WAKE TRANSITION AND BLOCKAGE EFFECTS ON CYLINDER BASE PRESSURES

Thesis by

Patrick D. Weidman

In Partial Fulfillment of the Requirements

For the Degree of

Aeronautical Engineer

California Institute of Technology

Pasadena, California

1968

(Submitted May 24, 1968)

ACKNOWLEDGEMENTS

The author wishes to express his gratitude to Dr. Anatol Roshko for his interest and encouragement in this work. His suggestions during the preparation of the thesis were particularly helpful. Many of the drawings were prepared by Mrs. Betty Wood, whose patience is much appreciated. The manuscript was typed by Mrs. Dottie Neely and corrections were made by Mrs. Elizabeth Fox.

ABSTRACT

Base pressure measurements of circular cylinders at Reynolds numbers from 100 to 3×10^6 were obtained in a low speed wind tunnel. Pressure distributions from $R_d = 10^3$ to 3×10^6 were also obtained.

In the Reynolds number region from the first appearance of an unsteady wake to the critical Reynolds number the base pressure coefficient shows two maximums and two minimums. The first maximum ($R_d \simeq 50$) coincides with the first appearance of the Karman vortex street. The succeeding minimum ($R_d \simeq 300$) probably corresponds to the movement of the onset of transition from the end of the vortex-formation region into the free shear layers. The following maximum ($R_d \simeq 2200$) is accompanied by a small discontinuity in the base pressure curve and a decrease in the Strouhal number. The final minimum corresponds to the end of the Schiller-Linke region, at which point transition to turbulence occurs in the free shear layers very near to the shoulder of the cylinder.

A comparison of the blockage correction theories of Maskell and Allen and Vincenti was made at $R_d = 6 \times 10^4$. The value of the base pressure coefficient in an unlimited stream at this Reynolds number was found to be $C_{p_b} = -1.215$ for cylinders of one particular roughness, though this value depends on other unit Reynolds number effects. These effects can also result in a significant Reynolds number shift of the base pressure coefficients.

TABLE OF CONTENTS

TABLE OF CONTENTS
(concluded)

LIST OF FIGURES

LIST OF SYMBOLS

English

C_D	drag coefficient
$C_p = p_s/\frac{1}{2}\rho U^2$	static pressure coefficient
$C_{p_{min}}$	minimum cylinder static pressure coefficient
C_{p_b}	base pressure coefficient
$(C_{p_b})_{ave}$	average pressure coefficient in base region
D	cylinder diameter
d	orifice diameter
H	tunnel height
$k^2 = 1 - C_{p_b}$	base pressure correction parameter
ℓ	cylinder length
n	shedding frequency
p	cylinder pressure
p_b	base pressure
p_∞	free stream static pressure
$p_s = p - p_\infty$	cylinder pressure referred to free-stream
R_d, $R = UD/\nu$	Reynolds number
$(R_d)_{crit}$	critical Reynolds number
$S = nD/U$	Strouhal number
U	free-stream velocity
u'/U	free-stream turbulence level

LIST OF SYMBOLS
(concluded)

Greek

ϵ	average surface roughness
θ	corrected pressure orifice angle with respect to free-stream velocity
θ_1	angular position of pressure orifice with respect to free-stream velocity
$\theta(C_{p_{min}})$	angle of minimum static pressure coefficient
θ_s	angle of laminar separation; angle of the inflection point in the pressure rise on the cylinder
λ	average turbulence scale
ϕ_s	angular correction increment
μ	10^{-6}
ν	kinematic viscosity
ρ	density

Subscripts

c	corrected value
o	reference condition

I. INTRODUCTION

Incompressible flow around a circular cylinder has been of interest to scientists in fluid mechanics for several decades. Recent investigations of hypersonic wakes have helped to bring about a revival in these studies. The cylinder is a typical bluff body, and a comprehension of the separated flow about a cylinder will aid in the understanding of flows about bluff bodies in general.

Recently there has been little progress in obtaining theoretical solutions of the problem other than variations and elaborations of the works of Kirchhoff and von Karman. However, there have been some theoretical advances in the region of low Reynolds number ($R_d < 60$); the recent numerical computations of Keller and Takami [Ref. 1] are of particular interest. For larger Reynolds numbers the problem is rendered difficult by the appearance of an unsteady wake (Karman vortex street) and the strong influence of transition on the flow field in the near-wake.

The contributions of von Karman and Kirchhoff deal with the *potential flow near the cylinder and the downstream wake.* These two regions are joined by what is called the near-wake. For a cylinder, the near-wake extends several diameters downstream and it is in this region that the separated shear layers roll up into vortices. For this reason the near-wake is called the vortex formation region. Figure 1 exhibits the flow regions for further reference. Flow separation, vortex formation, the base pressure, and transition all interact in the near-wake to determine the initial conditions for the quasi-steady

downstream wake and influence the potential flow around the cylinder.

Because the drag coefficient over the Reynolds number range $10^2 < R_d < 10^5$ does not vary greatly from a value of about 1, it is often assumed that there are no important changes in the near-wake over this range. A look at the base pressure indicates, in fact, a more interesting situation. Other than the work of Thom [Ref. 2], there seems to be no consistent determination of cylinder base pressures over a wide range of Reynolds numbers. A review of the literature [Refs. 2 to 11] was made to assemble some of the existing measurements. These data* are presented in Fig. 2. Though individual endeavors appear consistent, there is considerable scatter between the measurements of different authors. Undoubtedly the inconsistency of the various curves can be attributed, at least in part, to the different experimental conditions, particularly the wind tunnel turbulence level.

Because of the diversity of the measurements described above, it was decided to try to define more precisely the variation of the cylinder base pressure over as wide a range of Reynolds numbers as possible, having each test model subjected to approximately the same free-stream turbulence level. The present experiments were initiated for that purpose. In addition, the cylinder pressure distributions were obtained throughout a large part of the same Reynolds number range.

---

* The measurements have been corrected for tunnel blockage, when possible, by Maskell's correction formula [Ref. 20].

II. EXPERIMENTAL APPARATUS AND TECHNIQUES

1. Wind Tunnels

The majority of the experiments were conducted in the GALCIT 20- x 20-inch Low-Speed Wind Tunnel of the open-circuit type. The wind tunnel has a speed range from approximately 50 to 2,200 cm/sec. Measurements indicated a turbulence level of 0.15%, though it has been lower (about 0.03%) in the past. Further information may be obtained in Ref. 12.

Higher speeds were attained in the Merrill Wind Tunnel*, which is a closed-circuit tunnel having a test section of 32 x 43 inches. Wind speeds range from 1,200 to 6,000 cm/sec, the maximum attainable speed being less with the introduction of blockage. The turbulence level was about the same, possibly a little greater than that of the 20- x 20-inch tunnel.

2. Test Models and Measuring Equipment

A diversity of circular cylinders ranging in diameter from 0.013 to 3.50 inches was used. Table 1 presents a list of the various cylinders, including their average surface roughness as measured with a profilimeter. All cylinders were long enough to fully span the tunnel test section, thus simulating two-dimensional flow. A pressure tap was drilled normal to the cylinder at the center of its length. The

---

* Now being relocated.

sizes of these orifices are also presented in Table 1. The smallest cylinders were made out of stainless steel, while the rest were of brass, copper, or glass.

Standard manometry and hot wire equipment were used throughout the course of the experiments. The hot wire was used to determine shedding frequencies and to obtain a measure of the free-stream turbulence level. In conjunction with the hot wire, the following electronic equipment was incorporated: (1) Hewlett-Packard Model 2028 low-frequency oscillator, (2) Hewlett-Packard Model 522 3L electronic counter, (3) Krohn-Hite Model 330-M ultra-low frequency band-pass filter, and (4) Tektronix Type 522 oscilloscope.

Three micromanometers were used; two of the manometers had a precision of about ±0.02 mm of manometer fluid while the third, a Kendall manometer, was appreciably more precise due to its fine optical system. The free-stream static pressure served as the reference pressure for all measurements. Butyl Alcohol (specific gravity = 0.807) was used in each of the three manometers.

When taking frequency or turbulence measurements, the hot wire was mounted on a traversing mechanism which was located on the top of the test section. The traverse allowed for optimum positioning of the hot wire to obtain a clear signal of the vortex shedding [Fig. 3]. Frequency measurements were obtained by observing Lissajous figures on the oscilloscope and then recording the matched frequency on the electronic counter.

3. Experimental Techniques

The larger cylinders presented little difficulty in mounting. In each tunnel the cylinders were mounted so that the blockage ratio D/H was the smallest. For all diameters larger than 0.50 inch, the cylinder was sufficiently rigid to position from just one side of the tunnel. A large circle was scribed on each side of the tunnel and marked off in degrees. With a long pointer arm attached to its end, the cylinder could be rotated to any particular angle within ± 0.5 degree. The holes drilled in the tunnel mounting ports provided enough friction so that the cylinder would remain stationary at each position.

The smaller cylinders, however, could not be positioned from one side of the tunnel since the cylinder itself would twist. Consequently, for all the brass and copper cylinders smaller than 0.50 inch, each end had to be positioned with a special positioning block. As shown in Fig. 4, the cylinder could be put in tension by tightening the four bolts inserted through the cylinder positioning block. An aluminum washer was placed between the bolts and the wooden tunnel mounting port to facilitate rotation of the apparatus.

The three smallest cylinders were used in measuring the base pressure only. The positioning ($\theta = 180$ degrees) of these three cylinders was obtained visually. A sleeve was soldered on each end of the cylinders to fit snugly into holes drilled through the tunnel mounting ports. Then, by crawling into the tunnel and viewing the pressure tap through a magnifying glass, it was possible to position the small cylinder to within approximately 5 degrees of the base.

The angle $\theta = 0$ of all the larger cylinders was obtained by positioning the cylinder with the orifice facing upstream and measuring the static pressure in this neighborhood. The maximum (dynamic) pressure obtained was taken to be the angle $\theta = 0$; this position could be determined to within an accuracy of ± 1 degree.

In measuring the pressure distribution around each cylinder it was desirable to have very small orifices drilled in the cylinders to provide good angular resolution. Clearly, it was easy to obtain good resolution for the larger cylinders. For the smaller cylinders it became increasingly more difficult to drill a pressure orifice which was many times smaller than the overall cylinder diameter. The smallest cylinder, for example, was 0.013 inch in diameter and had a pressure orifice of 0.0059 inch. A study of the effect of hole size on measuring pressure distributions was made by Thom [Ref. 2]. He concluded that the pressure distributions around the front portion of each cylinder can be brought into substantial agreement if it is assumed that the pressure inside the hollow cylinder is not the pressure at the center of the hole, but that at a point half way along the hole radius towards the front of the cylinder. In other words, if θ_1 is the angular position of the hole with respect to the free-stream velocity, the measured pressure corresponds to the angle

$$\theta = \theta_1 - \frac{1}{2}\,\frac{d}{D} \quad \text{(radians)}$$

where d is the orifice diameter and D is the cylinder diameter. As a measure of the angular resolution of the orifices, the following

definition is then employed:

$$\text{angular resolution} = \theta_c = \frac{90}{\pi}\,\frac{d}{D} \quad \text{(degrees)}$$

This is the angular correction increment which is applied to the smaller cylinders. The values for each cylinder are listed in Table 1.

4. Velocity Measurements

A pitot-static probe, located 3.50 inches off the bottom of the test section as shown in Fig. 3, served to record the free-stream dynamic pressure for most of the measurements. For the three smallest cylinders, however, the free-stream velocity was obtained by calibrating the shedding frequency from a 0.125 inch cylindrical rod placed upstream of the test section (Fig. 3). This method, described by Roshko in Ref. 12, has the advantage that frequencies are easier to measure than pressures, especially at low speeds. In the Merrill tunnel the free-stream dynamic pressure at the center of the test section was calibrated with the dynamic pressure measured by a piezometer ring at the settling chamber. Pressures measured at the piezometer ring were then used to record the free-stream conditions.

While taking the pressure distribution around various cylinders it was noticed that the free-stream velocity drifted considerably over a 40- to 50-minute run. The change, probably due to a heating up of the control rheostats, was usually a slow decrease in dynamic pressure, the final pressure being about 10 per cent lower than the initial. This was taken into account in one of two ways. Either the velocity was held

constant by adjusting the tunnel speed or, more frequently, the free-stream dynamic pressure was measured throughout the run. Only an average Reynolds number could be recorded for the latter case.

5. Discussion of Pressure Measurements

A. Note on the Pressure Measurements

The reference pressure for the cylinders was located 8.0 inches upstream of the cylinder models as shown in Fig. 3. The upstream influence on the static pressure at the wall was found to be significant for cylinders greater than 1.0 inch in diameter. This static pressure change was taken into account by inviscid theory calculations.

Since the separated flow on the rear of the cylinder was unsteady for all the measurements presented here, mention should be made of the averaging process employed in recording the pressures. The unsteadiness in the base pressure became increasingly more pronounced for Reynolds numbers greater than 2,000. Below $R_d \simeq 2,000$, the observed fluctuations of the manometer fluid were only a very small percentage of the average measured pressure and consequently presented no difficulty in recording. The fluid oscillations for the larger Reynolds numbers, however, appeared random in nature and constituted as much as 10 per cent of the average measured pressure. (Fluctuations became significant only for angles $\theta > 40$ degrees.) The measured values were simply recorded by taking a visual average of the random fluctuations.

That the intensity of the fluctuations becomes greater with Reynolds number in the range described above is in agreement with

measurements of the oscillating lift coefficients on a cylinder by Gerrard [Ref. 13]. He has shown that the magnitude of the oscillating pressure coefficient at the fundamental (i.e., shedding) frequency at θ = 150 degrees increases almost two orders of magnitude from $R_d \simeq 3,000$ to $R_d \simeq 10^5$. Though the intensity at the base was reported to be significantly less than at θ = 150 degrees, it is expected that it undergoes a similar change.

Apparently the increase in the intensity of the observed fluctuations is due to the fact that the end of the formation region and the onset of turbulence both move toward the base of the cylinder at the higher Reynolds numbers, thus causing an increase in the turbulent activity on the rear of the cylinder.

The pressures presented in this investigation are then an average of observed fluctuations of the manometer fluid. Whether this represents the true average pressure on the cylinder is at present unknown.

B. Note on the Measurements at Low Reynolds Numbers

The three smallest cylinders used to measure the base pressure at low Reynolds numbers presented particular difficulties. In the first place the cylinders, though not under significant tension, were observed to vibrate, sometimes emitting a sound of a particular frequency. Since forced oscillations were not of interest in this investigation, the problem was corrected by placing the tubes in a slight compressive bend, yet leaving the center section (laterally displaced about 1.5 inches from its original position) normal to the

free stream. The bend inhibited all visible and audible vibrations, apparently by rendering the tubes more rigid.

In the second place, the 0.013 inch and the 0.025 inch cylinders restricted the flow through the pressure orifice (0.0059 inch diameter) in such a way that the recorded pressure would oscillate very slowly (over a period of minutes) around an average value. It was suspected that a comparable restriction on the static pressure side of the manometer would nullify the oscillations. Such was not the case and, after some effort to rectify the problem, it was decided to take an average of the maximum and minimum pressures of the oscillation. For these two cylinders it took as long as 40 to 50 minutes to record 5 maximums and 5 minimums. The 0.018 inch cylinder had a pressure orifice of 0.0091 inch which was still small enough to throttle the flow; with this cylinder the pressure oscillations were not observed and the manometer fluid came to rest within 15 to 20 minutes.

The magnitude of the noted oscillations was observed to be independent of the average measured pressure; in fact the manometer fluid began to oscillate once pressure tubing was connected from the cylinder to the manometer. The following table lists pertinent dimensions of the three cylinders and also an average of the amplitude of the oscillations observed.

Cylinder Diameter (D ~ in)	Orifice Diameter (d ~ in)	Cylinder Inside Diameter	Average Amplitude of Oscillation (mm alcohol)
0.013	0.0059	0.006	±0.50
0.018	0.0091	0.009	0
0.025	0.0059	0.0125	±0.30

Since similar results were obtained for the base pressure coefficients for all of the three cylinders (Fig. 10, to be discussed) one is led to believe that the pressure oscillations observed with the 0.013- and 0.025-inch cylinders were a characteristic of the cylinder-manometer system rather than very low frequency oscillations of the flow at the base of the cylinder.

A natural question arises in connection with the low Reynolds number measurements of base pressures. What is the accuracy of such measurements if the angular resolution is so poor? In fact, the smallest cylinder had a pressure orifice which was nearly half its diameter; the included angle of the pressure orifice was 54 degrees! The base pressure measurement is then an average over 54 degrees of the base. The situation is not nearly so bleak as one might first suspect. Fortuitously, the pressure distributions measured by Thom have shown that the positive pressure gradient on the aft part of the cylinder is small for the low Reynolds numbers of concern. At worst the base pressure changes only 10 per cent in the base region, though usually much less. For the most unfavorable condition, then, the average pressure sensed by the orifice would be only 5 per cent in error.

III. PRESENTATION OF RESULTS

1. Pressure Distributions

The cylinder pressure distributions measured over a wide range of Reynolds numbers are presented in Appendix I [Figs. 20 to 46]. Though smaller Reynolds numbers were obtainable, no distributions were measured below $R_d = 1,000$ because of the poor resolution of the pressure orifices in the smallest cylinders. The pressure distributions should be of particular interest to theoreticians for the interesting changes exhibited in the region of separated flow.

One observation which should be made concerns the pressure gradient in the separated flow region. Assuming that the separation point on the cylinder is located near the inflection point in the pressure rise, one can see that the region of separated flow is characterized by a negative pressure gradient for $R_d \simeq 4,000$. For $R_d \simeq 2,000$ the gradient is positive and intermediate Reynolds numbers [Figs. 23 to 26] are characterized by approximately constant pressure (p_b) on the rear of the cylinder. Thom's measurements [Ref. 2] show similar results. His pressure distributions indicate that the positive pressure gradient persists to Reynolds numbers as low as 28. Consequently, a basic change in the flow (perhaps in the mechanism of separation) might be expected in the neighborhood $2,000 < R_d < 4,000$.

It is of interest to follow the Reynolds number variation of characteristic points of the pressure distributions. Figures 5, 6, and 7 show the Reynolds number variations of the angle of zero pressure

coefficient $\theta(C_p = 0)$, the minimum pressure coefficient $C_{p_{min}}$, and the angle of the minimum pressure coefficient $\theta(C_{p_{min}})$, respectively. These points are illustrated in the following sketch.

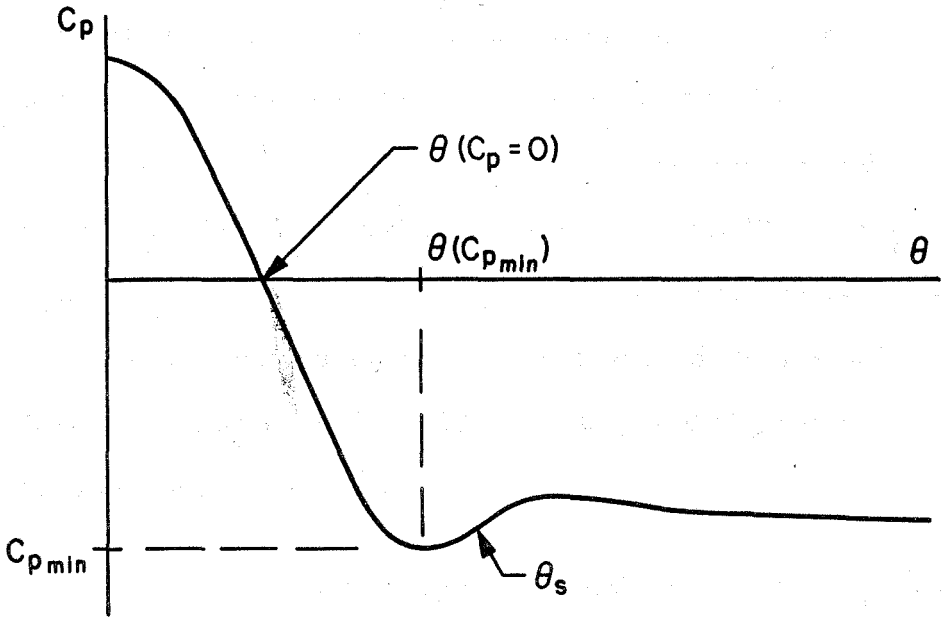

If it can be assumed that the inflection point in the pressure rise is approximately the point of separation of the flow around the cylinder, one can also show the variation of the angle of laminar separation θ_s over a wide range of subcritical Reynolds numbers [Fig. 8]. Also included in these figures are some recent measurements by the author [Ref. 11] on a cylinder in the supercritical Reynolds number regime. The above figures exhibit the fact that the flow about a cylinder is continually changing up to and even beyond the critical Reynolds number, contrary to the often made assumption that turbulent base flows show little Reynolds number effect. In particular, consider the curve for laminar separation. Though it is often stated that separation occurs near $\theta = 81$ degrees [Ref. 14], the measurements indicate it can vary from 76 to 85 degrees in the range $10^3 < R_d < 3 \times 10^5$.

2. Base Pressures

Figure 9 is a presentation of the base pressure coefficients measured for all the cylinders. (In this figure the data are presented without correction for wind tunnel blockage.) The base pressure curve between the first appearance of an unsteady wake and the critical Reynolds number ($R_d \simeq 3.5 \times 10^5$) is characterized by a minimum near $R_d = 300$, a maximum near $R_d = 2{,}000$, and a second minimum near $R_d = 1.0 \times 10^5$. The discussion of base pressures will be divided into the following sections: Low Reynolds Numbers ($100 < R_d < 2{,}000$), Reynolds Numbers Near $R_d = 2{,}000$, and High Reynolds Numbers ($2{,}000 < R_d < 3 \times 10^5$).

A. Low Reynolds Numbers ($100 < R_d < 2{,}000$)

The base pressure measurements at the lowest Reynolds numbers recorded are presented in Fig. 10. Included for comparison are some recent numerical calculations by Keller and Takami [Ref. 1] for steady two-dimensional viscous flow, and some recent experimental results obtained by Acrivos, et al. [Ref. 10] in an oil tunnel. A predominant feature of the base pressure measurements is the shifting of the curve with a change in cylinder diameter; though the minimum remains relatively constant ($C_{p_b} \simeq -0.90$), the curve shifts towards larger Reynolds numbers with each increase in cylinder diameter. The three cylinders were of approximately equal surface roughness, the average being about 4 μin. This diameter

dependence was observed at all Reynolds numbers where the surface roughness of a group of cylinders was approximately constant*.

A description of characteristic changes in the flow field will be presented in order to bring the present measurements into proper perspective. For increasing Reynolds numbers approaching $R_d \simeq 50$ the flow is laminar and steady, though symmetrical eddies are attached to the base of the cylinder. At a Reynolds number of 40 or 50 (depending on the quietness of the flow, the tunnel blockage, etc.) a laminar vortex street is produced behind the eddies due to an instability in the wake. We infer that the maximum in Acrivos' measurements [Fig. 10] occurs at this point of instability. If so, it is at the rather high value of $R_d = 60$. (The blockage ratio, however, was 0.05 for which Shair, et al. [Ref. 15] gives the value $R_d = 55$ for the onset of instability.) The appearance of the vortex street was first observed at $R_d = 43.5$ for the smallest cylinder (0.013 inch) in these measurements.

For $90 < R_d < 150$ the laminar vortex street originates at the base of the cylinder [Tritton, Ref. 16], the lee eddies having completely disappeared. A sketch of this flow is offered in Fig. 1a. In the Reynolds number region $50 < R_d < 150$ the flow is everywhere laminar; the shedding frequency is easily detected. In the Reynolds number range $150 < R_d < 300$ [Roshko, Ref. 12] or $200 < R_d < 400$ [Bloor, Ref. 17] the shedding frequencies are observed to be sporadic and difficult to measure. Above this "transition" range the vortex street reappears as fairly well-defined turbulent, periodic motion.

---

* See section entitled Unit Reynolds Number Effects

The minimum in the base pressure curve is seen to occur near R_d = 300 for the cylinders and free-stream turbulence level in this investigation; apparently it falls within the transition range described above.

Bloor's measurements are particularly interesting inasmuch as she has followed the movement of the region of laminar-turbulent transition throughout a large range of Reynolds numbers ($200 < R_d < 4.5 \times 10^4$). She has observed that below the transition range, i.e., below $R_d = 200$, the wake is laminar and periodic, without any trace of turbulent motion. For $200 < R_d < 300$ she has observed that low frequency irregularities, originally formed in the formation region, begin to grow in the far wake, eventually rendering it turbulent. In the Reynolds number region $300 < R_d < 400$ transition to turbulence moves into the end of the formation region (marked by the disappearance of the low frequency irregularities until at $R_d \simeq 400$ it is difficult to decide if the vortices are laminar or turbulent on formation. Above $R_d \simeq 400$, however, the transition occurs in the separated shear layers, the vortices being turbulent on formation. Moreover, the transition region does not move appreciably for Reynolds numbers up to $R_d \simeq 1,300$, though the length of the formation region increases from 2 to 2.7 diameters. (All downstream lengths are referred to the center of the cylinder.)

Since the turbulence level in Bloor's measurements is reported to be considerably less ($u'/U = 0.03\%$) than that of the low-speed tunnel used in this investigation ($u'/U = 0.15\%$), the minimum of the base pressure coefficients reported here at $R_d \simeq 300$ possibly

corresponds to $R_d \simeq 400$ in Bloor's tunnel, i.e., the minimum point corresponds to the passage of the transition point through the end of the formation region. On the low Reynolds number side of the minimum the base pressure coefficients are seen to decrease with increasing Reynolds number, apparently due to the increasing Reynolds stresses in the laminar near-wake [Roshko and Fiszdon, Ref. 18]. It is not quite understood, however, exactly why the base pressure begins to rise again once the transition moves into the separated shear layers, though Roshko suggests that the minimum (i.e., a maximum in Reynolds stress) may be due to intermittencies connected with the development of other periodic modes and their interaction with the vortex-shedding mode..

B. Reynolds Numbers Near $R_d = 2,000$

An especially interesting phenomenon was observed while measuring the base pressures at the maximum near $R_d = 2,000$. If close enough increments were taken, a distinct jump or discontinuity in the base pressure coefficient could be discerned at $R_d \simeq 2,200$ for the 0.125 inch cylinder. In pursuit of this observation it was decided to make a close survey of the base pressure and the shedding frequency in this region. Figure 11 clearly exhibits the discontinuity at $R_d = 2,200$ for the 0.125 inch cylinder. Figure 12, a plot of the shedding frequency, shows that at $U = 1,100$ cm/sec (i.e., $R_d = 2,200$) the cylinder experiences a distinct break in the slope of the frequency-velocity curve. An enlargement of the figure showed that the data moved from one curve to the other over the region $1,000 < U < 1,150$ cm/sec

(i.e., $2,000 < R_d < 2,300$). A plot of the same data in dimensionless form is presented in Fig. 13; the equations for the two straight lines have also been transformed into dimensionless form and are plotted for comparison, assuming a break at $R_d = 2,200$. Here one can distinctly see a continuous change in the Strouhal number around $R_d \simeq 2,200$, suggesting that the flow is flipping back and forth between two modes of vortex shedding. Also plotted in Fig. 13 is the $S(R_d)$ equation fitted to a band of data measured by Roshko [Ref. 12]. The present measurements lie on the upper edge of that band.

The measurements show, then, that the maximum in the base pressure curve is attended by a small discontinuity which is most likely brought about by a particular change in the mechanism of vortex shedding. It is of interest to remember that the pressure gradient on the back of the cylinder changes sign near this same Reynolds number. Furthermore, the maximum in the curve of the base pressure coefficient corresponds closely to the maximum in the length of the formation region as measured by Bloor [Ref. 17].

C. High Reynolds Numbers $(2,000 < R_d < 3 \times 10^5)$

According to Fig. 9, the pressure coefficient at the base of the cylinders is seen to decrease from a value of approximately $C_{p_b} = -0.75$ at $R_d \simeq 2,000$ to $C_{p_b} = -1.65$ at $R_d \simeq 10^5$. The nature of the curve for the individual cylinders is considerably different. In the first place, the data in Fig. 9 have not been corrected for tunnel blockage, and this correction becomes especially important for $R_d > 10^4$. Secondly, the band of measurements in the figure obscures

the diameter dependence of the base pressures. Finally, it has been shown that the base pressure depends on the turbulence level of the free stream. In fact Gerrard [Ref. 9] has called this region of decreasing base pressure a "disturbance-sensitive Reynolds number range."

This region was probably first studied by Thom in 1928. In 1933, Schiller and Linke [Ref. 6] showed that the onset of transition moves from 1.4 to 0.7 diameter downstream of the center of the cylinder as R_d increases from 3,500 to 8,500. Bloor has shown that the length of the formation region decreases in much the same manner as the base pressure, i.e., from a maximum of 2.7 to 1.4 diameters for a 0.250 inch cylinder in the same Schiller-Linke region. A representative sketch of the separated flow in this Reynolds number regime is provided in Fig. 1b.

The diameter dependence of the base pressure curve becomes readily apparent in Fig. 14, which shows the base pressure coefficients for various cylinders of approximately equal surface roughness (ϵ = 15 μin). The blockage effect is indicated by the gradual decrease of the minimum of each successive curve.

Two cylinders (1.00 and 3.50 inches diameter) of equal surface roughness (ϵ = 15 μin) were tested in the Merrill wind tunnel. The base pressure measurements are included in Fig. 9. The base pressure coefficients are seen to rise rapidly beyond $R_d = 2 \times 10^5$; this trend is expected since it has been demonstrated [Weidman, Ref. 11] that a maximum of $C_{p_b} \simeq -0.30$ (uncorrected for 11 per cent blockage) occurs in the supercritical regime at $R_d \simeq 6.x\ 10^5$.

A final comment with reference to Bloor's measurements should be made. Not only does the shape of the curve describing the length of the formation region follow the same trend as the base pressure coefficient curve (which verifies her suggestion that the length of the formation region is related to the pressure at the rear of the cylinder), but it exhibits the same diameter dependence. That is, the curve experiences a positive Reynolds number shift with an increase in cylinder diameter. This shift is much larger than the expected Reynolds number increase due to blockage effects; these effects will be discussed in the following section.

3. The Problem of Blockage

Blockage constraints for symmetrical two- and three-dimensional bodies have been considered in some detail in the past. Wind tunnel walls give rise to a simple increase in the free-stream velocity attributed to the volume distribution of the body (solid blockage) and also provide a serious constraint on the growth of the wake (wake blockage). Velocity corrections have been successfully computed for streamline bodies which result in thin wakes. Attempts have been made to obtain velocity corrections for bluff bodies where the displacement effect of the wake becomes of significant importance. Allen and Vincenti [Ref. 19] have obtained the formulas

$$\frac{U_c}{U} = 1 + \frac{1}{4} C_d (D/H) + 0.82 (D/H)^2 \qquad (1)$$

$$\frac{C_{d_c}}{C} = 1 - \frac{1}{2} C_d (D/H) - 2.5 (D/H)^2 \qquad (2)$$

(subscript c denotes corrected value and D/H is the blockage ratio) for the case of two-dimensional flow about a circular cylinder by using image doublets and sources to represent the wall interference on the cylinder and wake, respectively. Maskell [Ref. 20] has considered the flow about both two- and three-dimensional symmetric bluff bodies. His theory is based on an approximate relation describing the momentum balance in the flow outside the wake and two empirical auxiliary relations. The correction for two-dimensional flow is expressed in the form

$$\frac{U_c^2}{U^2} = \frac{C_{d_c}}{C_d} = \frac{k^2}{k_c^2} = 1 + \frac{C_d}{k_c^2 - 1} (D/H) \qquad (3)$$

where $$k^2 = 1 - \left(C_{p_b}\right)_{ave}$$

The equation is best solved through an iterative procedure. Maskell's correction theory is well supported by experiments on sharp-edged square flat plates of small blockage ratios.

Both of the above theories do not take into account possible interference effects on the separation point, the region of transition, and the structure of the near-wake. These considerations may be of particular interest for bluff bodies where the separation point is not fixed.

The Reynolds number region in which the base pressure coefficient of each cylinder reaches a minimum (Fig. 14) provides an area in which a comparative study of blockage corrections can possibly be made. The qualification is mentioned because a correlation of this nature can only be carried out if the magnitude of the minimum base pressure coefficient is independent of so-called unit Reynolds number effects. The maximum at $R_d \simeq 2,200$ and the minimum at $R_d \simeq 300$ were seen to be relatively insensitive to these effects as long as the turbulence level remained constant. Therefore it will be assumed that this is also the case at high Reynolds numbers. The curves for the smaller cylinders in Fig. 14 have been extended so that the minimum base pressure coefficient of five distinct cylinders can be compared at the single Reynolds number of $R_d = 6 \times 10^4$. Figure 15 shows the variation of this base pressure coefficient with the blockage ratio. An extrapolation yields a zero blockage coefficient of $C_{p_b} = -1.215$.

The blockage corrections of Maskell, and Allen and Vincenti have been applied to the measurements. Both correction schemes require knowledge of the uncorrected drag coefficient which was not available for all the cylinders in this comparison. Furthermore, Maskell's formula requires the measurement of the mean pressure in the separated region, i.e., the pressure average over the base of the body and the surface of the effective wake. For flat plates, discs, etc., this value is taken to be the base pressure coefficient. In the case of a circular cylinder, a better average may have to be employed. To obtain the above data, a pressure distribution was measured around each of the three largest cylinders near $R_d = 6 \times 10^4$. An

integration of the surface pressures was performed to obtain the drag coefficient, and the average base pressure coefficient defined as

$$\left(C_{p_b}\right)_{ave} = -\int_{\frac{\pi}{2}}^{\pi} C_p(\theta) \cos\theta \, d\theta \qquad (4)$$

was also calculated to be used as an approximate mean pressure coefficient for the separated region. The values of C_d and $\left(C_{p_b}\right)_{ave}$ for the 1.0 inch and 0.50 inch cylinders were obtained by an extrapolation to smaller D/H. The results are summarized in the following table.

Diameter ~ D (inches)	Blockage Ratio ~ D/H	$\left(C_{p_b}\right)_{ave}$	C_D
0.500	0.025	-1.155	1.210
1.00	0.050	-1.205	1.230
1.50	0.075	-1.235	1.260
2.25	0.1125	-1.340	1.320
3.50	0.175	-1.545	1.435

Equations (1) and (3) were then used to obtain the corrected values of velocity, and the corrected base pressure coefficient was obtained from the equation

$$\left(C_{p_b}\right)_c = 1 - \frac{U^2}{U_c^2}\left(1 - C_{p_b}\right) \qquad (5)$$

Both the average and measured base pressure coefficients were used

in Maskell's correction formula. The corrected coefficients are presented in Fig. 16. The corrected values obtained from Allen and Vincenti's correction formula deviate less than 3 per cent from the zero blockage coefficient; Maskell's correction formula yields maximum deviations of 8 or 12 per cent depending on whether the measured or averaged base pressure coefficient was used in the calculation.

The results are particularly interesting since good agreement is obtained with Allen and Vincenti's correction formula which, unlike Maskell's, does not require a measurement of the average pressure in the separated region. Though it appears that Allen and Vincenti's method is better than Maskell's for circular cylinders, one should be aware of the sometimes important influence unit Reynolds number effects can have on base pressures.

4. Unit Reynolds Number Effects

Throughout the investigation the dependence of the base pressure curve on cylinder diameter (other than through the Reynolds number) manifested itself. This is the so-called "unit Reynolds number effect." For small blockage ratios (or equal blockage ratios) the important dimensionless parameters which may influence the flow are the aspect ratio ℓ/D, the relative surface roughness ϵ/D, the turbulence scale parameter λ/D, and u'/U, a measure of the turbulence level. Since the curves were found to shift for the smallest cylinders, it is evident that there is a Reynolds number shift other than that due to blockage effects. As the flow is essentially two-dimensional one would not expect a large influence due to the

aspect ratio. (All but two of the cylinders had aspect ratios greater than ten.) Though the turbulence scale spectrum may be important, we shall simply assume that the turbulence scale λ is fixed in a given tunnel, and so the parameter λ/D only varies with D. In the ensuing discussion only the three dimensionless parameters λ/D, ϵ/D, and u'/U will be considered.

In Gerrard's base pressure measurements [Ref. 9] u'/U was varied while ϵ/D remained constant; λ/D must have also changed since an increased turbulence level was introduced with the use of a 1 inch mesh grid. His results indicate that the base pressure curve experiences a decrease in Reynolds number with an increase in u'/U. In addition, however, there is a considerable effect on the magnitude of the pressure coefficient; it decreases with an increase in the turbulence level. (It may also be due to changes in λ/D.) The present measurements seem to correspond with Gerrard's observations on a 1.00 inch cylinder in a 20- x 20-inch tunnel. The following table is a comparison of the base pressure coefficient minimums at the end of the Schiller-Linke region for cylinders of equal diameter and blockage ratio.

	Turbulence Level u'/U (%)	C_{p_b} (minimum)
Gerrard	0.015	-1.03
Present Investigation	0.15	-1.23
Gerrard	1	-1.22 (or less)

In the present investigation it was found that the cylinders of equal roughness (ϵ) exhibited a strong Reynolds number shift in the low Reynolds number region, with only a weak (if any) effect on the magnitude of the base pressure coefficient. At higher Reynolds numbers the shift again becomes readily apparent, but evidence of a base pressure change is unobtainable since blockage effects dominated. (The Reynolds number shifts observed are much larger than the increase in Reynolds number due to the tunnel wall constraints which can be estimated from the results in the previous section.) Since the turbulence level was fairly constant ($u'/U \simeq 0.15\%$), the Reynolds number shift in this case could be due to either a decrease in ϵ/D, λ/D, or both.

To investigate the effect of surface roughness, three glass cylinders ($\epsilon \simeq 1.5\ \mu$in) were prepared for testing. The base pressure measurements are presented in Fig. 17. Also shown are the coefficients for the copper cylinders (an order of magnitude rougher) of the nearest diameters. One can see that though λ/D and u'/U are approximately constant for each pair of cylinders, comparisons show no consistent dependence on ϵ/D; the smallest glass cylinder seems to be affected largely in the magnitude of the base pressure, and the second two cylinders appear to be perturbed in magnitude, Reynolds number, and even in the shape of the curve. But one interesting observation can be made, namely, the Reynolds number variation of the base pressure coefficient seems to occur much more rapidly on the smoother cylinders. This is evidenced by the sudden upward trend of the base pressure for the two largest glass cylinders

and suggests a stronger Reynolds number shift for cylinders of smaller ϵ/D, with u'/U and λ/D remaining constant. It might be noted that this effect is very similar to the effects of surface roughness on the drag coefficient of a circular cylinder as investigated by Fage and Warsap [Ref. 21].

Recent measurements presented in a paper by Roshko and Fiszdon [Ref. 18] provide a comparison of base pressure changes on a circular cylinder due to changes in the free-stream turbulence level. These results, like Gerrard's, indicate a significant base pressure coefficient decrease for each pair of equally smooth cylinders as u'/U is increased. (Again the turbulence level was changed by placing wire mesh grids in the flow, so λ/D probably also changed.) Nevertheless, there appears to be some Reynolds number shift; the results are inconclusive since it is difficult to separate out the two effects when the base pressure curve is steep. The situation is undoubtedly more difficult to analyze than simply trying to relate the shifts in the base pressure curve to simple changes in λ/D, u'/D, and ϵ/D. The magnitude of cylinder pressures in the region of separated flow are seen to be affected by changes in the free-stream turbulence level. In addition the Reynolds number shift appears to be primarily due to changes in λ/D, ϵ/D, or some combination thereof.

To obtain a quantitative idea of the diameter dependence, the relative Reynolds number shift was plotted against the accompanying relative change in cylinder diameter with ϵ as a parameter. This was accomplished by comparing the shifts of similar points on

displaced curves, if such points existed. In the case of the low Reynolds numbers, the similar point selected was $C_{p_b} = -0.80$, although the minimum base pressure would also have been a good choice. In the case of high Reynolds numbers, the value $C_{p_b} = -1.00$ was chosen (after all the curves in Fig. 14 had been shifted vertically so that their minimums coincided with the extrapolated value of C_{p_b} at zero blockage). For the case of the two largest glass cylinders the minimum point of the base pressure curves [Fig. 17] was selected as the similar point. The smallest glass cylinder had no point of comparison with the two larger cylinders.

Where there were more than two cylinders to compare, the relative shifts were taken always with respect to the smallest diameter and its corresponding Reynolds number at the similar point. The results, displayed in Fig. 18, indicate a certain uniformity and trend in spite of the paucity of data points. Figure 19 shows the variation of the slope $(\Delta R/\Delta D)$ of the curves in Fig. 18. These points, the rate of change of Reynolds number with diameter, are seen to fall on a monotonically decreasing curve which shows that the rougher (absolute) cylinders are less sensitive to unit Reynolds number effects.

The above results, though quantitative in nature, should be used only as qualitative guidelines for further investigations; however, the trends do exhibit the fact that there is by no means a unique curve for the base pressure coefficient for a circular cylinder and, probably, for the base pressure coefficients of bluff bodies in general. There may be one important exception to this hypothesis, namely bluff bodies where the separation point is fixed. But even in this case the free-

stream turbulence level (and the turbulence spectrum) will have an effect on the near-wake, which in turn affects the base pressure.

IV. SUMMARY AND CONCLUSIONS

The curve of the base pressure coefficient is seen to undergo a series of changes in the Reynolds number region between the first appearance of an unsteady wake and the critical Reynolds number. These observations along with observations made by Roshko at large Reynolds numbers suggest that the flow in the wake is in a continual state of transition up to $R_d \simeq 3.5 \times 10^6$ where transition to turbulence first appears in the boundary layer on the cylinder.

The base pressure curve in the subcritical regime is characterized by two maximums ($R_d \simeq 50$ and 2,000) and two minimums ($R_d \simeq 300$ and 10^5); the Reynolds number of these extrema depend on unit Reynolds number effects. The first maximum represents the onset of instability in the wake, after which the base pressure decreases due to the increasing Reynolds stresses in the laminar near-wake. The minimum at $R_d \simeq 300$ appears to correspond to the movement of the onset of transition from the end of the formation region into the free shear layers. After $R_d \simeq 300$ the formation region lengthens and the base pressure rises to the second maximum near $R_d = 2,200$. This extremum is distinguished by a small discontinuity in the base pressure coefficient and a decrease in the Strouhal number. The pressure coefficient then decreases in the Schiller-Linke region as the onset of transition moves up the free shear layers to the shoulder of the cylinder. A relatively flat minimum is then reached near $R_d = 10^5$ before the base pressure coefficient begins

to rise rapidly as it approaches the supercritical regime. To complete the picture one should add that the base pressure attains still another maximum near $R_d = 6 \times 10^5$ when a laminar separation bubble is formed on the rear of the cylinder. The base pressure coefficient reaches the very large value of $C_{p_b} \simeq -0.2$ due to the narrow wake that is characteristic of the supercritical Reynolds numbers. The base pressure drops off in the transcritical regime until at $R_d \simeq 3.5 \times 10^6$ it reaches a constant value (about $C_{p_b} = -0.85$). Here the separation bubble no longer exists and transition to turbulence occurs ahead of separation.

The base pressure measurements are observed to follow the same trends as the measurements of the length of the formation region obtained by Bloor. That is, the curves describing these two quantities increase from $R_d = 400$ to a maximum at $R_d = 2,000$, and decrease in the Schiller-Linke region to a flat minimum near $R_d = 10^5$. In addition, the curves exhibit a similar diameter dependence.

An extrapolation to zero blockage at $R_d = 6 \times 10^4$ gives the unlimited stream value of $C_{p_b} = -1.215$ for the "rough" cylinders ($\epsilon \simeq 15$ μin). A comparison of blockage theories at this Reynolds number shows that Allen and Vincinti's correction formula gives good agreement with the unlimited stream value, while Maskell's corrections compare less favorably. However, in the case of Maskell's corrections, only an approximate average pressure in the base region was calculated in lieu of the true mean wake pressure which he suggests should be used.

Finally, the base pressure curve is observed to be significantly dependent on unit Reynolds number effects. Not only can the curve shift in Reynolds number, but the actual magnitude of the base pressure coefficient is seen to change. Similar results are expected for other bluff bodies, especially when the separation point is not fixed by the geometry of the body.

REFERENCES

1. Keller, H. B. and H. Takami. On steady two-dimensional viscous flow of an incompressible fluid past a circular cylinder. To be presented at the International Symposium on High Speed Computing in Fluid Dynamics at Monterey, California, 19-24 August 1968.

2. Thom, A. 1928 An investigation of fluid flow in two dimensions. Aero. Res. Counc., R & M No. 1194.

3. Thom, A. 1928 The boundary layer of the front portion of a cylinder. Aero. Res. Counc., R & M No. 1176.

4. Fage, A. and F. M. Falkner. 1931 The flow around a circular cylinder. Aero. Res. Counc., R & M No. 1369.

5. Flachsbart, O. 1929 From an article by H. Muttray 1932. Handb. Experimentalphysik, 4, part 2 (Leipzig), 316.

6. Schiller, L. and W. Linke. 1933 Druck- und Reibungswiderstand des Zylinders bei Reynoldschen Zahlen 5000 bis 40000. Z. Flugtechnik u. Motorluftschiffahrt, 24:193.

7. Roshko, A. 1954 On the drag and shedding frequency of two-dimensional bluff bodies. NACA TN 3169.

8. Roshko, A. 1960 Experiments on the flow past a circular cylinder at very high Reynolds number. Journ. Fluid Mech., Vol. 10, part 3.

9. Gerrard, J. H. 1965 A disturbance sensitive Reynolds number range of the flow past a circular cylinder. Journ. Fluid Mech., Vol. 22, part 1.

10. Acrivos, A., L. G. Leal, D. D. Snowden, and F. Pan. 1968 (?) Further experiments on steady separated flows past bluff objects. Dept. of Chem. Engrg., Stanford University, Stanford, California. To be published in Journ. Fluid Mech.

11. Weidman, P. D. 1967 Investigation of high Reynolds number over a circular cylinder. T. C. E. A. Project Rept. 67-195, Rhode-Saint-Genese, Belgium.

12. Roshko, A. 1952 On the development of turbulent wakes from vortex streets. (Ph. D. thesis) California Institute of Technology, Pasadena, California.

13. Gerrard, J. H. 1961 An experimental investigation of the oscillating lift and drag of a circular cylinder shedding turbulent vortices. Journ. Fluid Mech. Vol. 11, p. 244.

14. Goldstein, S. (editor). 1965 Modern Development in Fluid Dynamics. Vol. 1, p. 61. Dover Publications, Inc., New York.

15. Shair, F. H., A. S. Grove, E. E. Peterson, and A. Acrivos. 1963 The effect of confining walls on the stability of the steady wake behind a circular cylinder. Journ. Fluid Mech. Vol. 17, p. 546.

16. Tritton, D. J. 1959 The flow past a circular cylinder at low Reynolds numbers. Journ. Fluid Mech. Vol. 6, p. 547.

17. Bloor, M. S. 1964 The transition to turbulence in the wake of a circular cylinder. Journ. Fluid Mech. Vol. 19, p. 290.

18. Roshko, A. and W. Fiszdon. 1967 On the persistence of transition in the near-wake. California Institute of Technology, Pasadena, California. (Invited contribution to 60th anniversary volume for Prof. L. I. Sedov to be published by U.S.S.R. National Committee on Theoretical and Applied Mechanics.)

19. Allen, H. J. and W. G. Vincenti. 1944 Wall interference in a two-dimensional-flow wind tunnel, with consideration of the effect of compressibility. NACA Rept. 782.

20. Maskell, E. C. 1963 A theory of the blockage effects on bluff bodies and stalled wings in a closed wind tunnel. Aero. Res. Counc., R & M No. 3400.

21. Fage, A. and J. H. Warsap. 1930 The effects of turbulence and surface roughness on the drag of a circular cylinder. Aero. Res. Counc., R & M No. 1283.

TABLE 1

TEST MODELS

Cylinder Diameter D (in)	Orifice Diameter d (in)	Material	Average Surface Roughness ϵ (min)	Angular Resolution ϕ_c (deg)
0.013	0.0059	Stainless steel	4	13.0
0.018	0.0091	Stainless steel	4	14.5
0.025	0.0059	Stainless steel	4	6.8
0.063	0.0110	Stainless steel	4	5.1
0.095	0.0135	Copper	15	4.1
0.114	0.010	Glass	1.5	2.5
0.125	0.0145	Copper	15	3.3
0.186	0.0145	Brass	20	2.2
0.250	0.0145	Copper	15	1.7
0.259	0.0100	Glass	1.5	1.0
0.375	0.0145	Brass	20	1.1
0.500	0.0135	Copper	15	0.8
0.517	0.015	Glass	1.5	0.8
1.00	0.0135	Copper	15	0.4
1.50	0.031	Copper	15	0.6
2.25	0.031	Copper	15	0.4
3.50	0.040	Copper	15	0.3

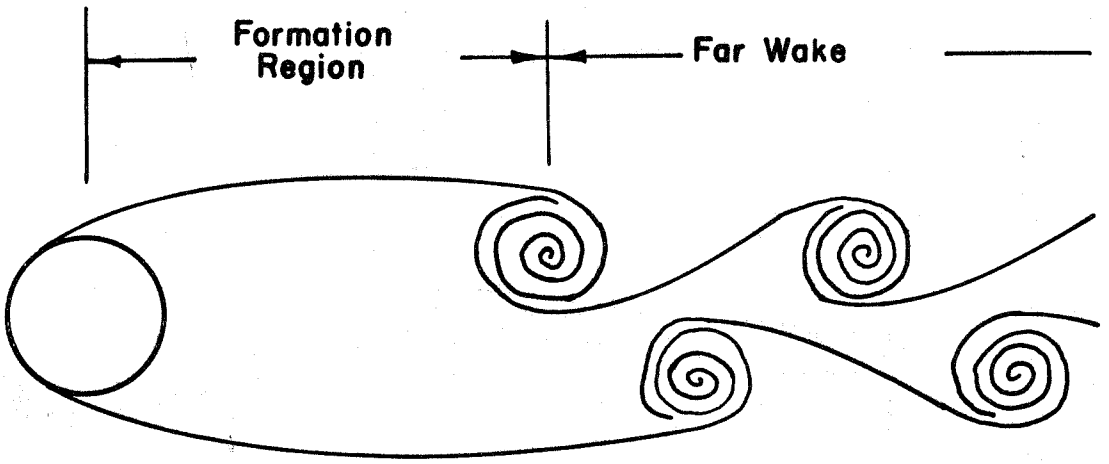

(a) Vortices Laminar On Formation

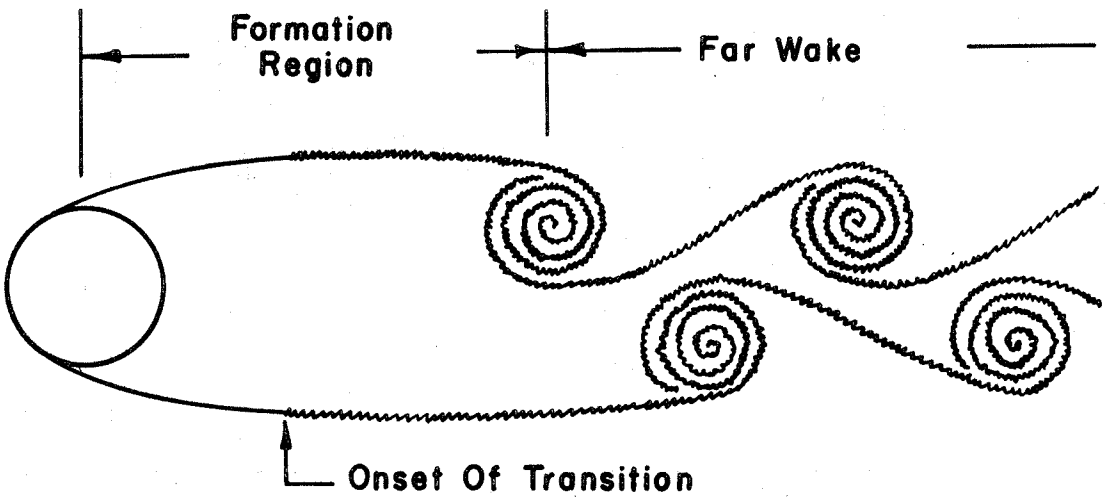

(b) Vortices Turbulent On Formation

FIGURE I IDEALIZED SEPARATED FLOW REGIONS IN THE WAKE OF A BLUFF BODY

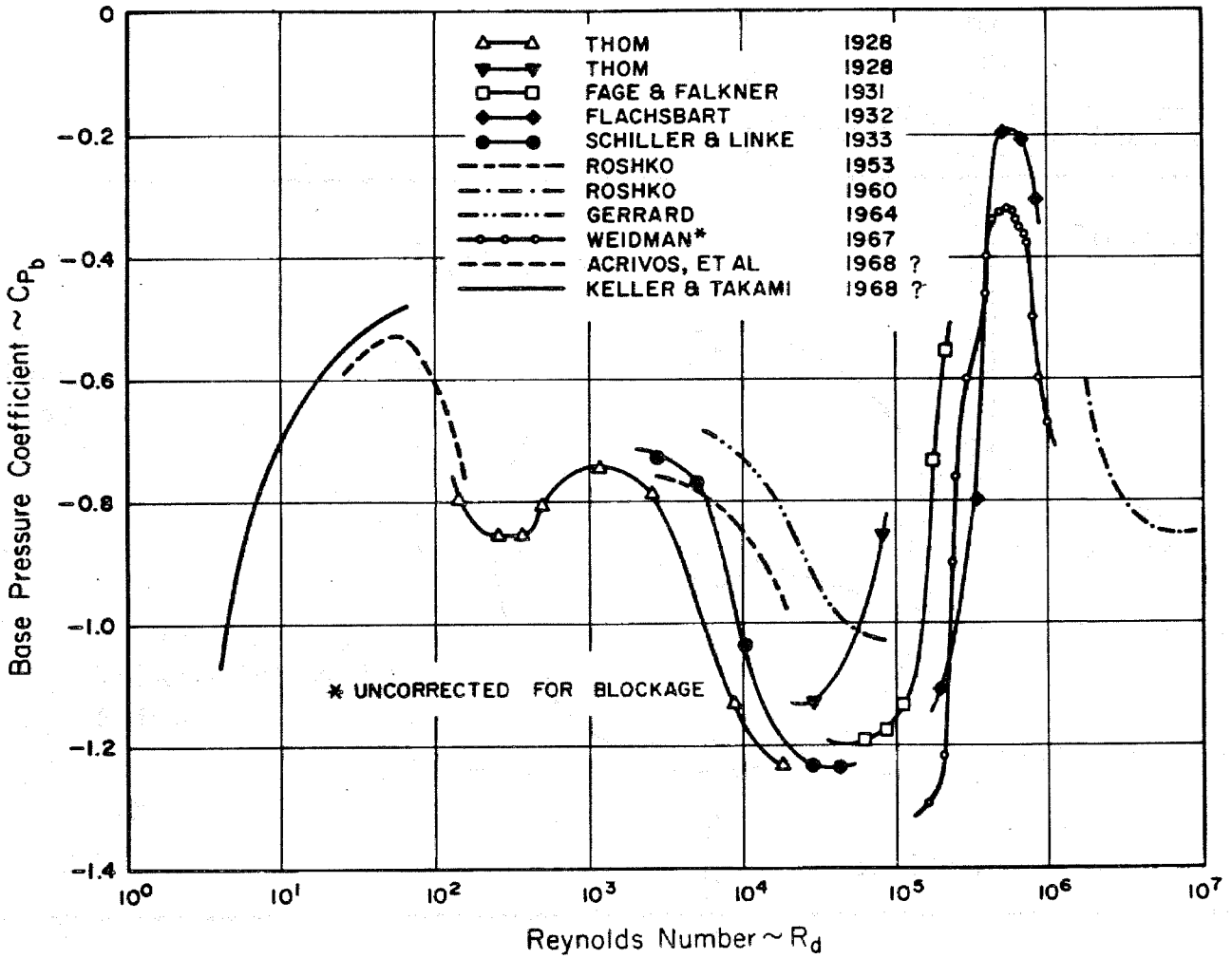

FIGURE 2 A SURVEY OF BASE PRESSURE MEASUREMENTS

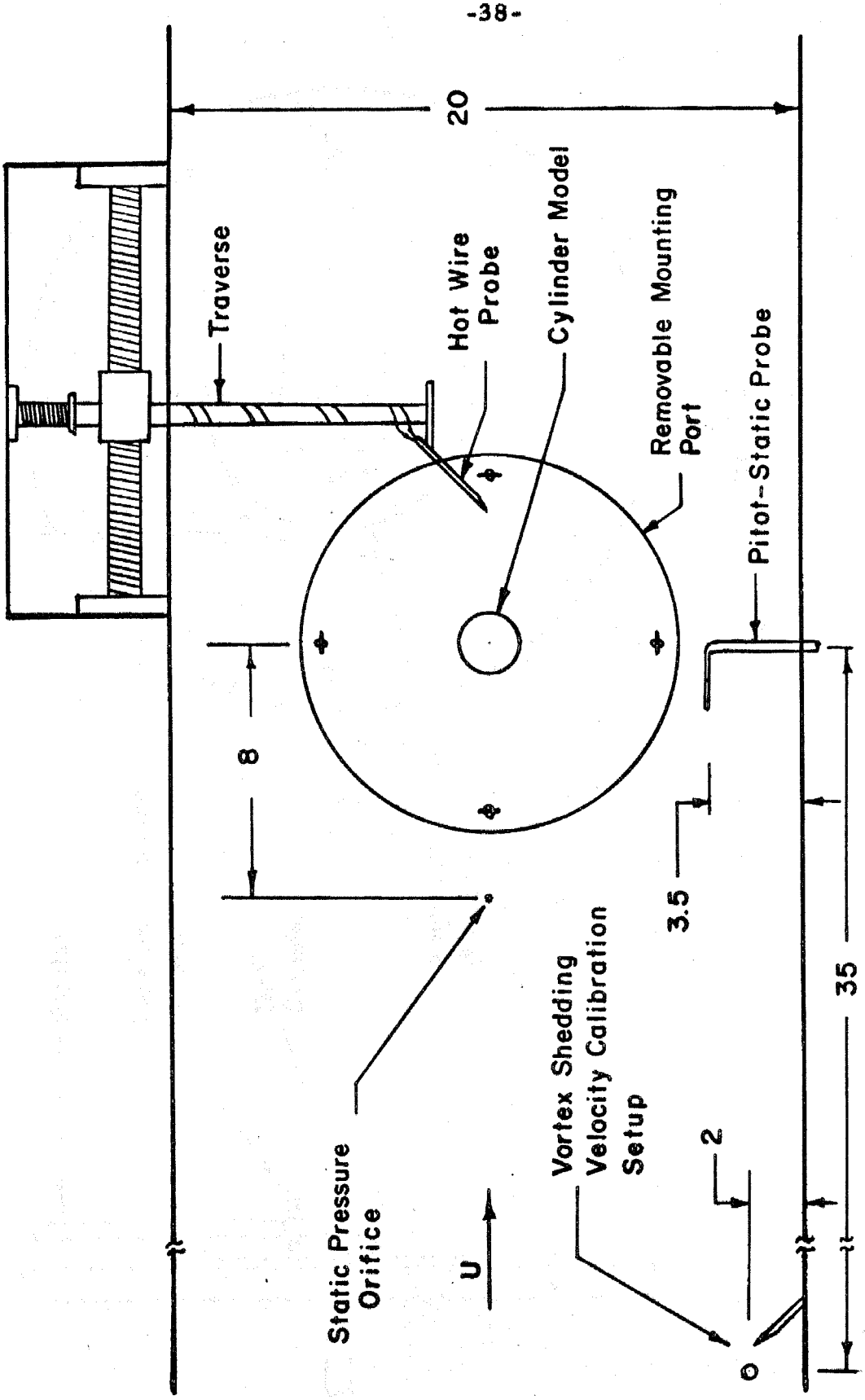

FIG.3 TEST SETUP IN THE LOW SPEED TUNNEL

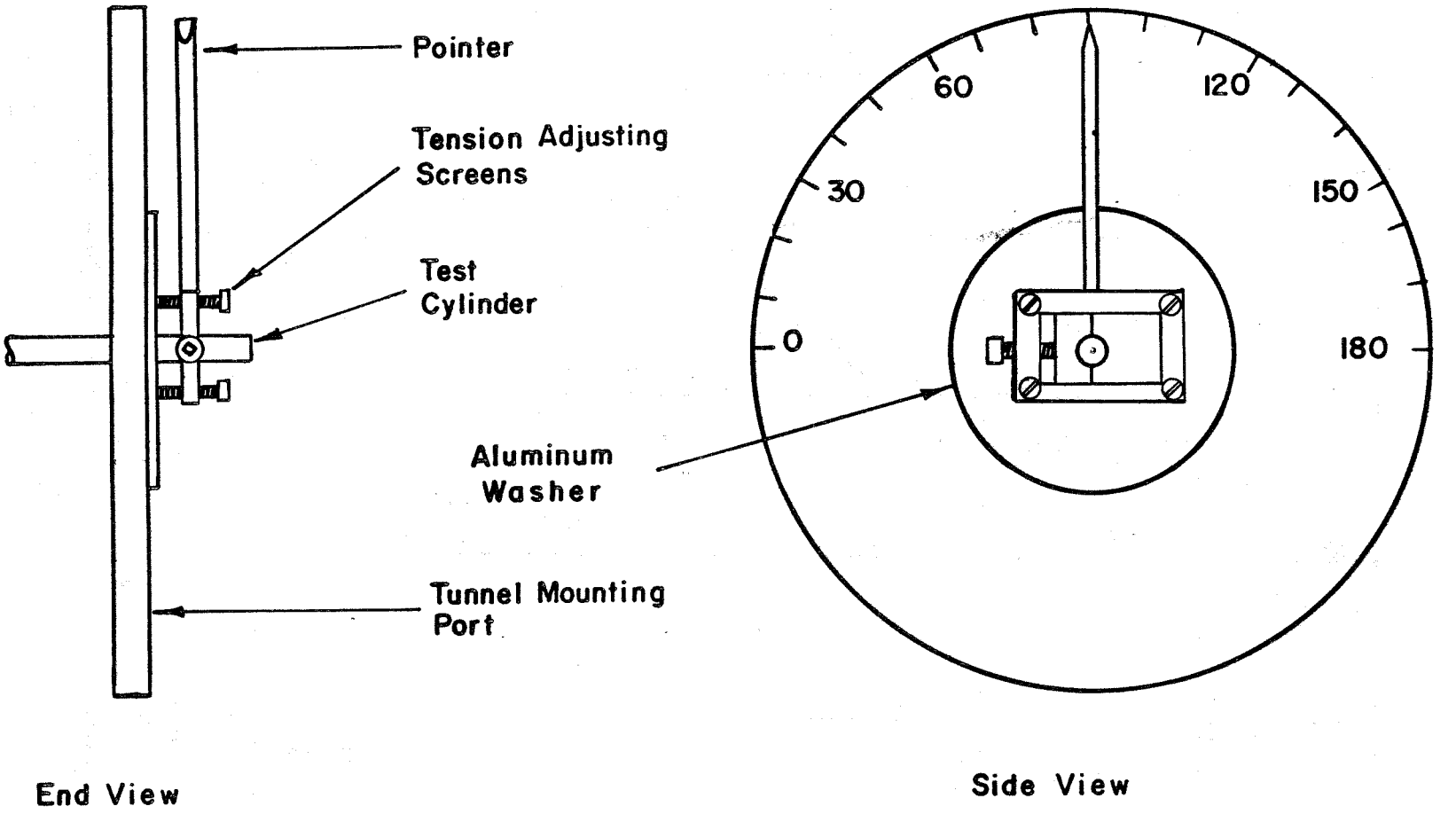

FIG. 4 CYLINDER POSITIONING BLOCK

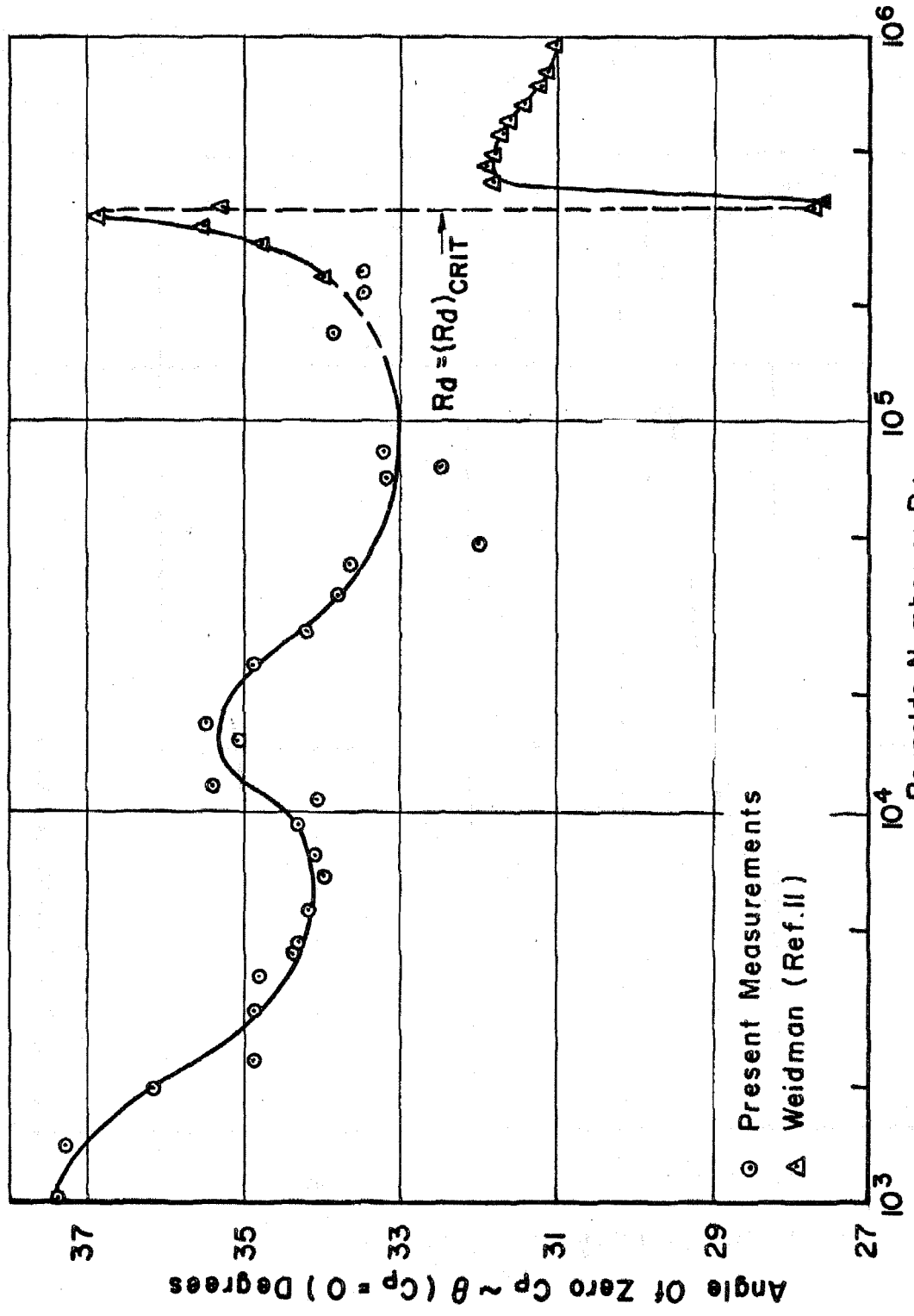

FIGURE 5 VARIATION OF ANGLE OF ZERO PRESSURE COEFFICIENT WITH REYNOLDS NUMBER

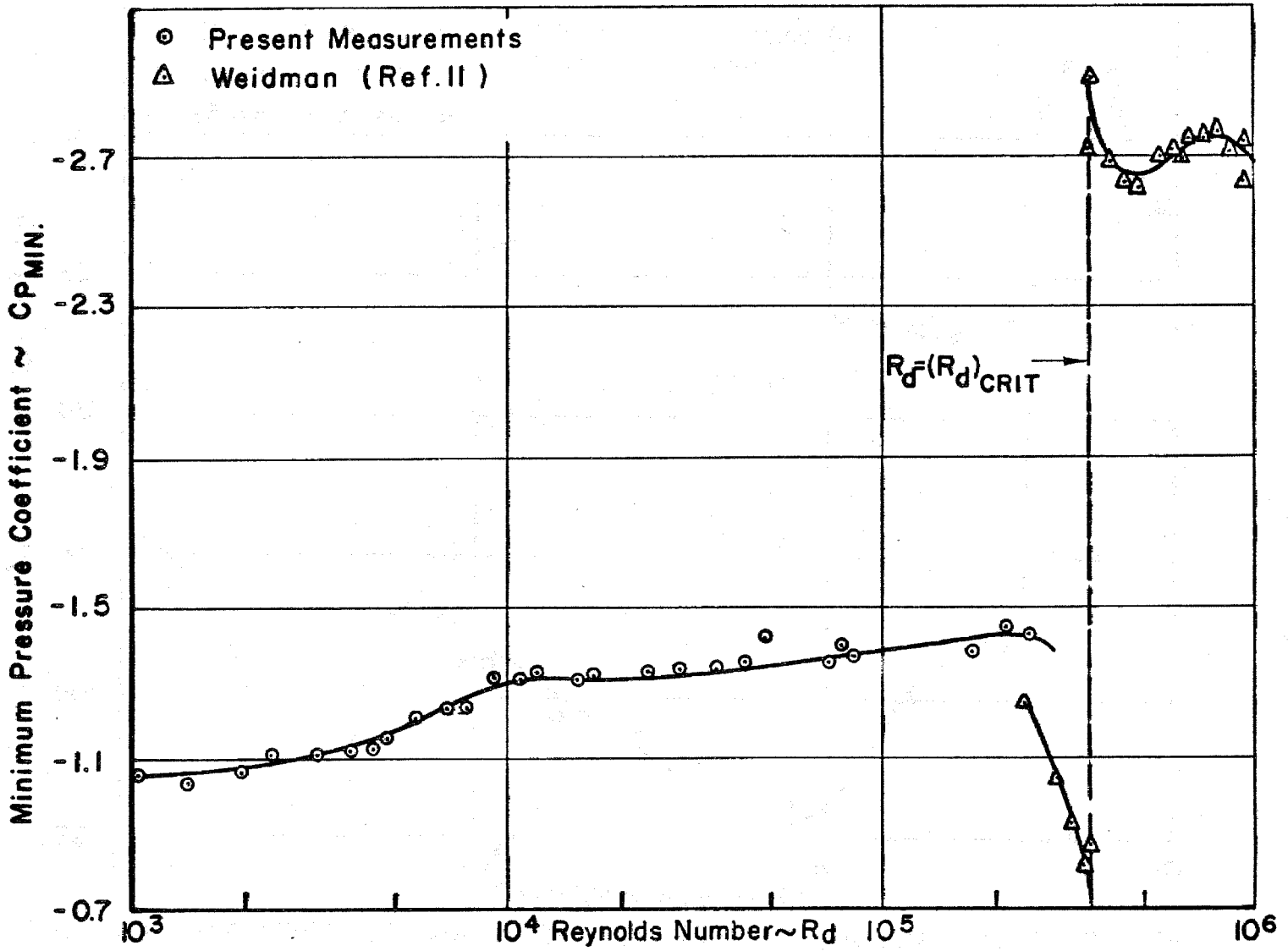

FIG. 6 VARIATION OF MINIMUM PRESSURE COEFFICIENT WITH REYNOLDS NUMBER

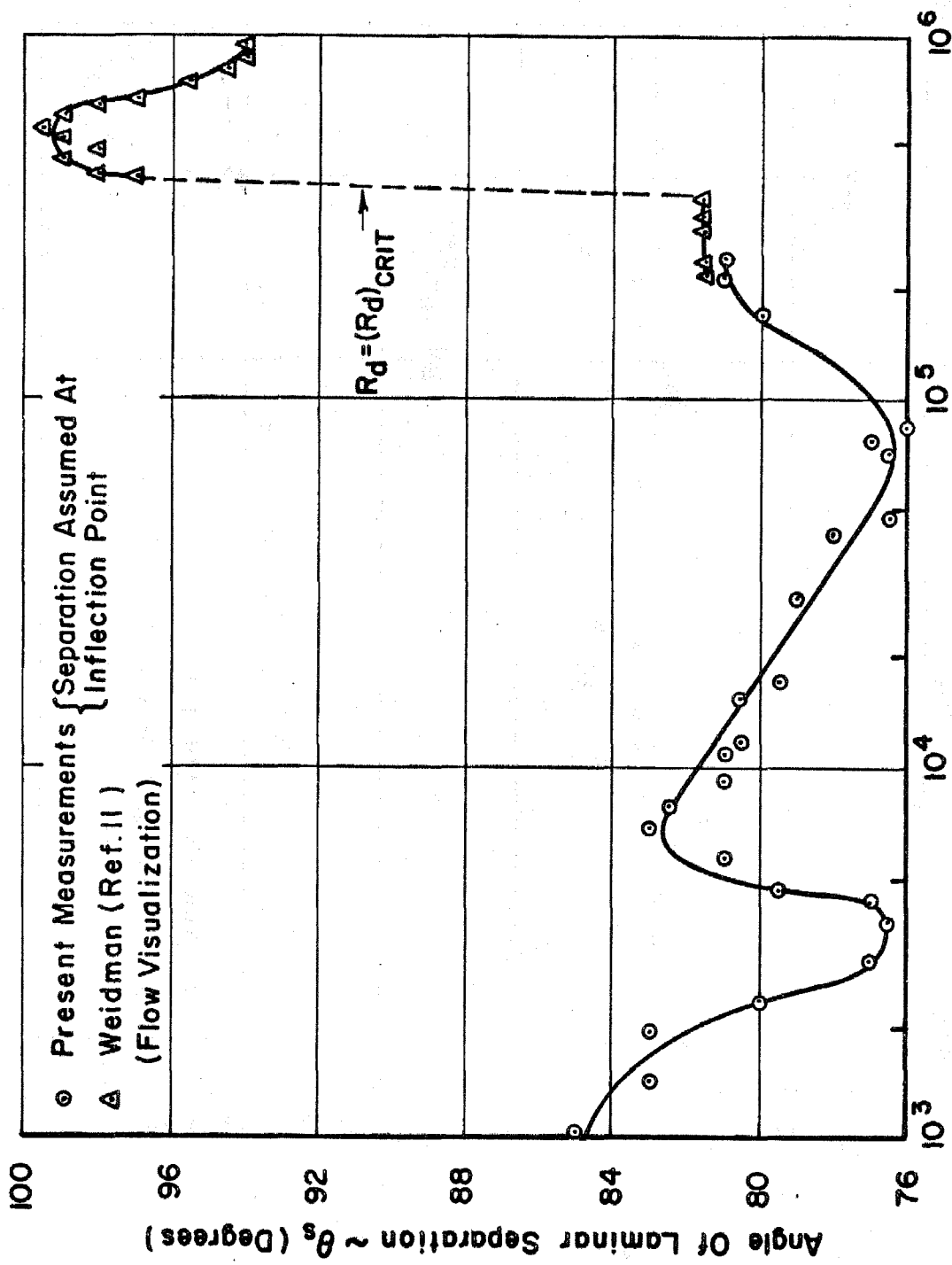

FIGURE 8 VARIATION OF ANGLE OF LAMINAR SEPARATION WITH REYNOLDS NUMBER

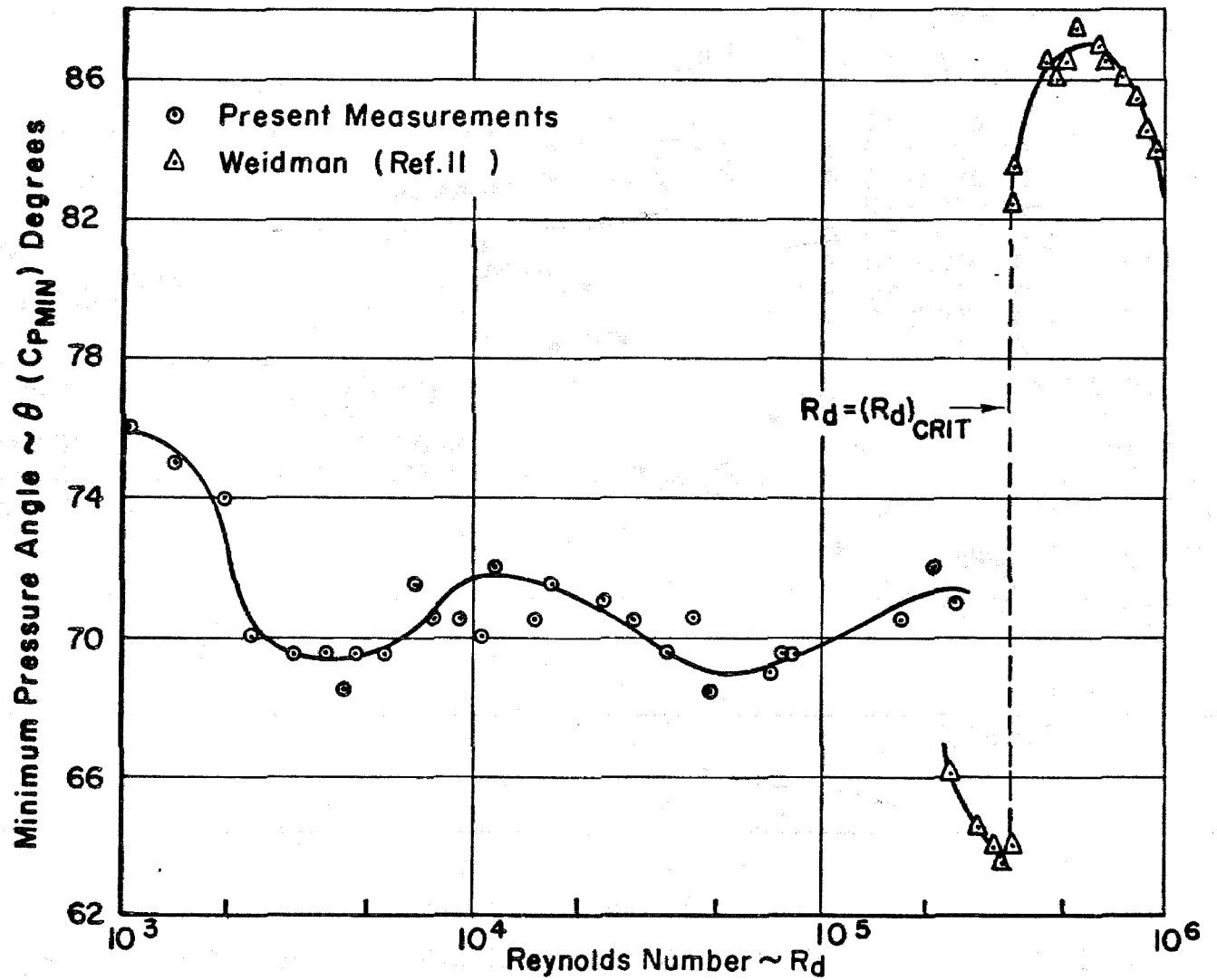

FIGURE 7 VARIATION OF ANGLE OF MINIMUM PRESSURE COEFFICIENT WITH REYNOLDS NUMBER

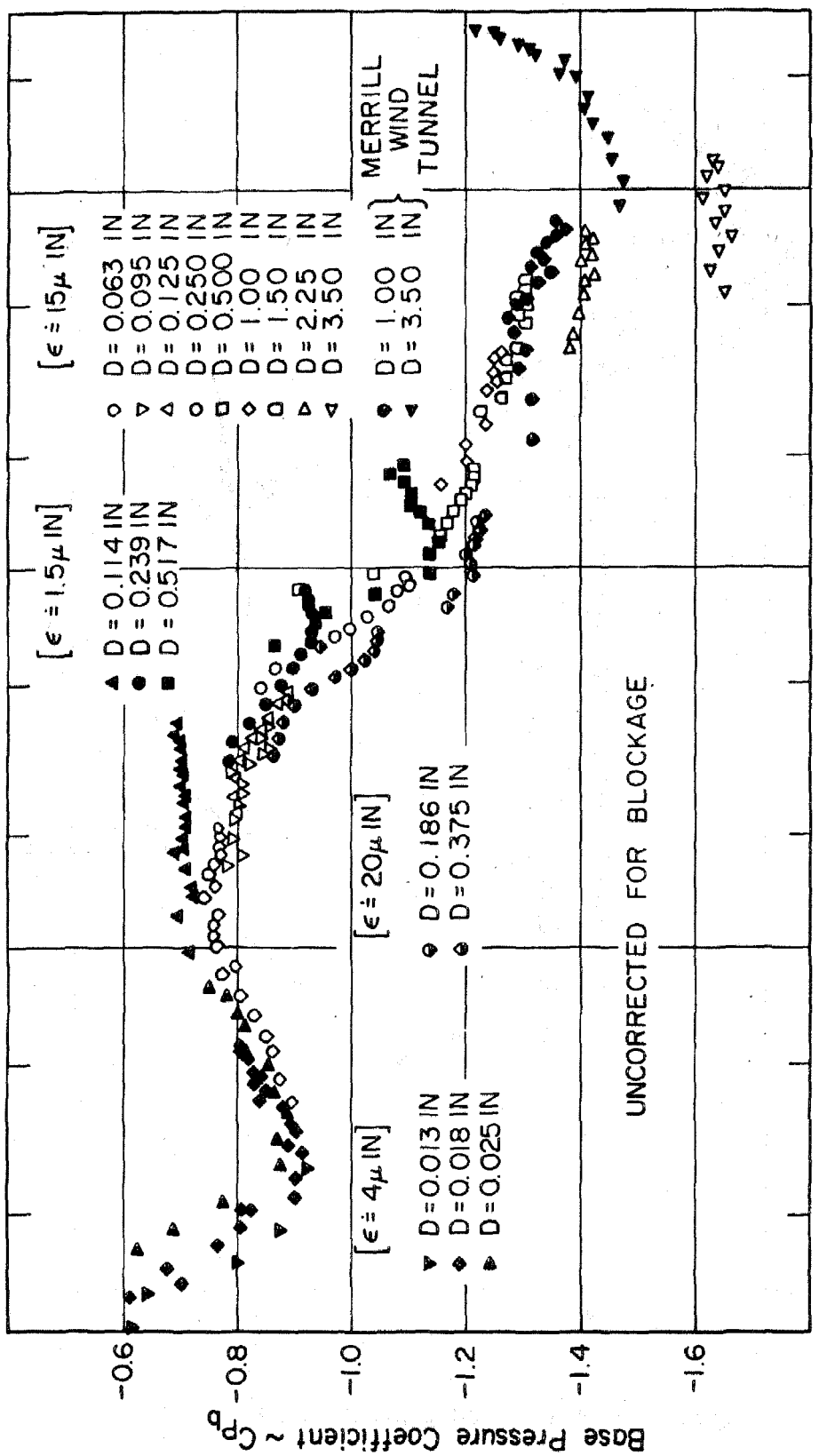

FIGURE 9 BASE PRESSURE COEFFICIENT AS A FUNCTION OF REYNOLDS NUMBER

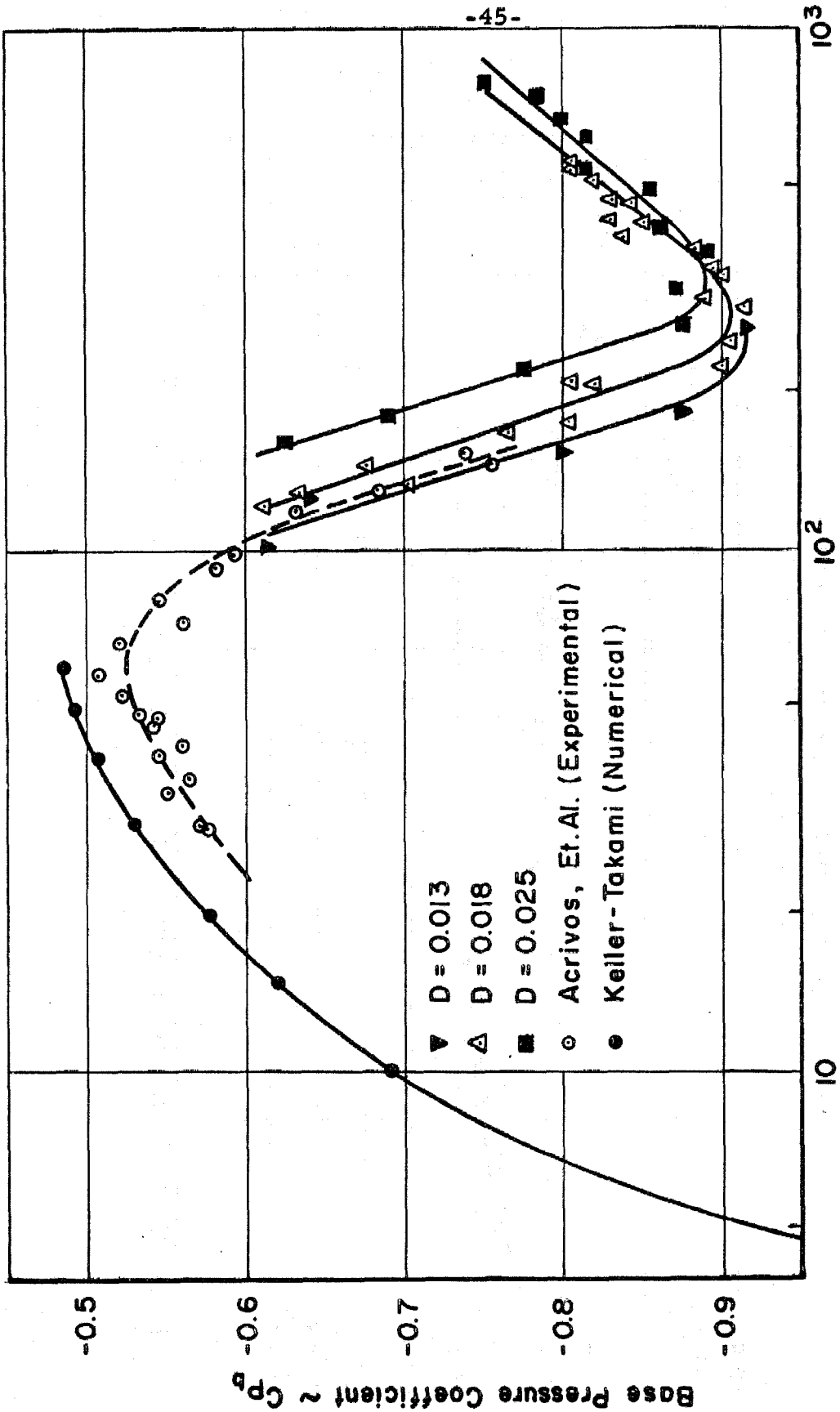

FIGURE 10 BASE PRESSURE COEFFICIENTS AT LOW REYNOLDS NUMBERS

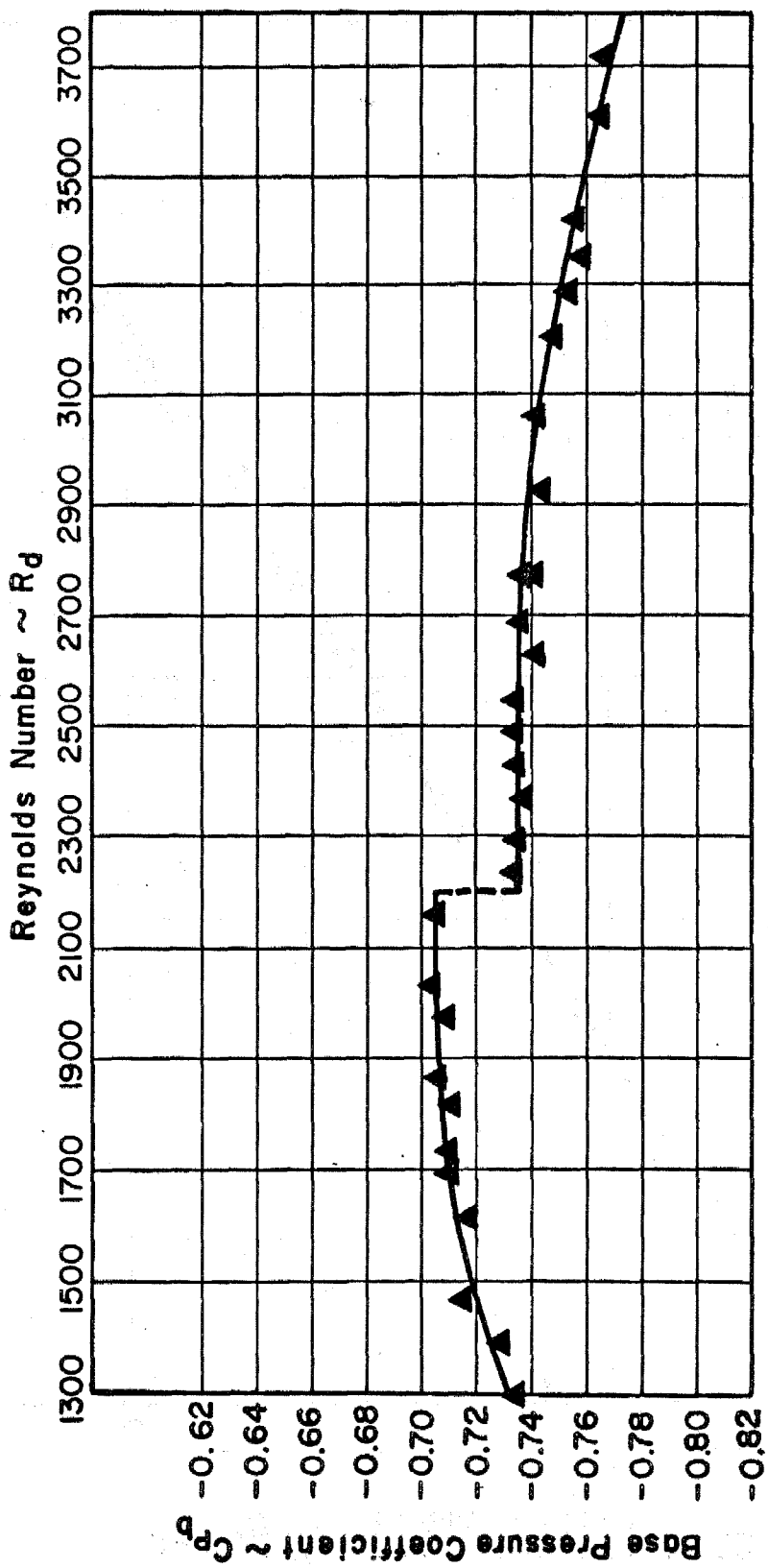

FIGURE II BASE PRESSURES FOR 0.125 IN. CYLINDER ACROSS NOTED "TRANSITION" POINT

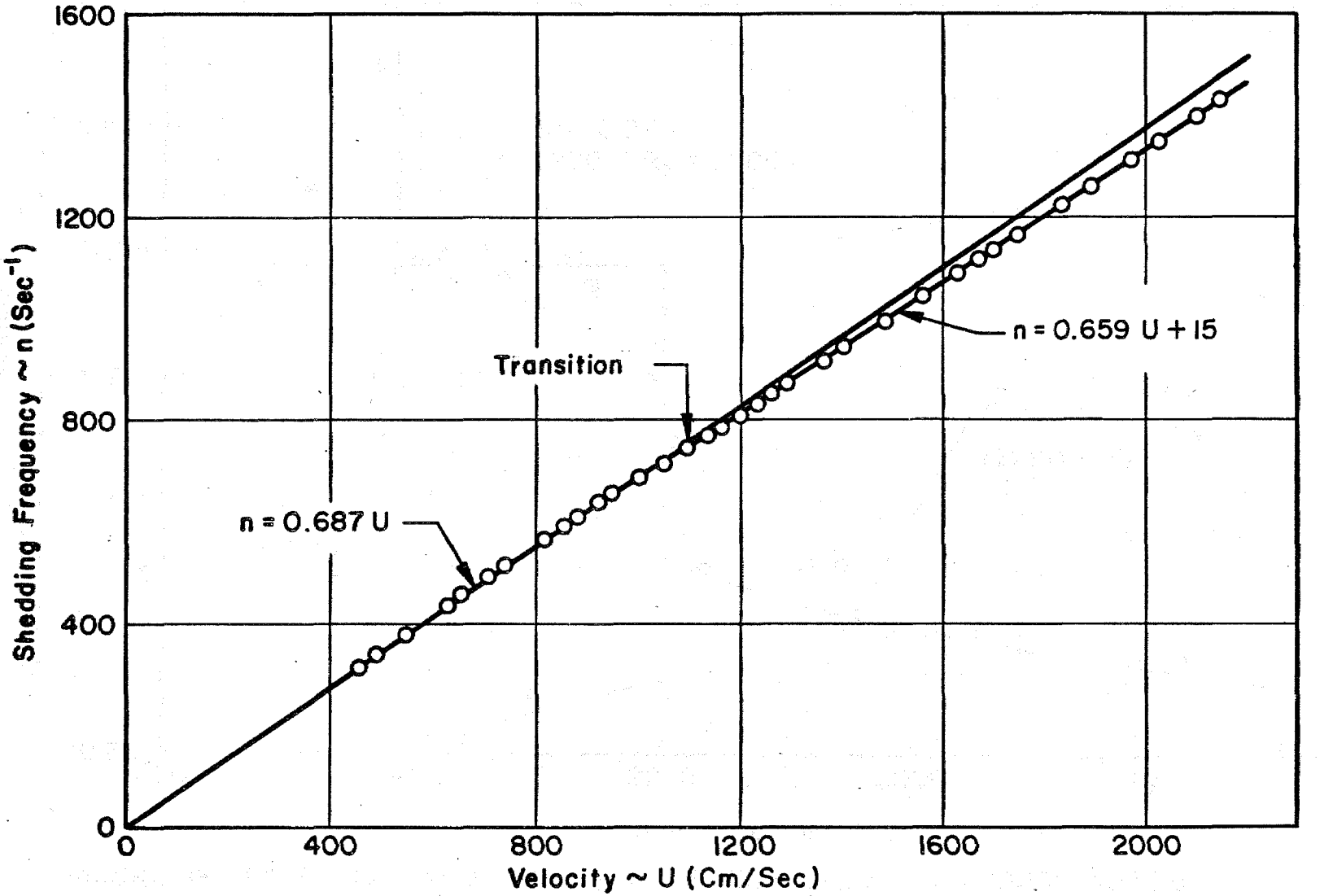

FIGURE 12 SHEDDING FREQUENCY AS A FUNCTION OF VELOCITY FOR 0.125 IN. CYLINDER ACROSS NOTED "TRANSITION" POINT

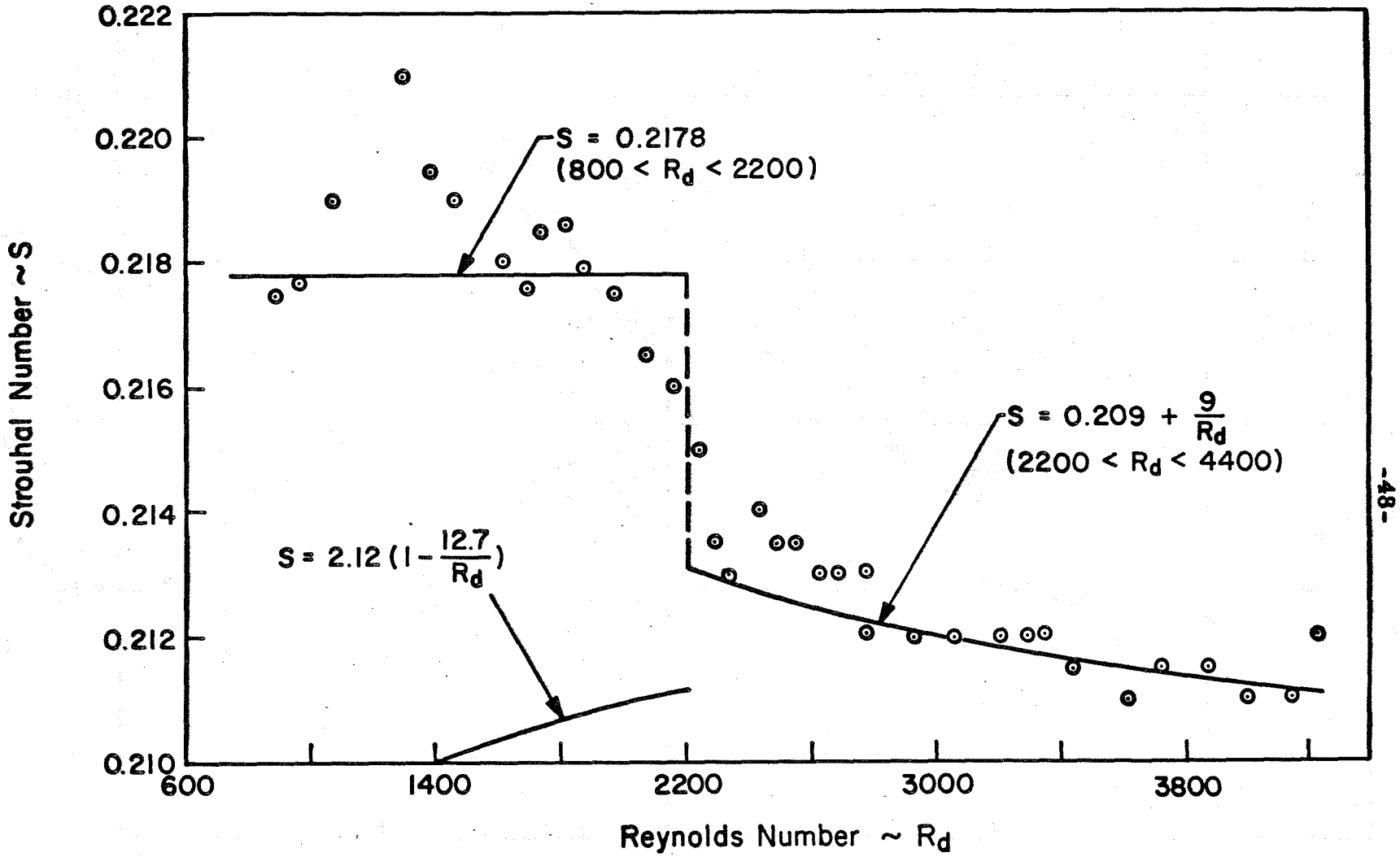

FIGURE 13 STROUHAL NUMBER FOR 0.125 INCH CYLINDER ACROSS NOTED "TRANSITION" POINT

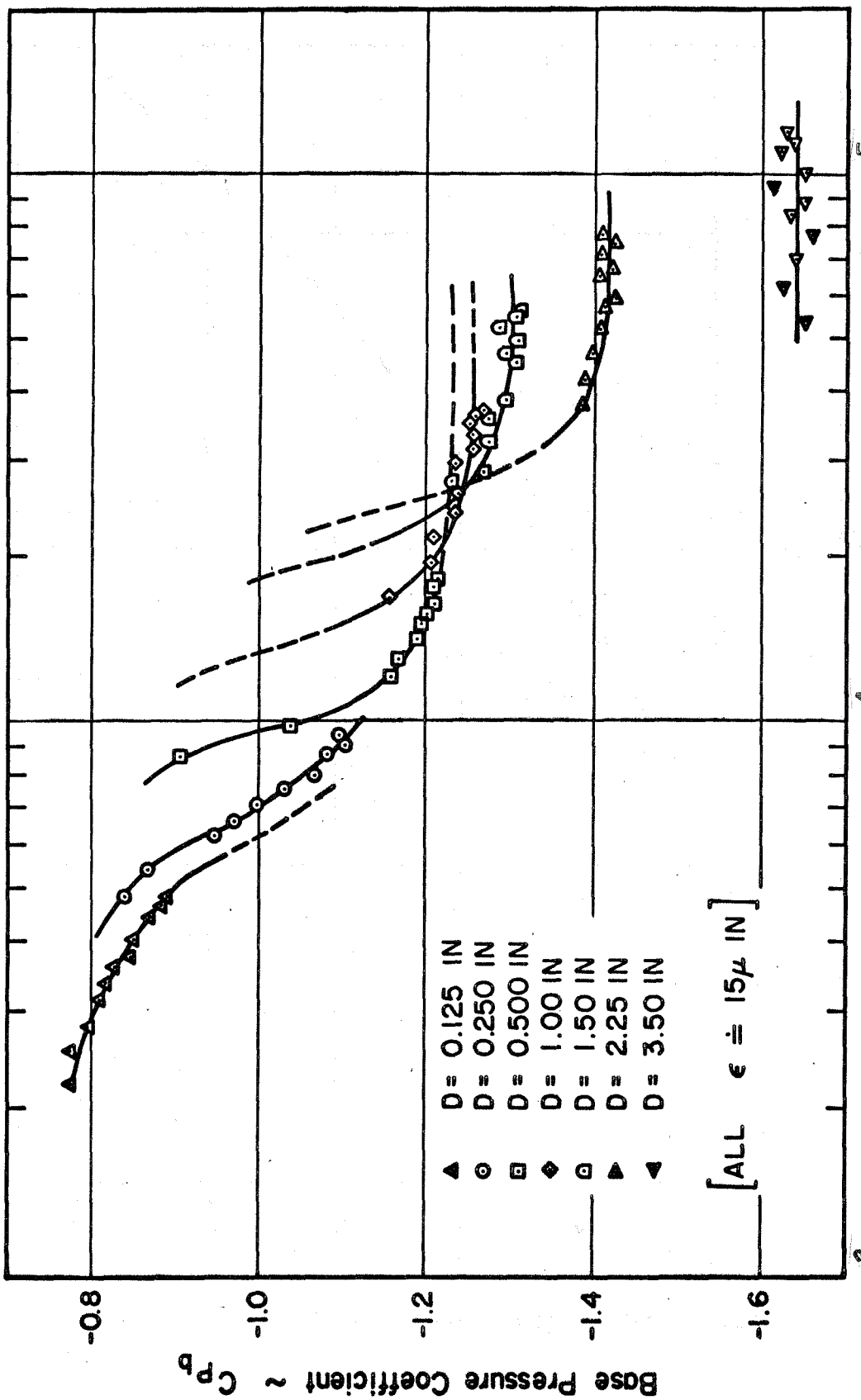

FIGURE 14 BASE PRESSURE COEFFICIENTS AT HIGH REYNOLDS NUMBERS

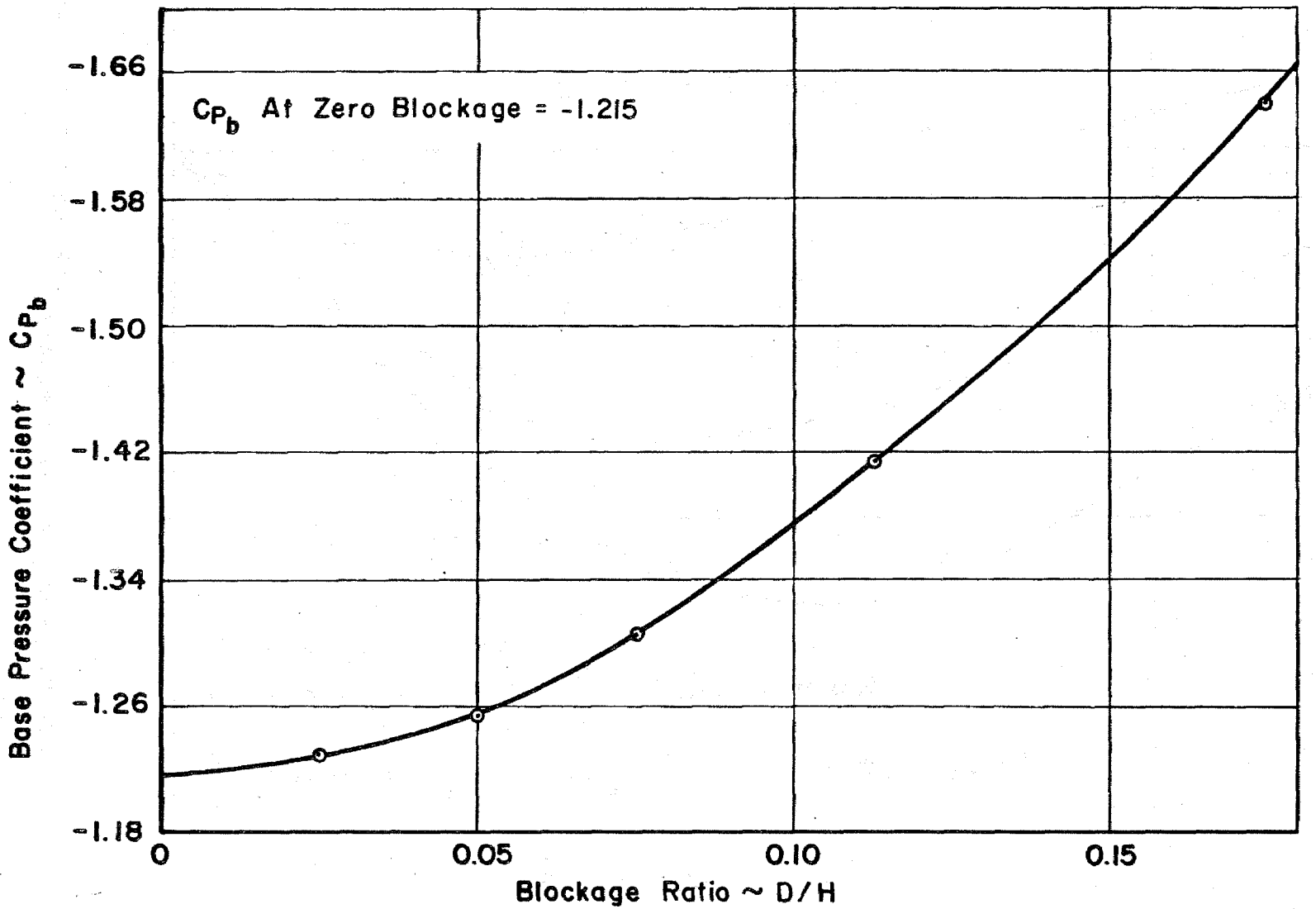

FIG.15 VARIATION OF THE BASE PRESSURE COEFFICIENT WITH BLOCKAGE RATIO

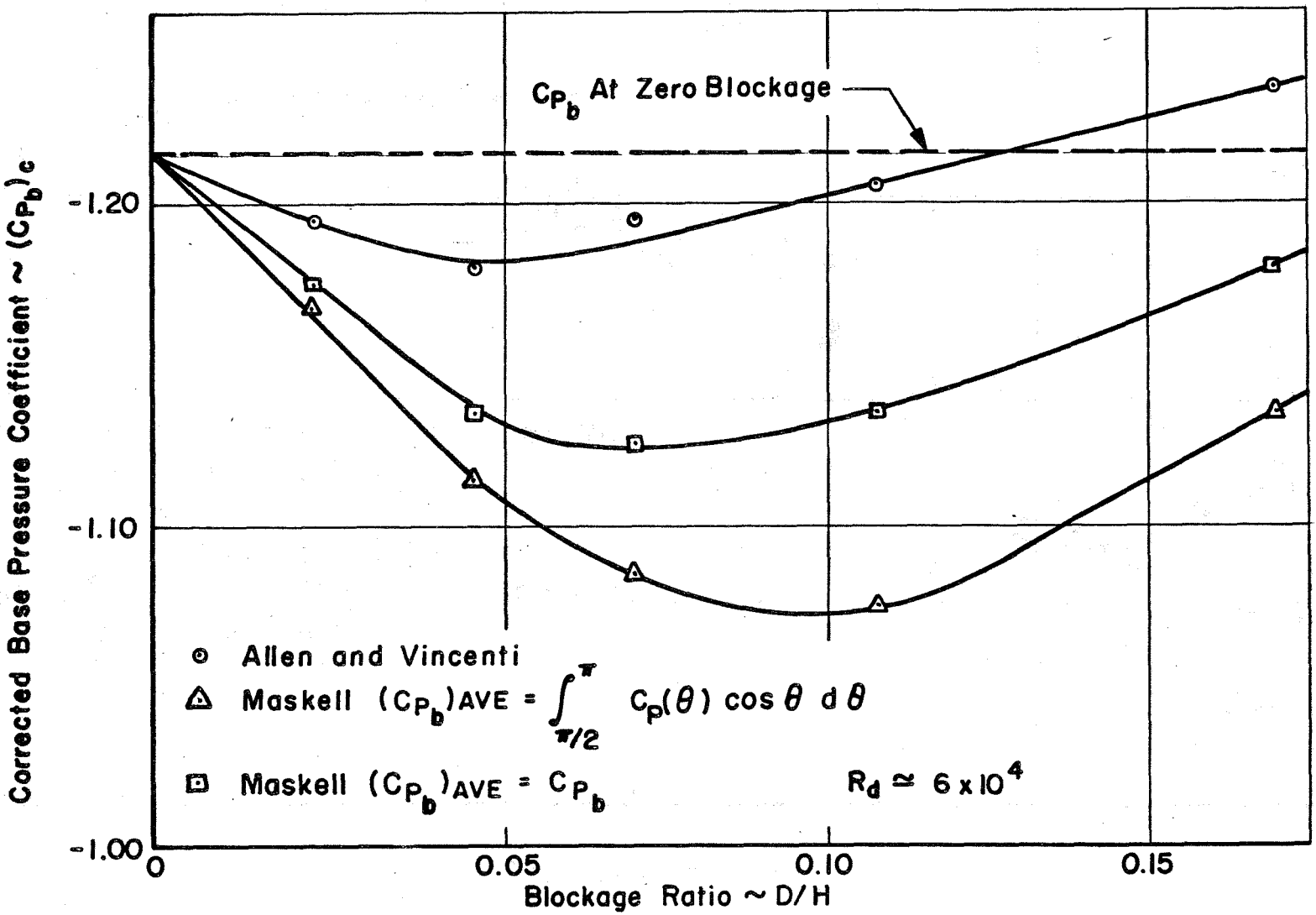

FIG. 16 A COMPARISON OF MASKELL'S AND ALLEN AND VINCENTI'S BLOCKAGE CORRECTIONS

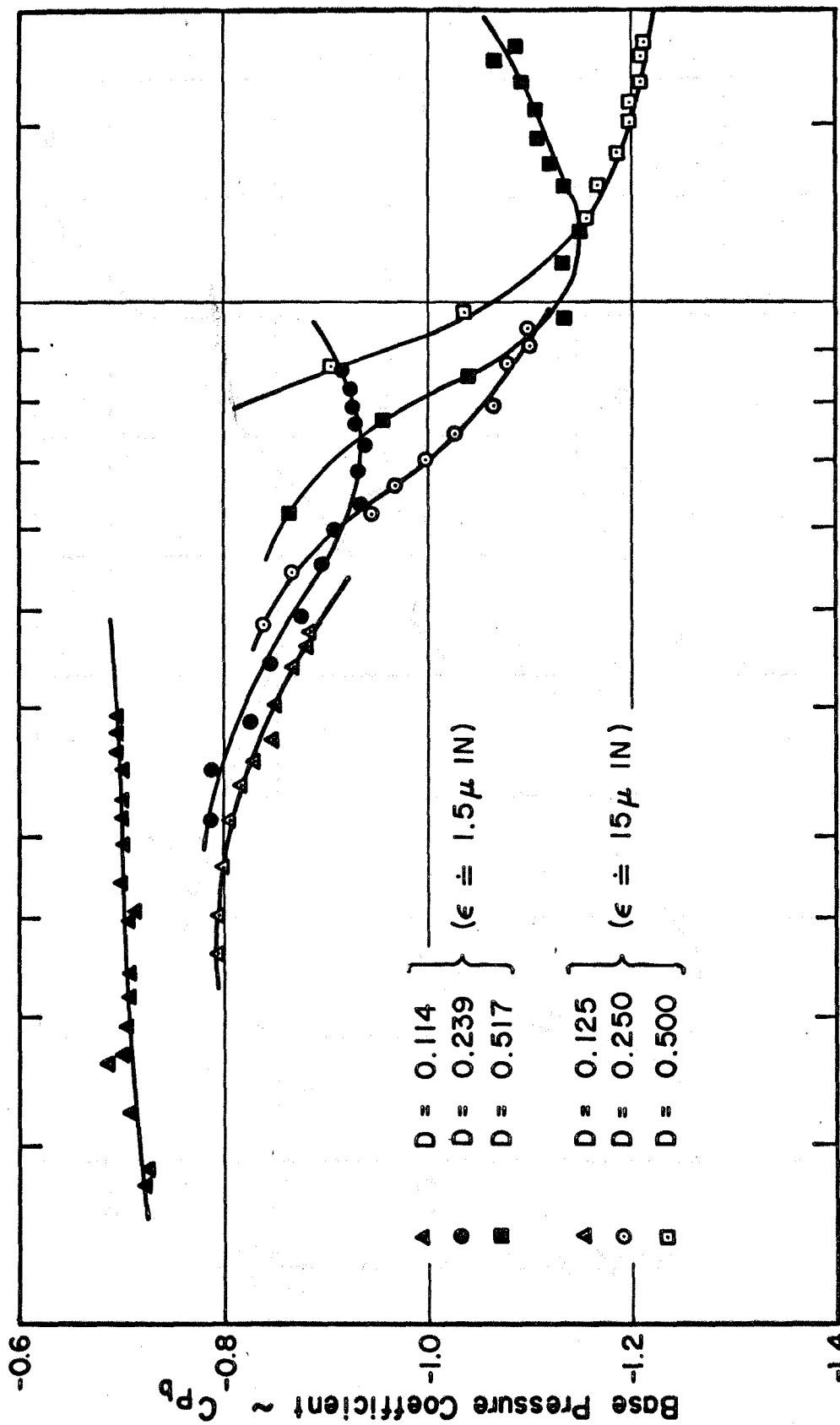

FIGURE 17 SURFACE ROUGHNESS EFFECTS ON THE BASE PRESSURE COEFFICIENT

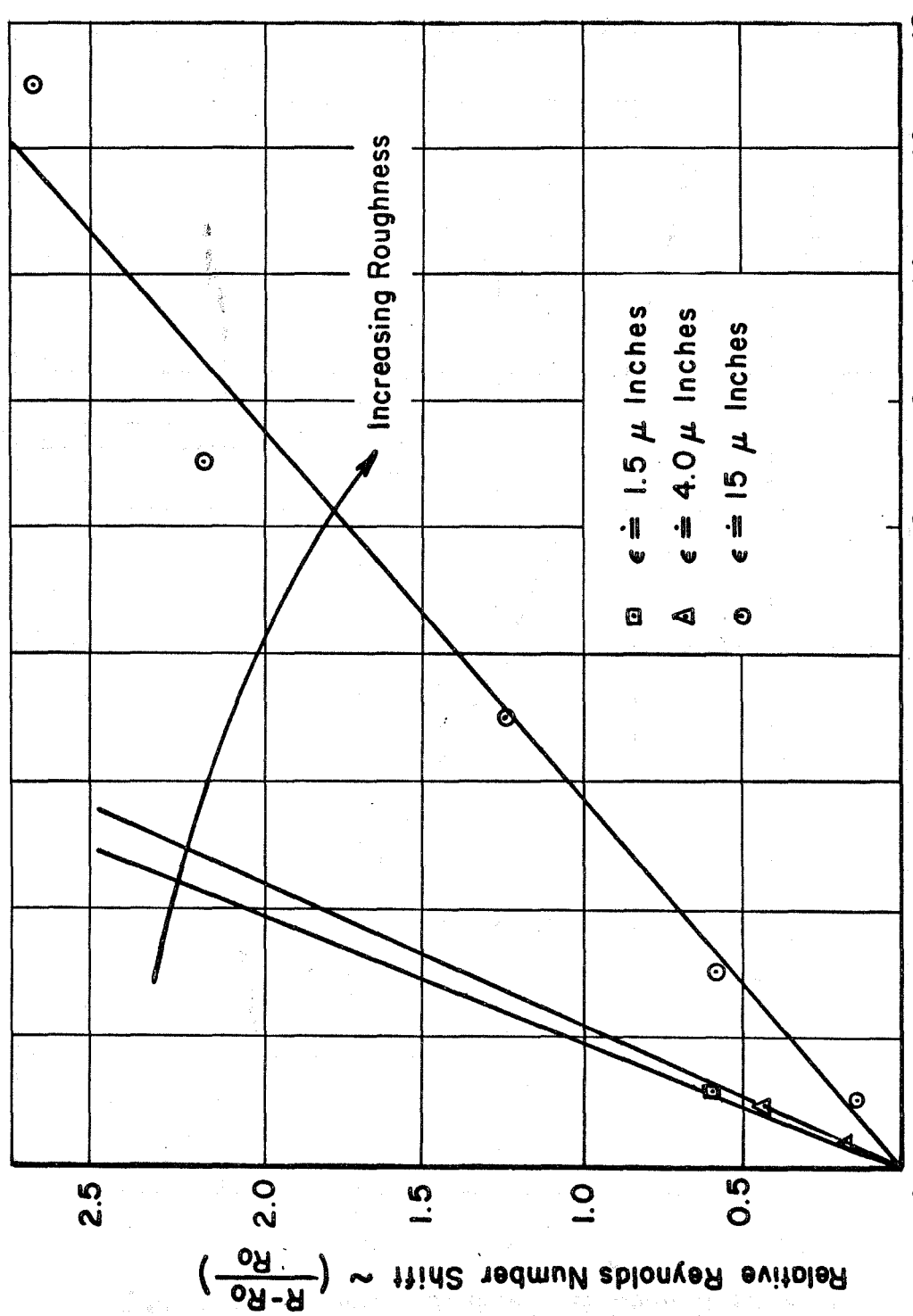

FIG. 18 REYNOLDS NUMBER SHIFT VS. DIAMETER SHIFT WITH SURFACE ROUGHNESS AS A PARAMETER

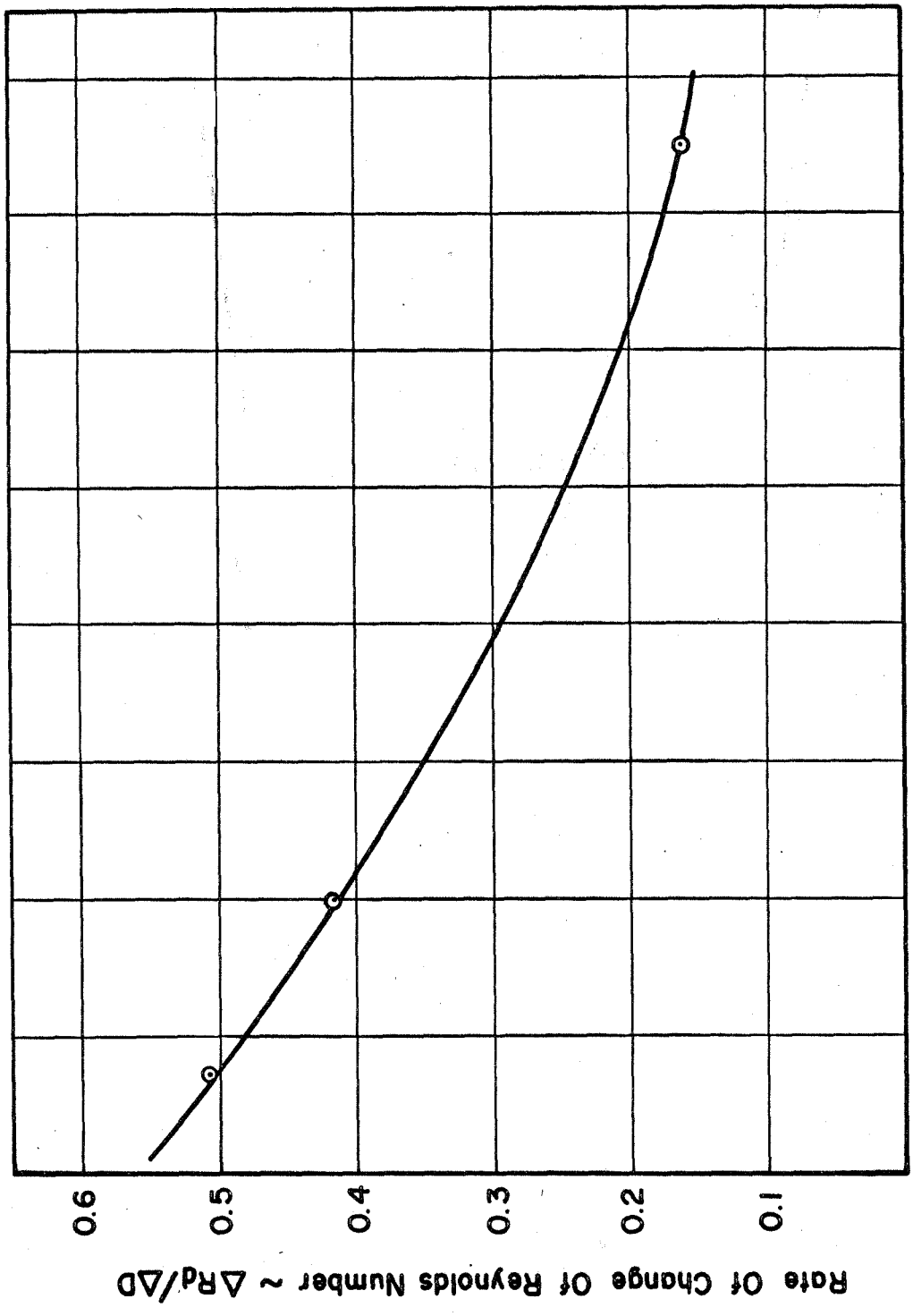

FIG.19 RATE OF CHANGE OF REYNOLDS NUMBER SHIFT AS A FUNCTION OF SURFACE ROUGHNESS

APPENDIX I

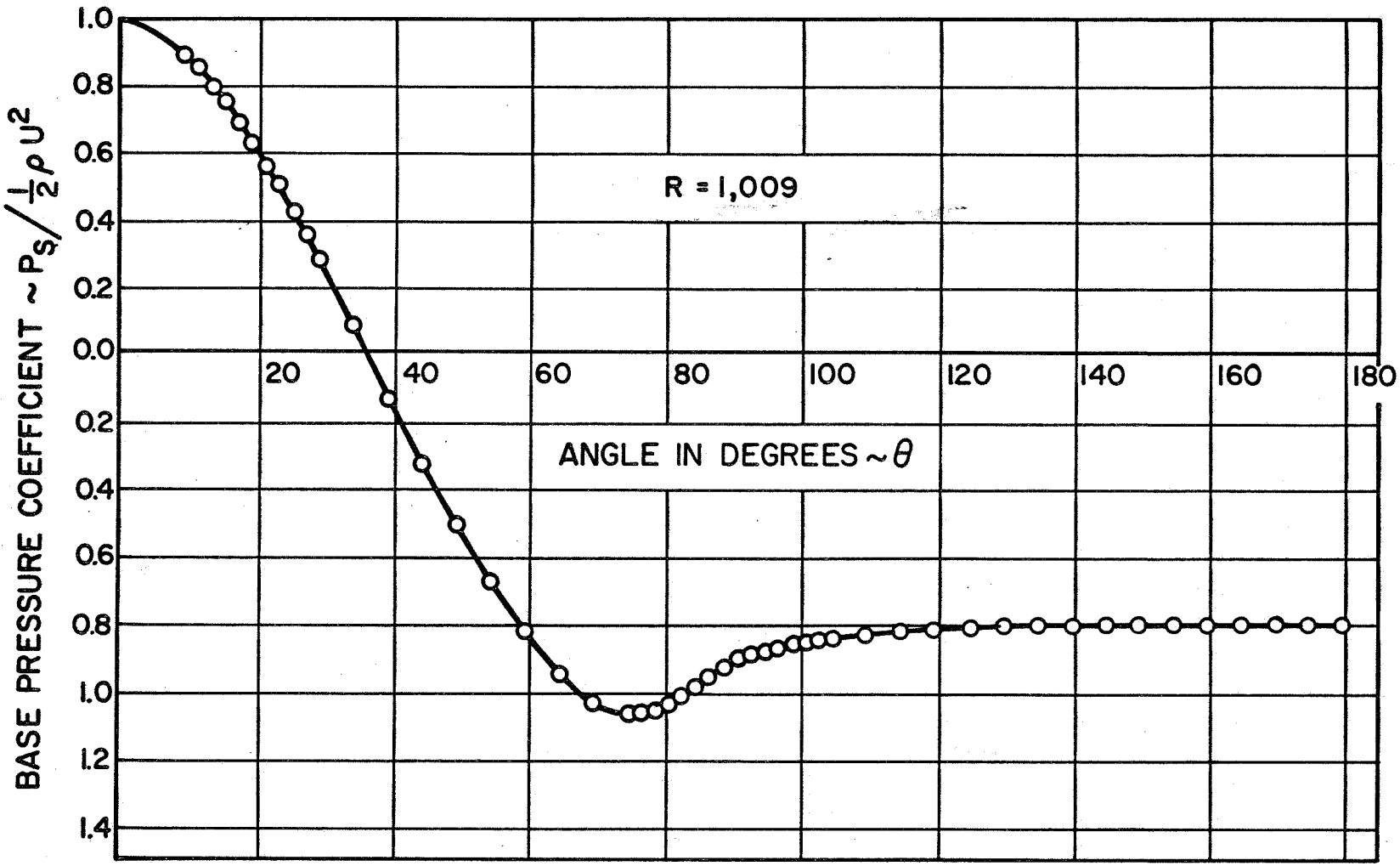

FIGURE 20 PRESSURE DISTRIBUTION OVER CIRCULAR CYLINDER, R = 1,009, D = 0.0625 IN.

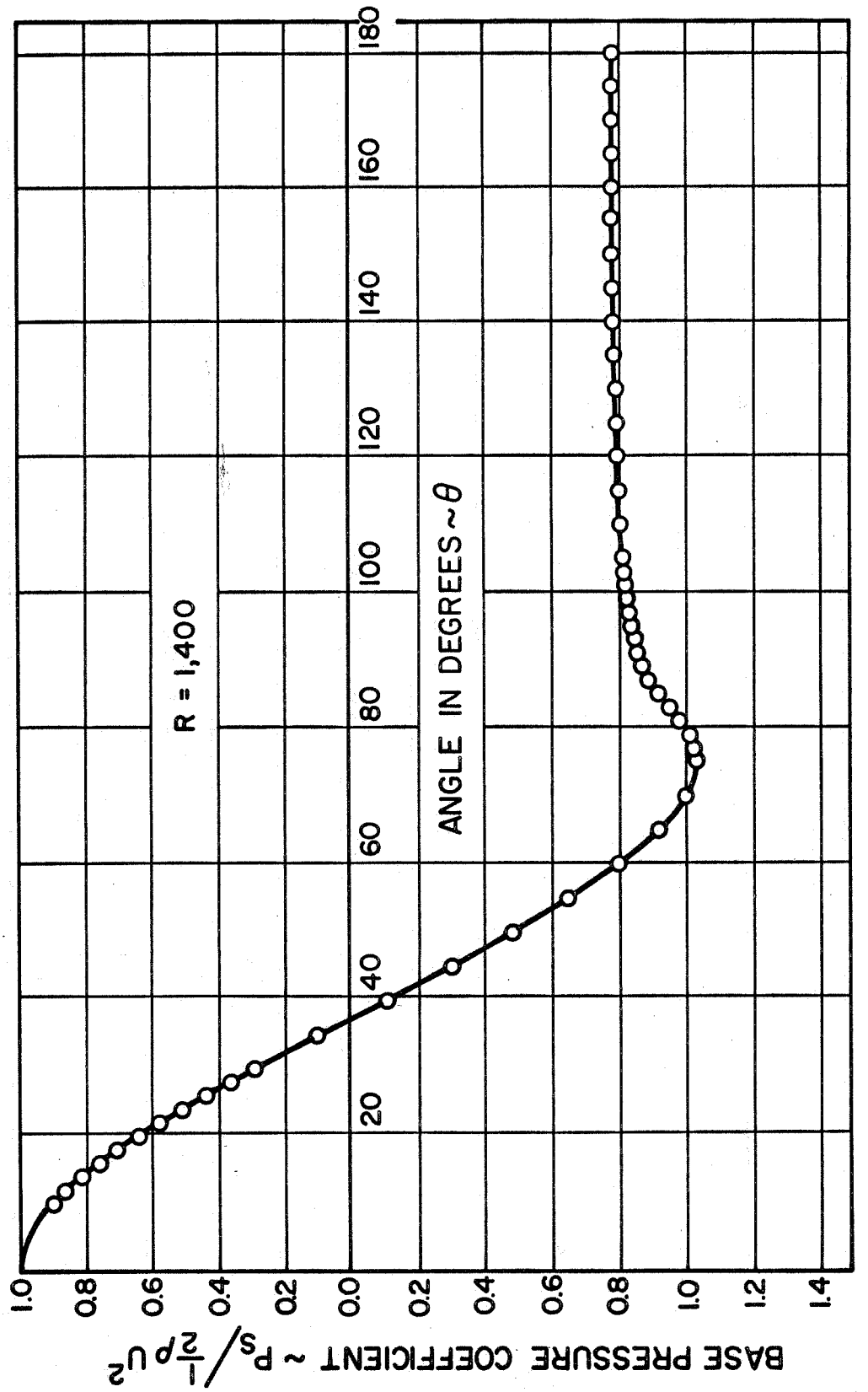

FIGURE 21 PRESSURE DISTRIBUTION OVER CIRCULAR CYLINDER, R = 1,400, D = 0.0625 IN.

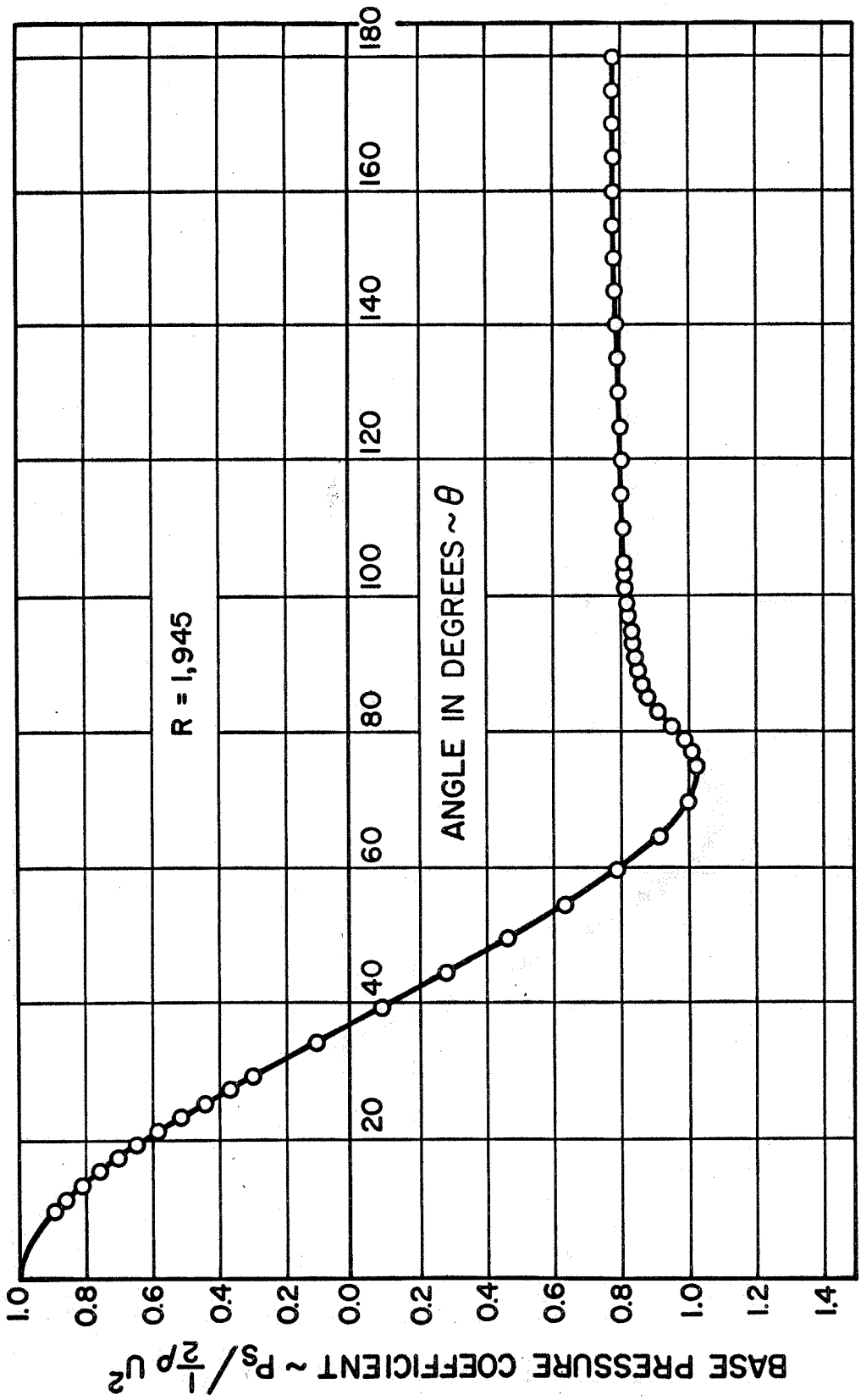

FIGURE 22 PRESSURE DISTRIBUTION OVER CIRCULAR CYLINDER, R = 1,945, D = 0.0625 IN.

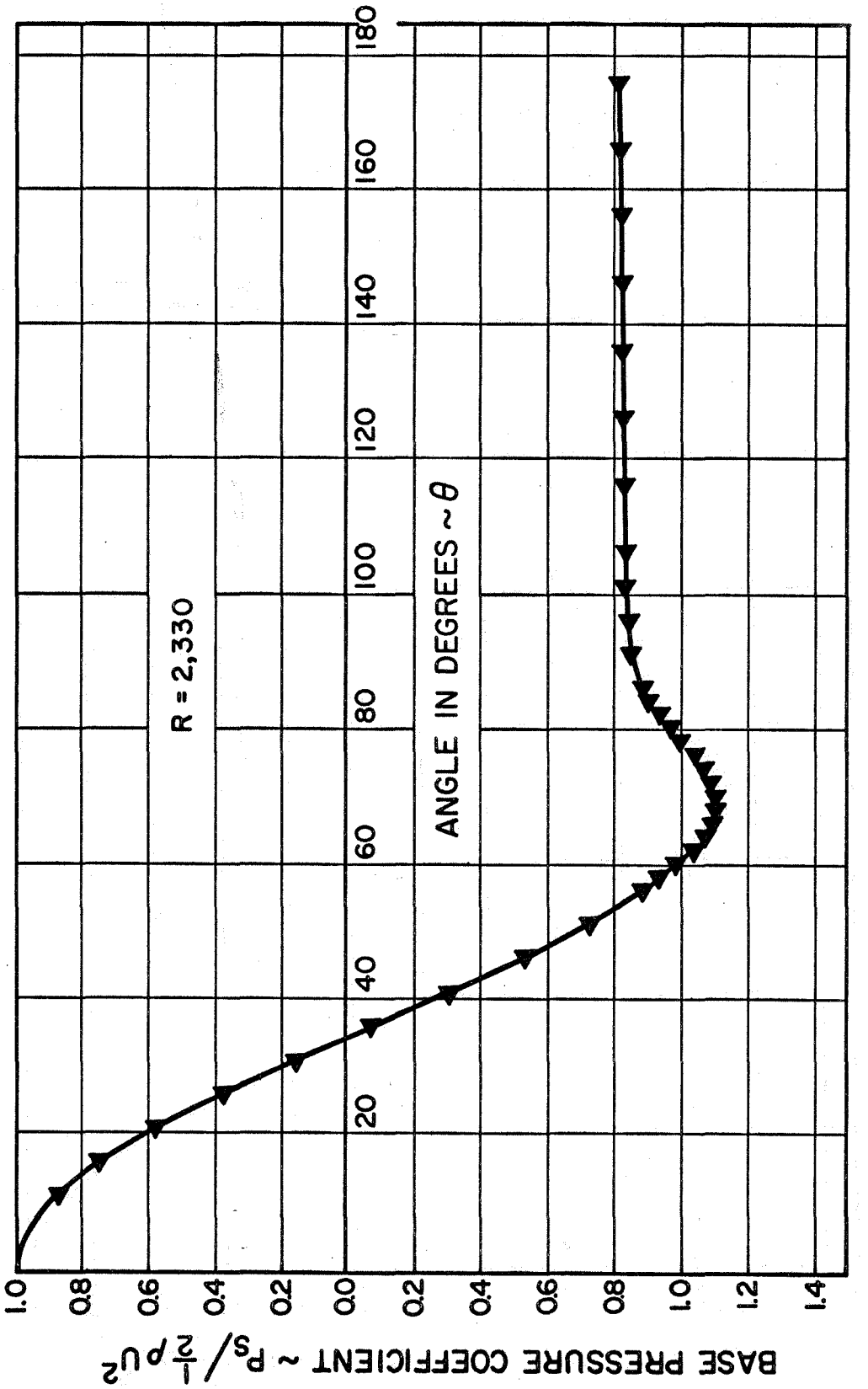

FIGURE23 PRESSURE DISTRIBUTION OVER CIRCULAR CYLINDER, R = 2,330, D = 0.125 IN.

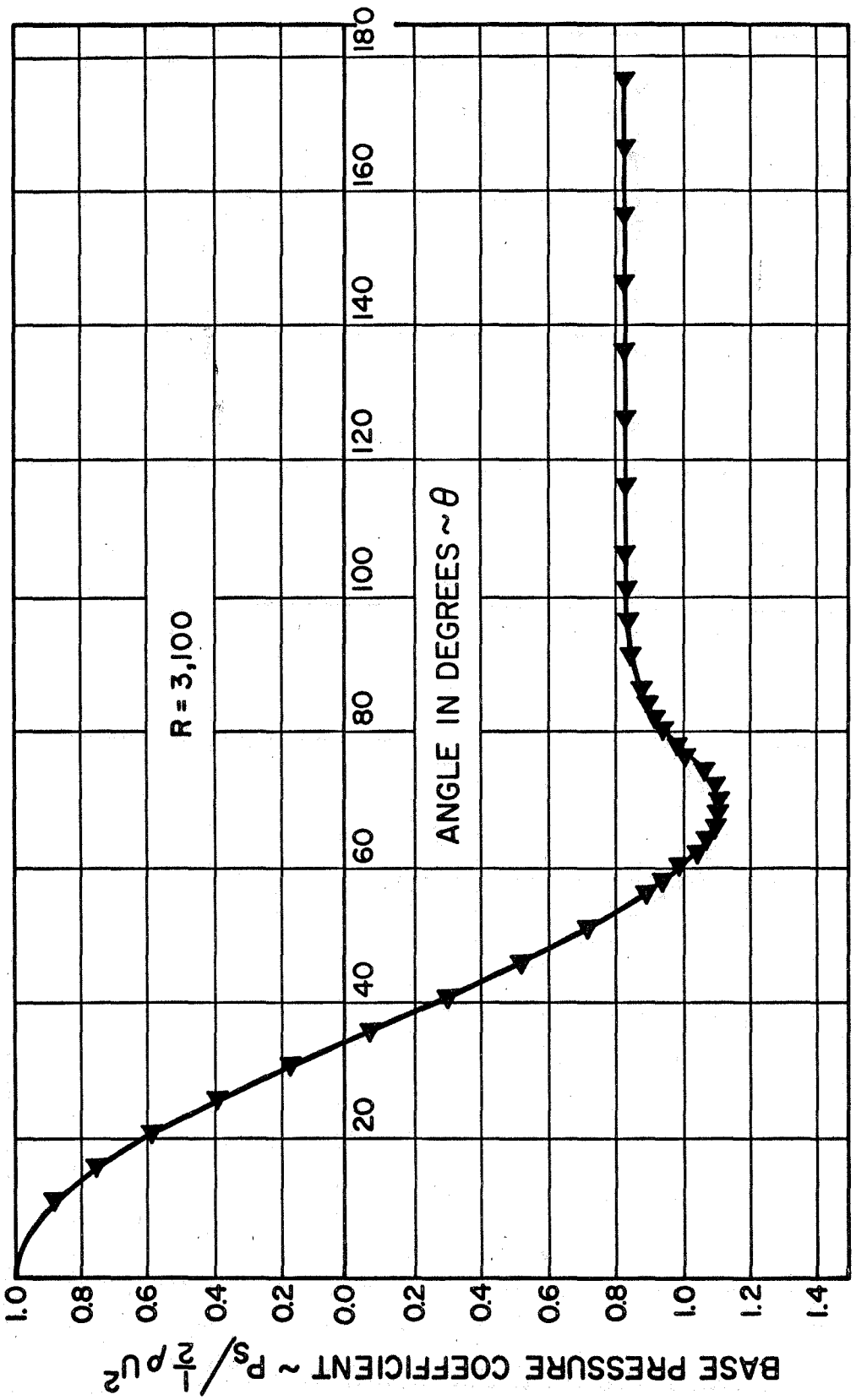

FIGURE 24 PRESSURE DISTRIBUTION OVER CIRCULAR CYLINDER, R = 3,100, D = 0.125 IN.

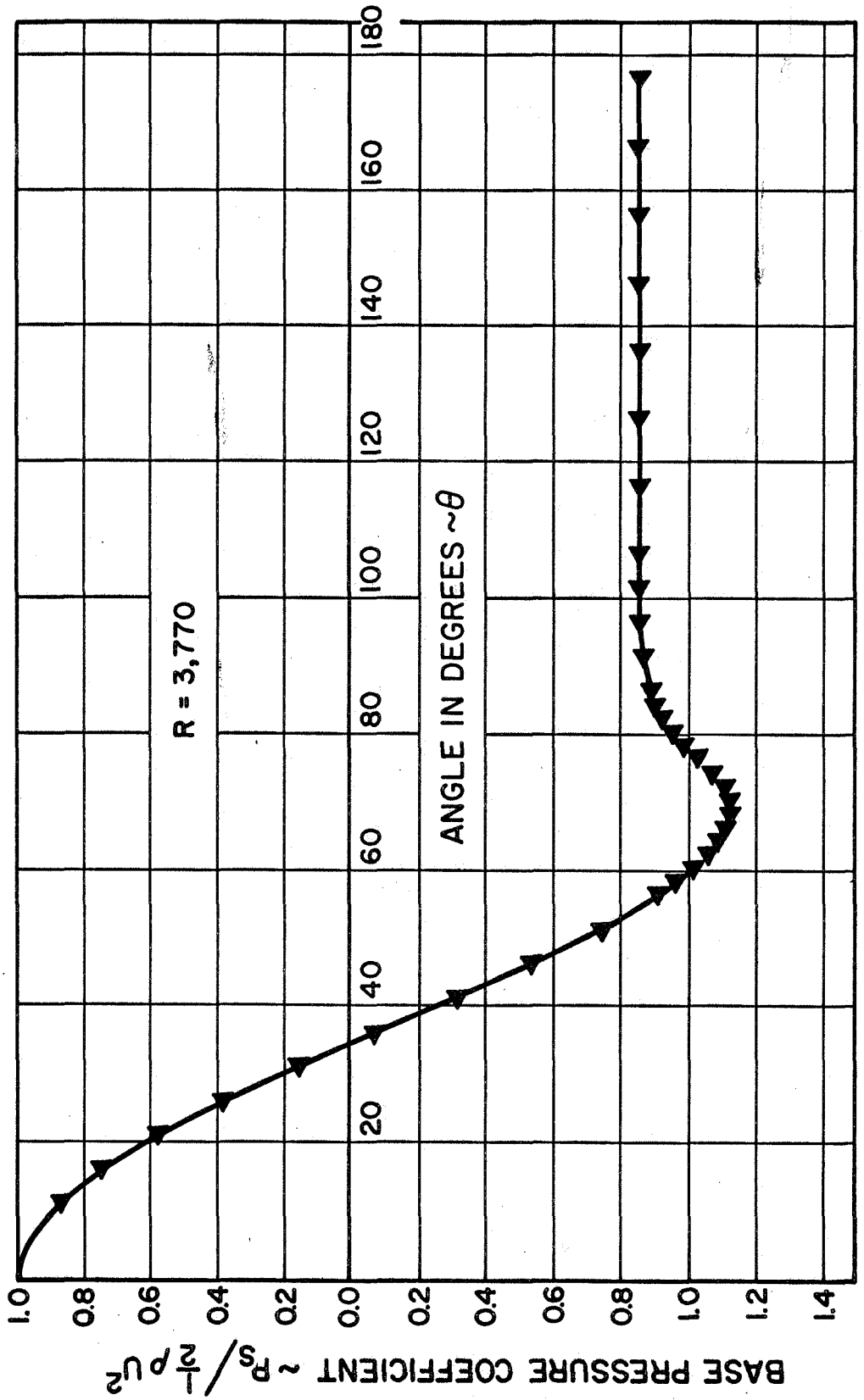

FIGURE25 PRESSURE DISTRIBUTION OVER CIRCULAR CYLINDER, R = 3,770, D = 0.125 IN.

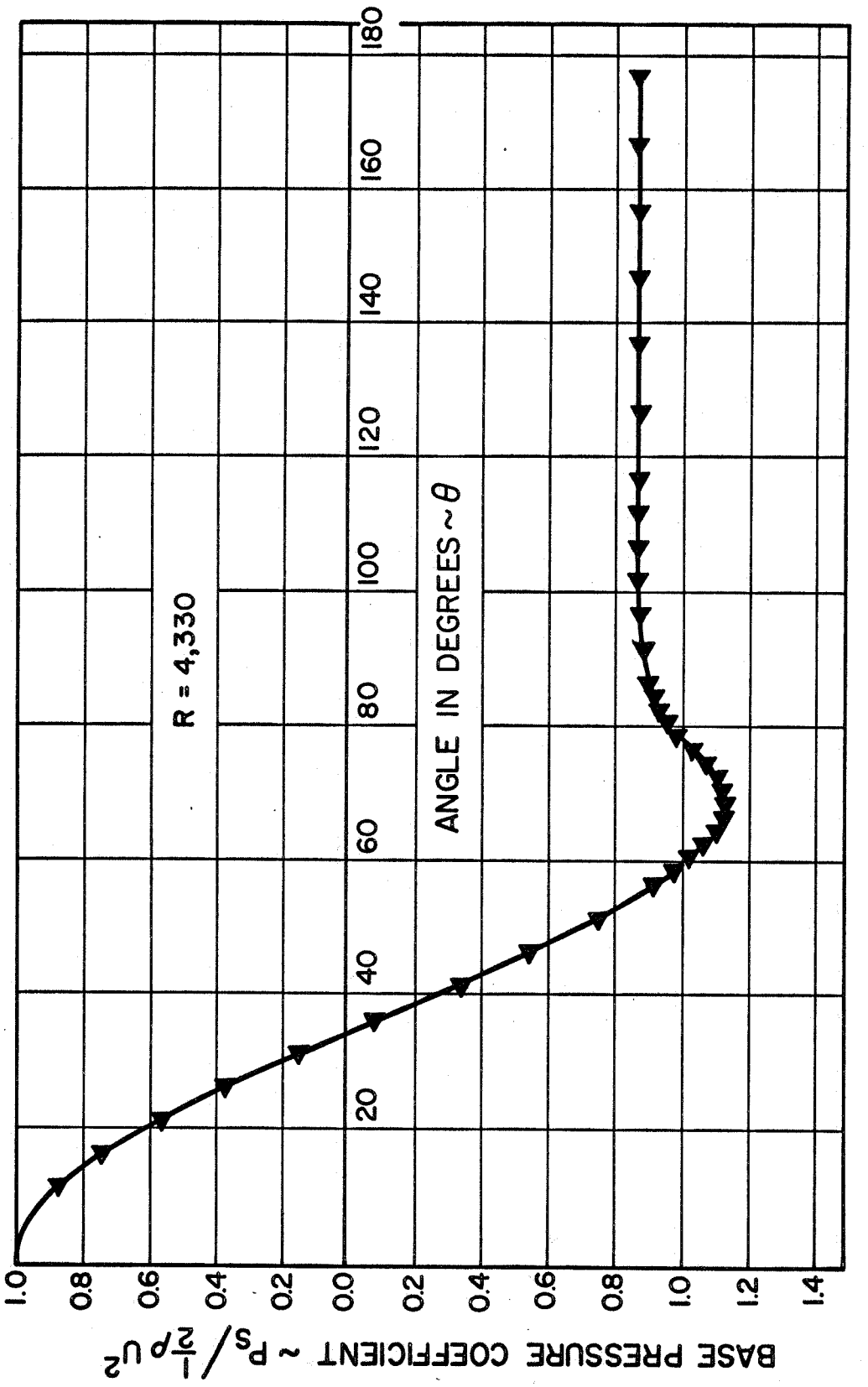

FIGURE 26 PRESSURE DISTRIBUTION OVER CIRCULAR CYLINDER, R = 4,330, D = 0.125 IN.

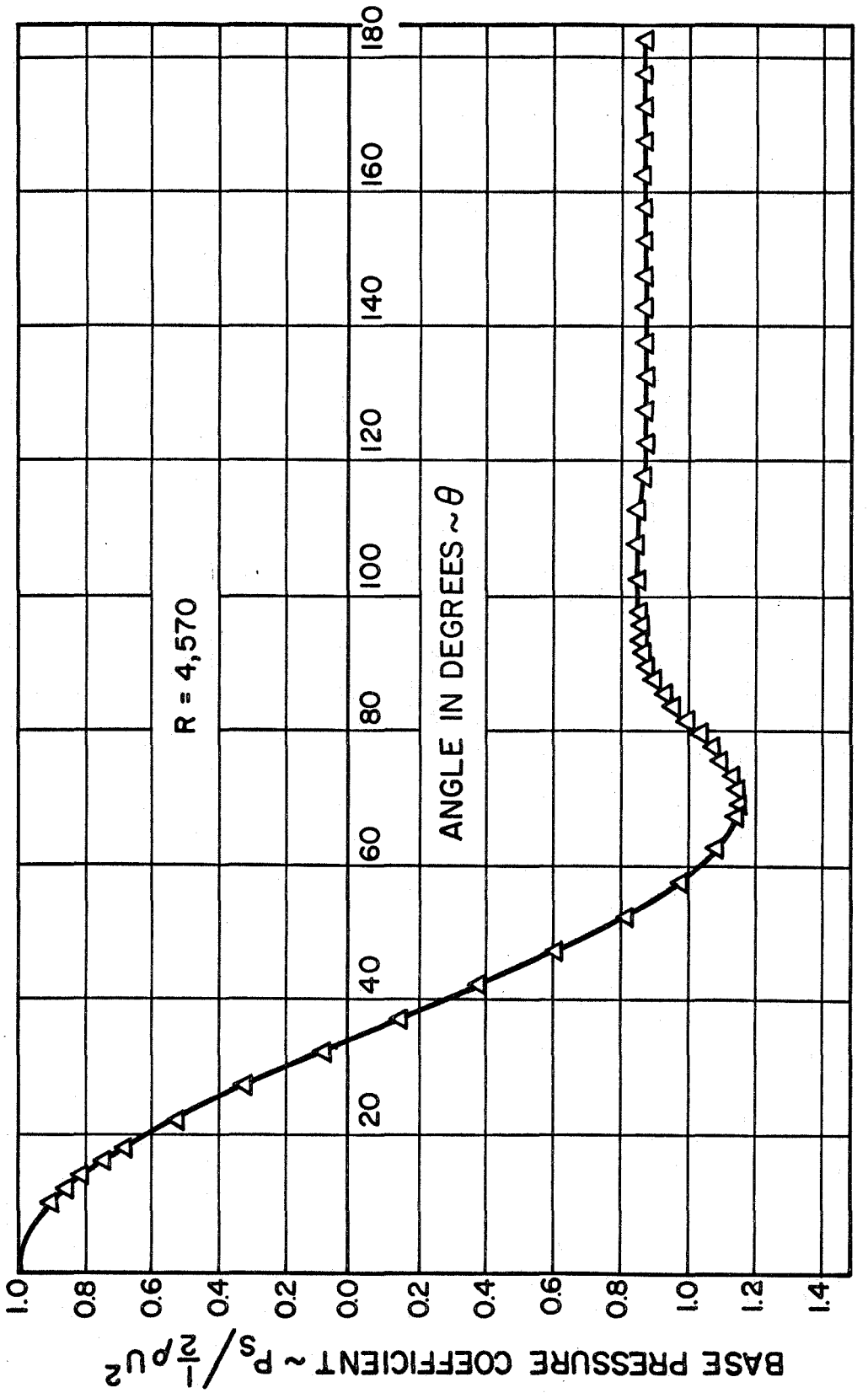

FIGURE 27 PRESSURE DISTRIBUTION OVER CIRCULAR CYLINDER, R = 4,570, D = 0.250 IN.

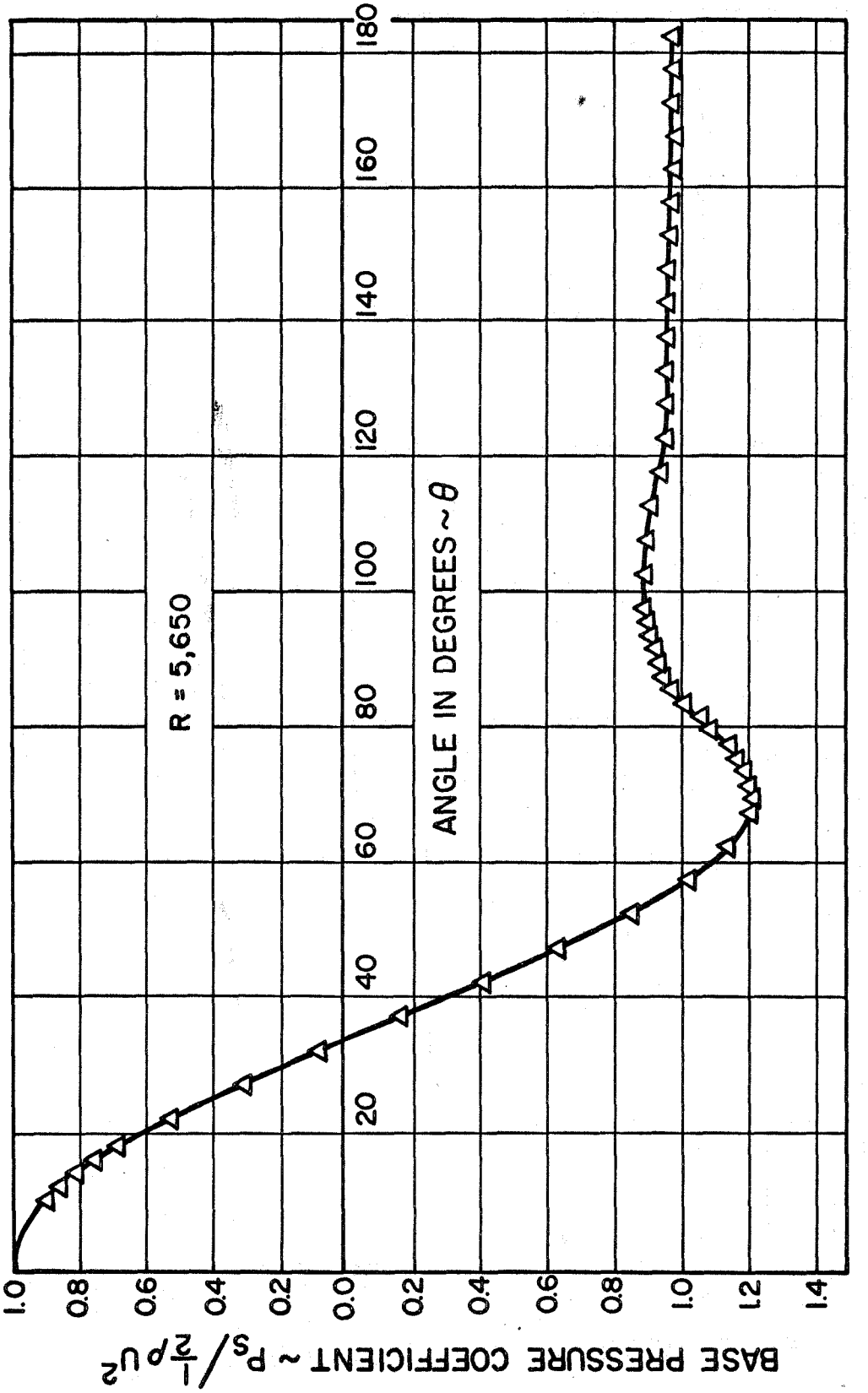

FIGURE 28 PRESSURE DISTRIBUTION OVER CIRCULAR CYLINDER, R = 5,650, D = 0.250 IN.

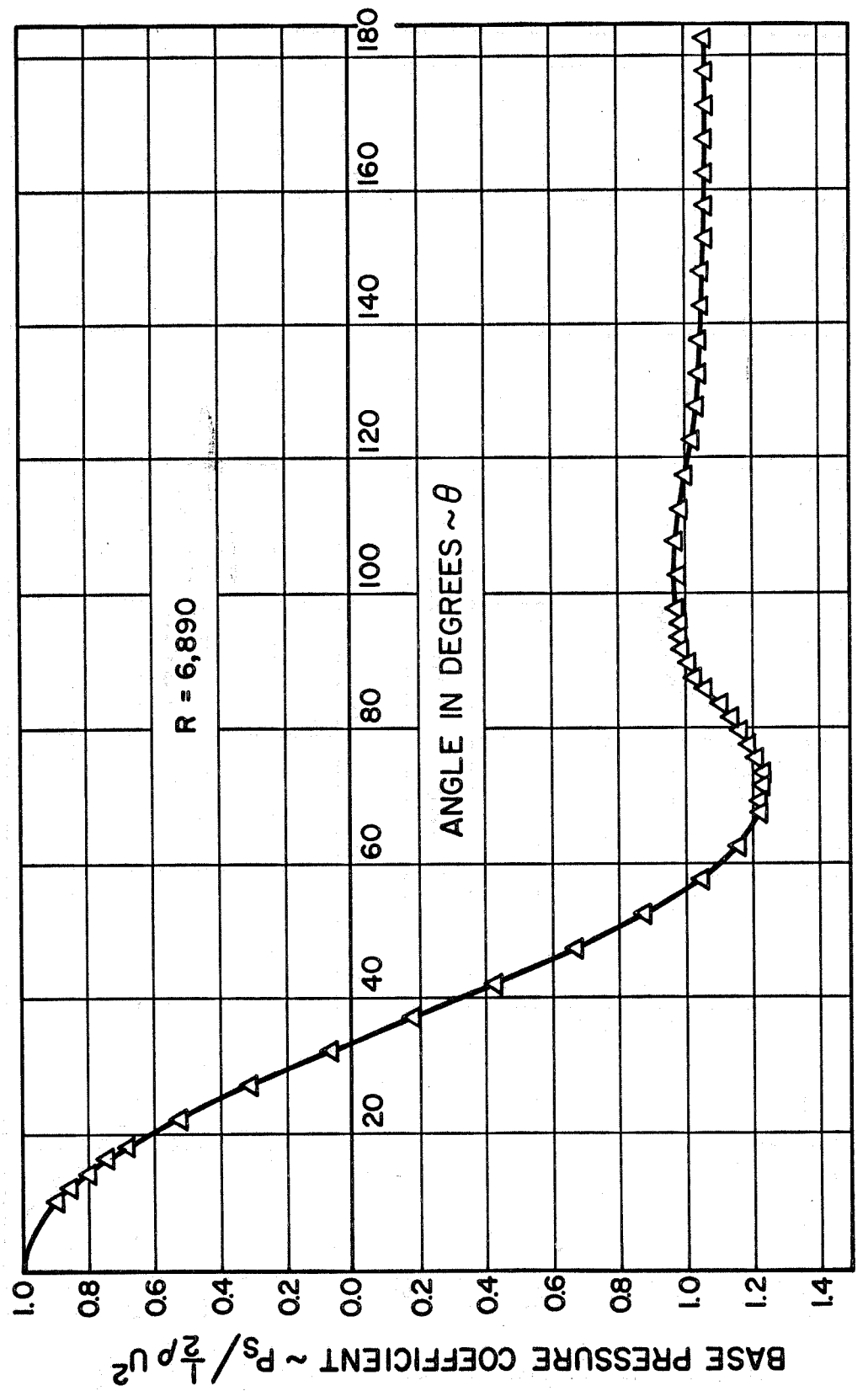

FIGURE 29 PRESSURE DISTRIBUTION OVER CIRCULAR CYLINDER, R = 6,890, D = 0.250 IN.

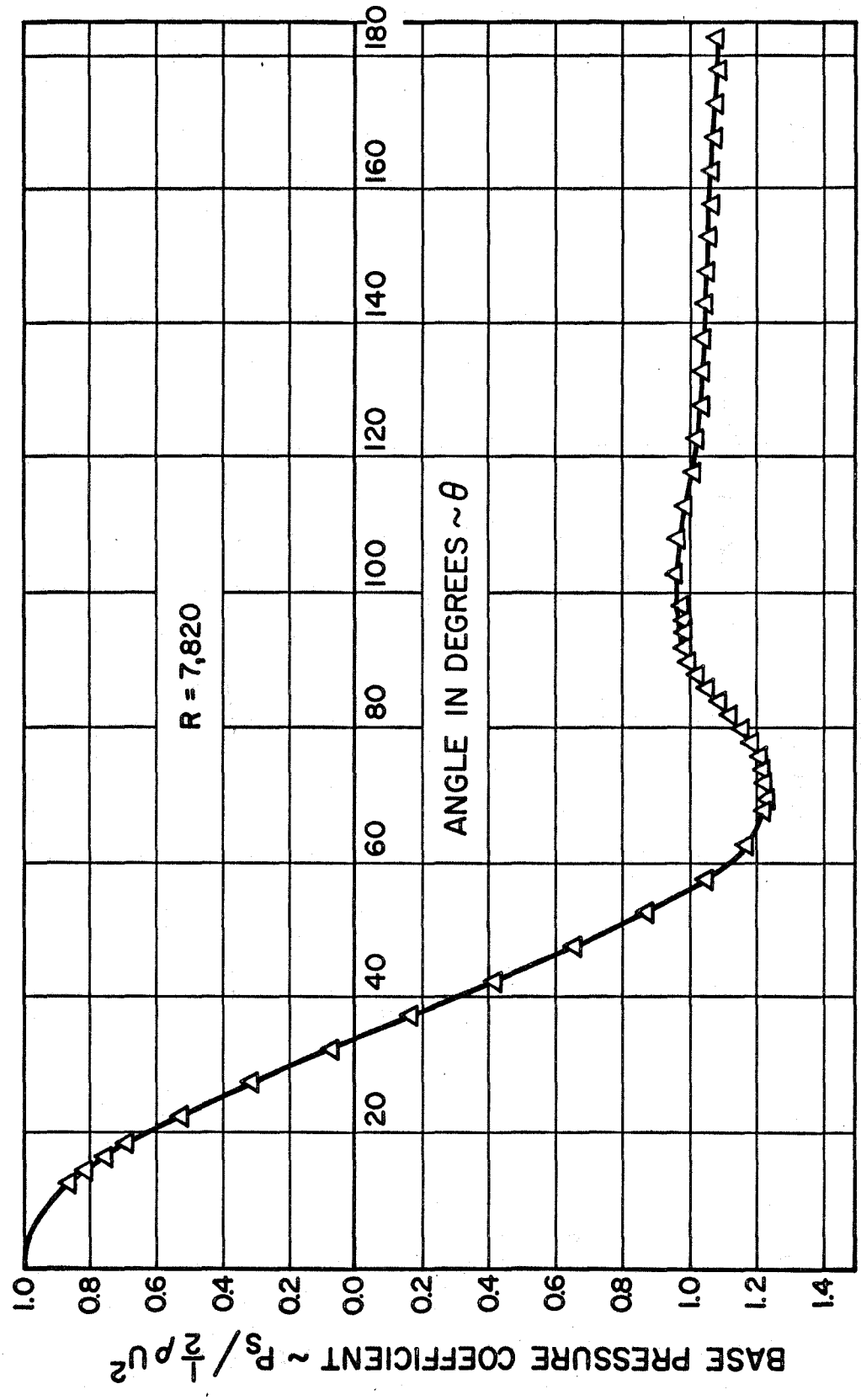

FIGURE 30 PRESSURE DISTRIBUTION OVER CIRCULAR CYLINDER, R = 7,820, D = 0.250 IN.

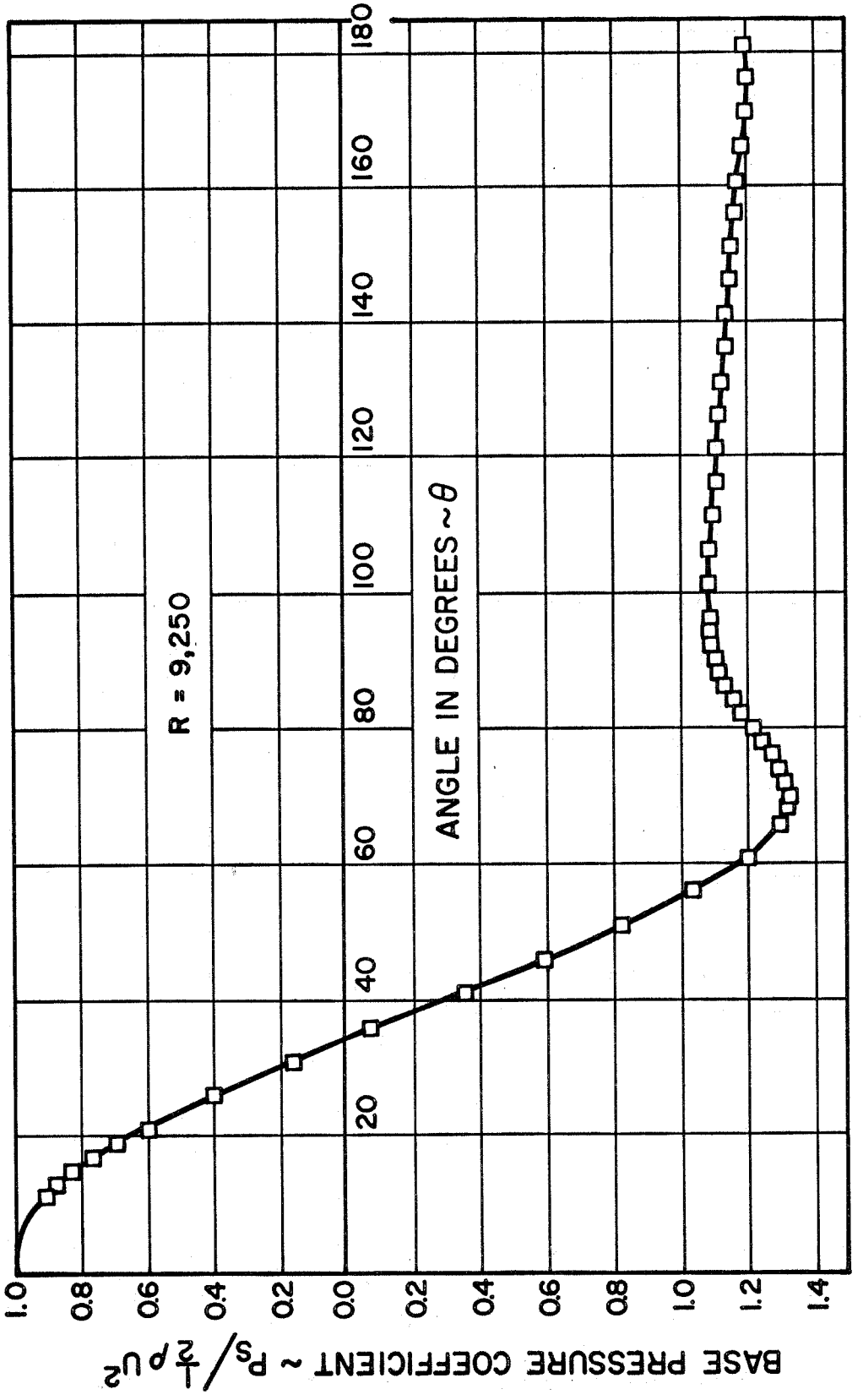

FIGURE 31 PRESSURE DISTRIBUTION OVER CIRCULAR CYLINDER, R = 9,250, D = 0.500 IN.

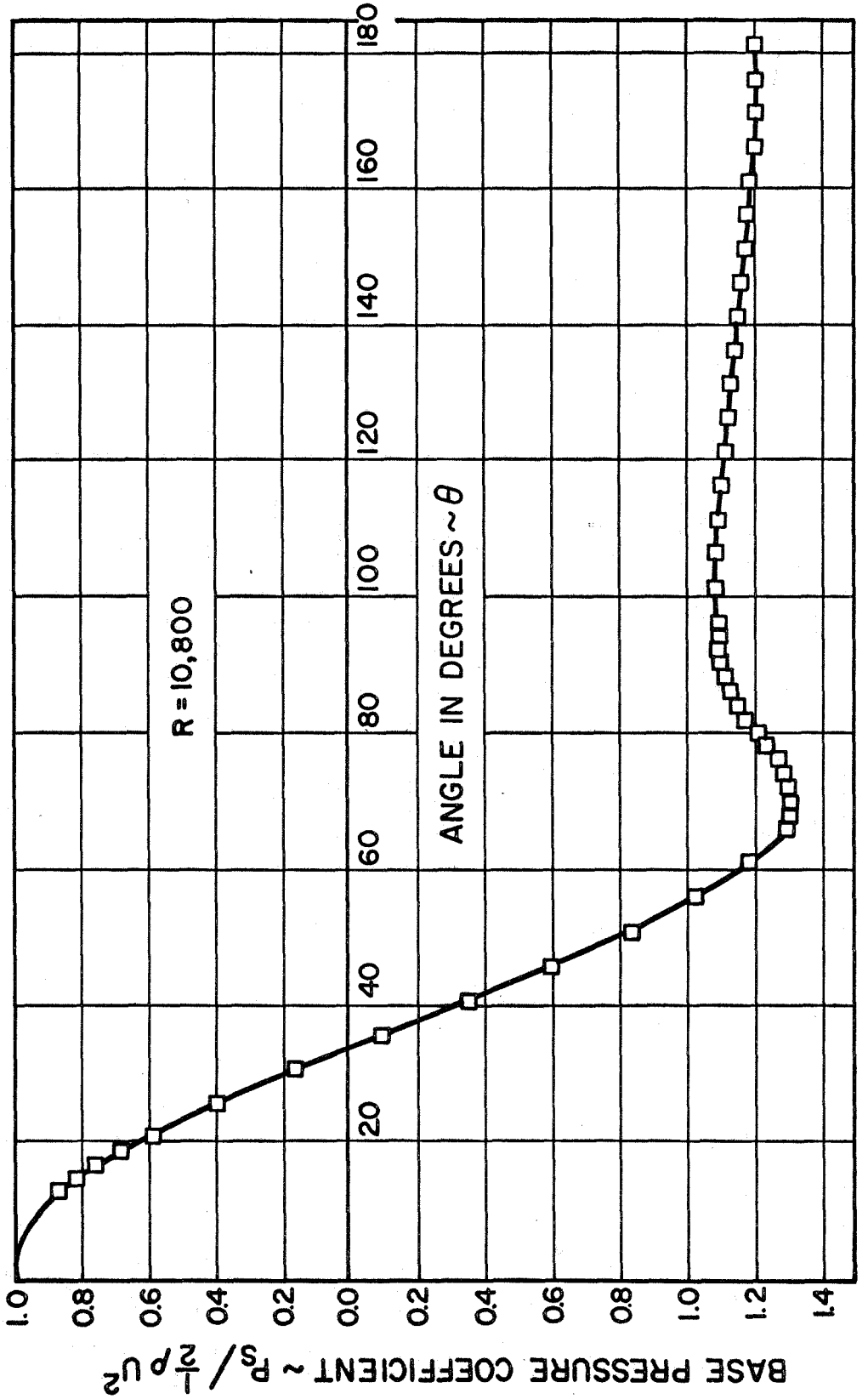

FIGURE 32 PRESSURE DISTRIBUTION OVER CIRCULAR CYLINDER, R = 10,800, D = 0.500 IN.

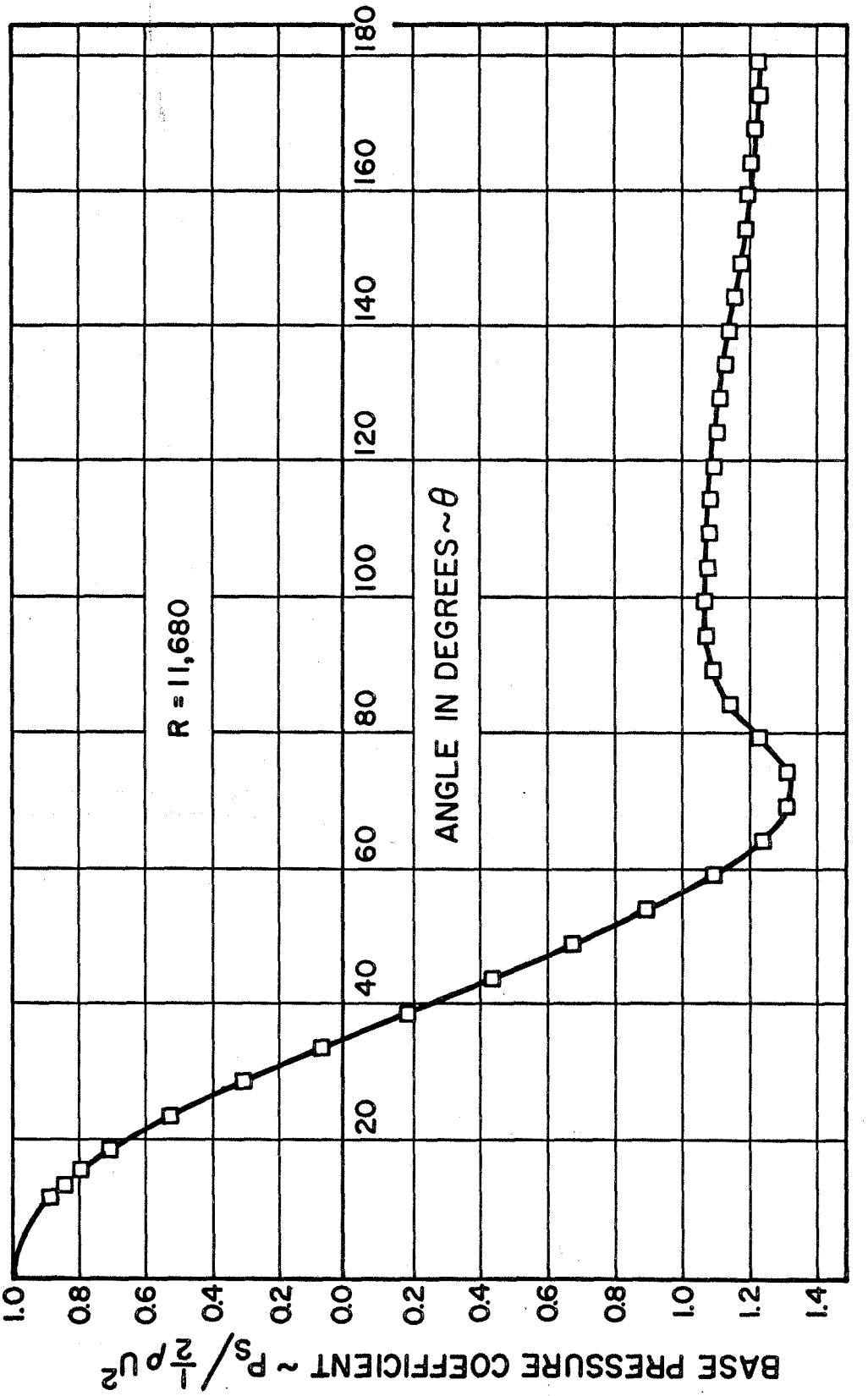

FIGURE 33 PRESSURE DISTRIBUTION OVER CIRCULAR CYLINDER, R = 11,680, D = 0.500 IN.

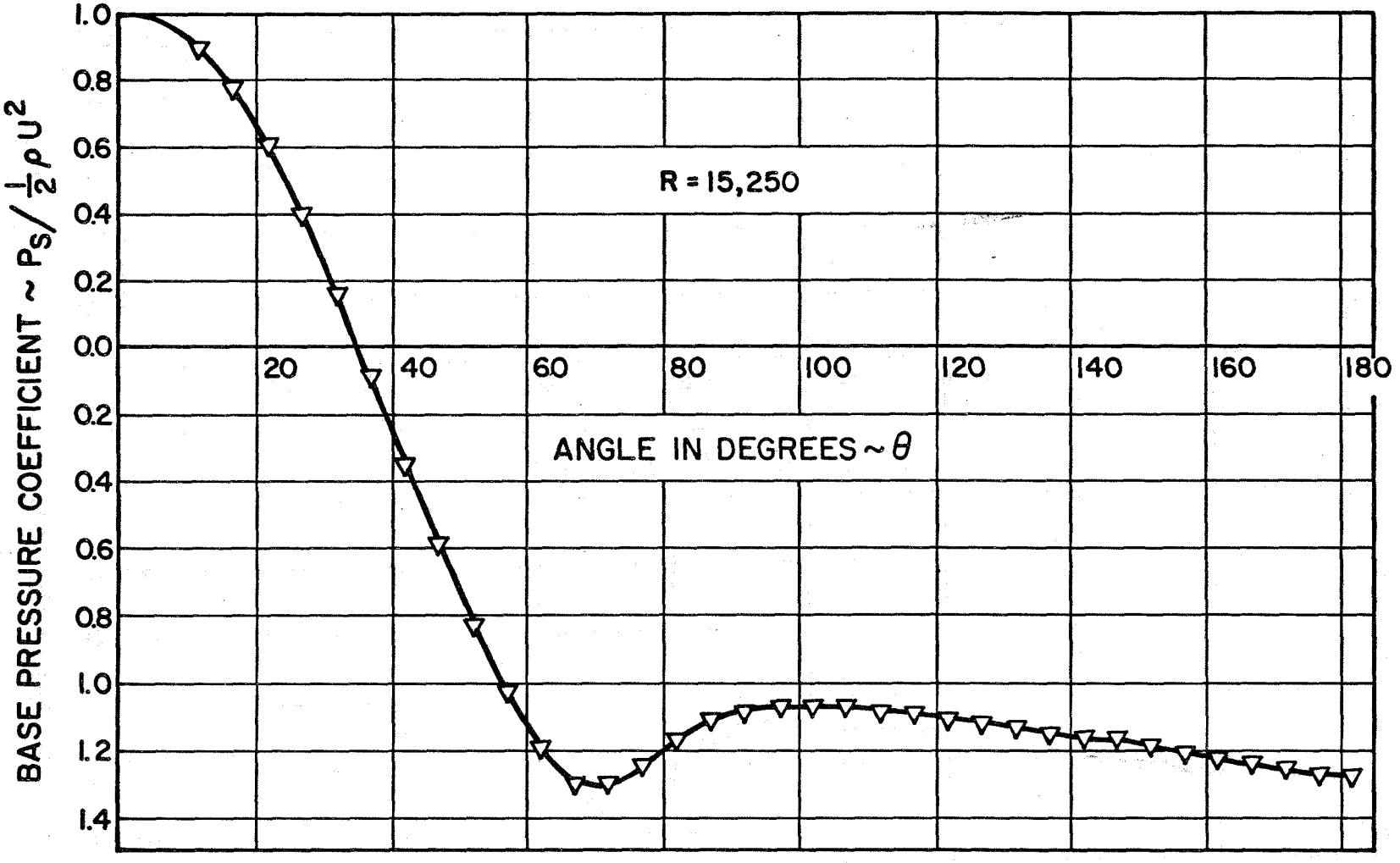

FIGURE 34 PRESSURE DISTRIBUTION OVER CIRCULAR CYLINDER, R = 15,250, D = 0.750 IN.

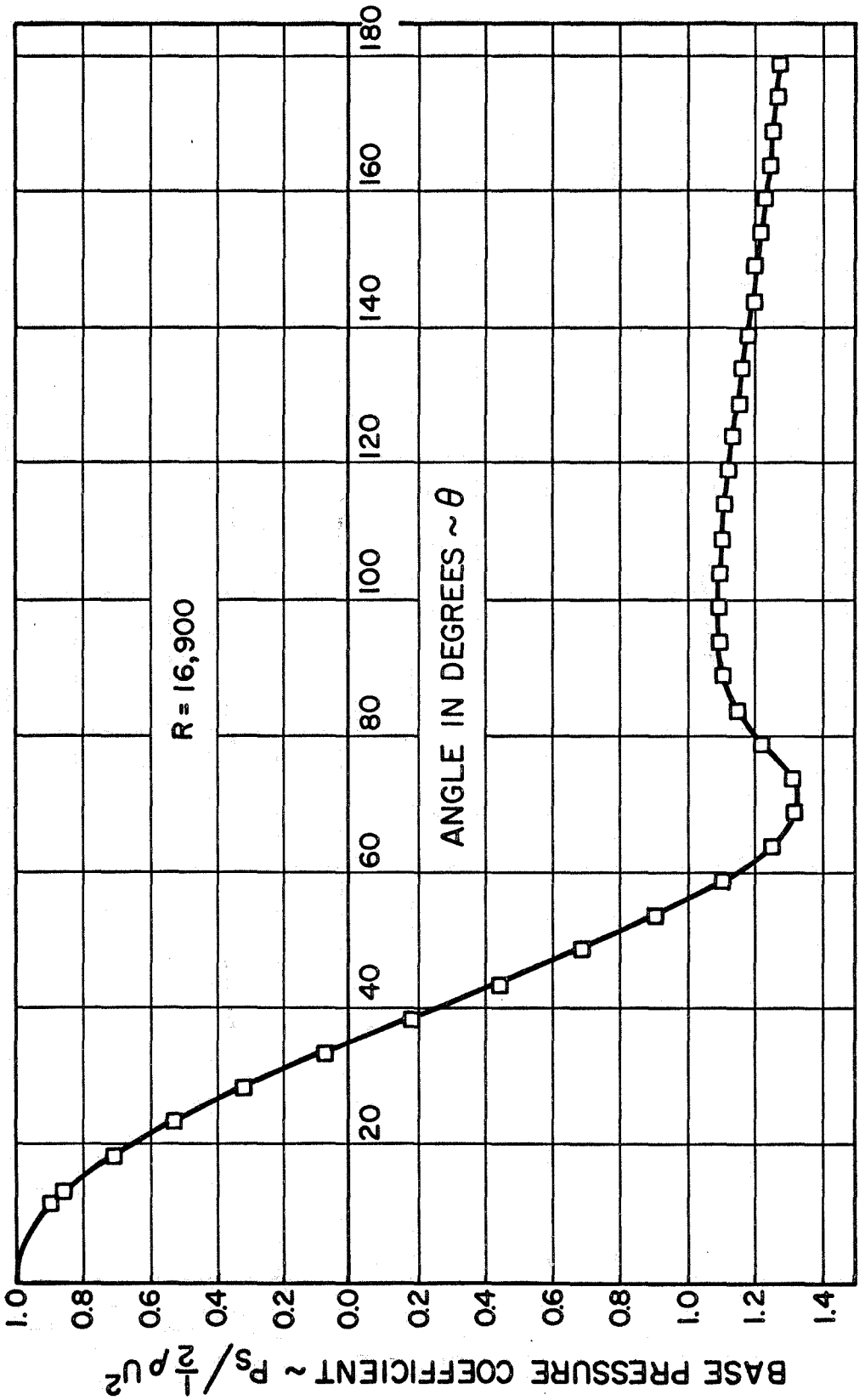

FIGURE 35 PRESSURE DISTRIBUTION OVER CIRCULAR CYLINDER, R = 16,900, D = 0.500 IN.

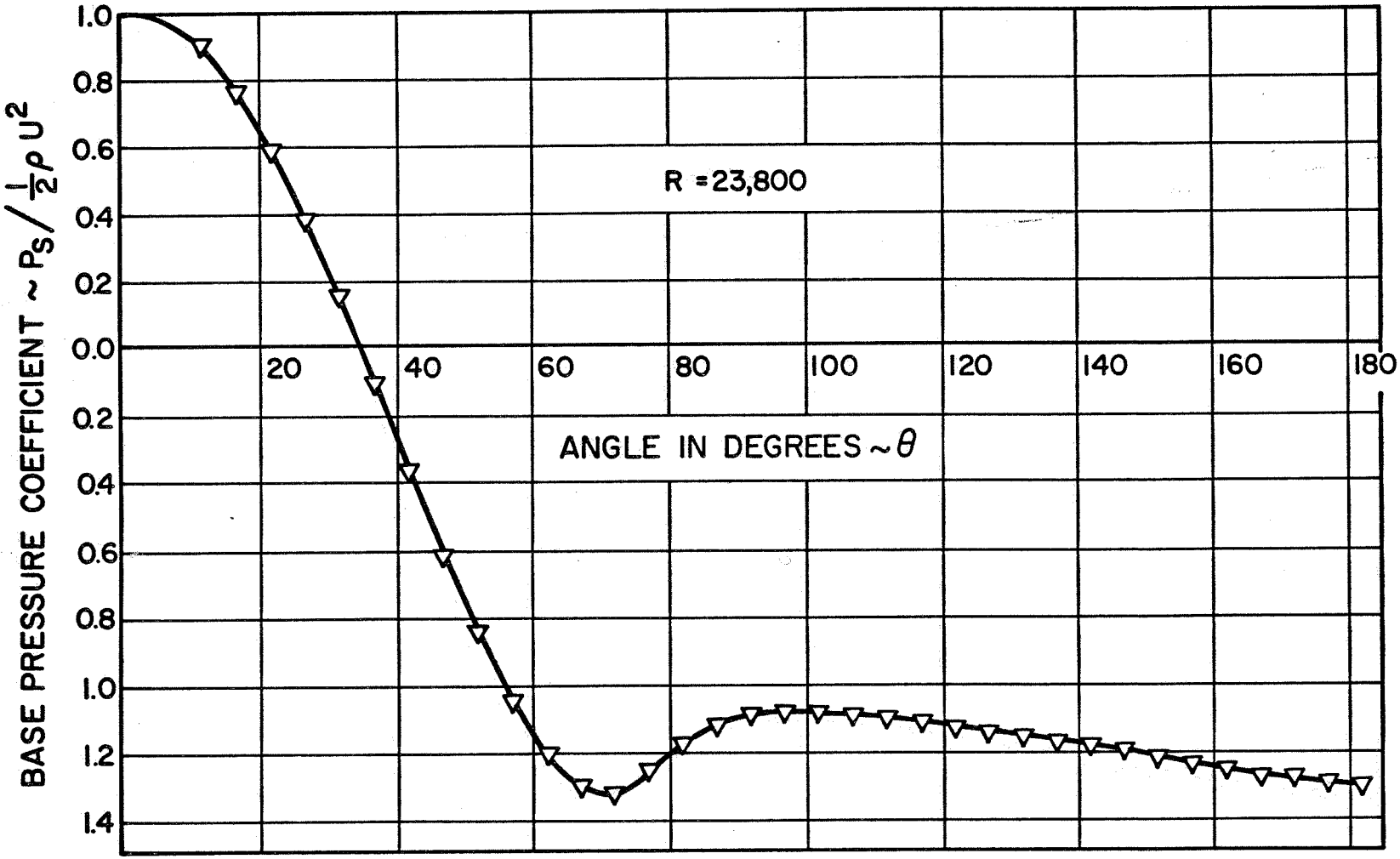

FIGURE 36 PRESSURE DISTRIBUTION OVER CIRCULAR CYLINDER, R = 23,800, D = 0.750 IN.

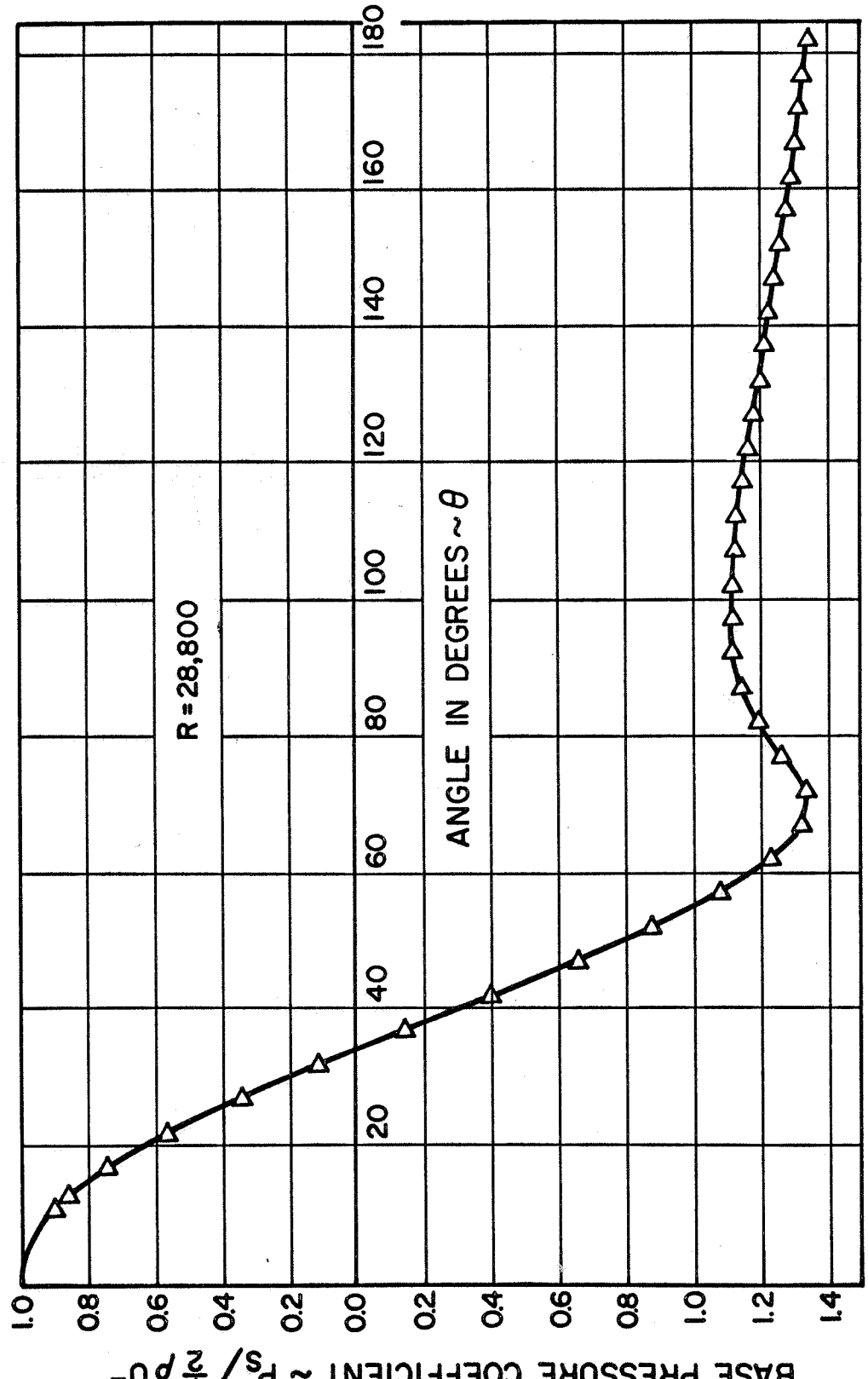

FIGURE 37 PRESSURE DISTRIBUTION OVER CIRCULAR CYLINDER, R = 28,800, D = 0.875 IN.

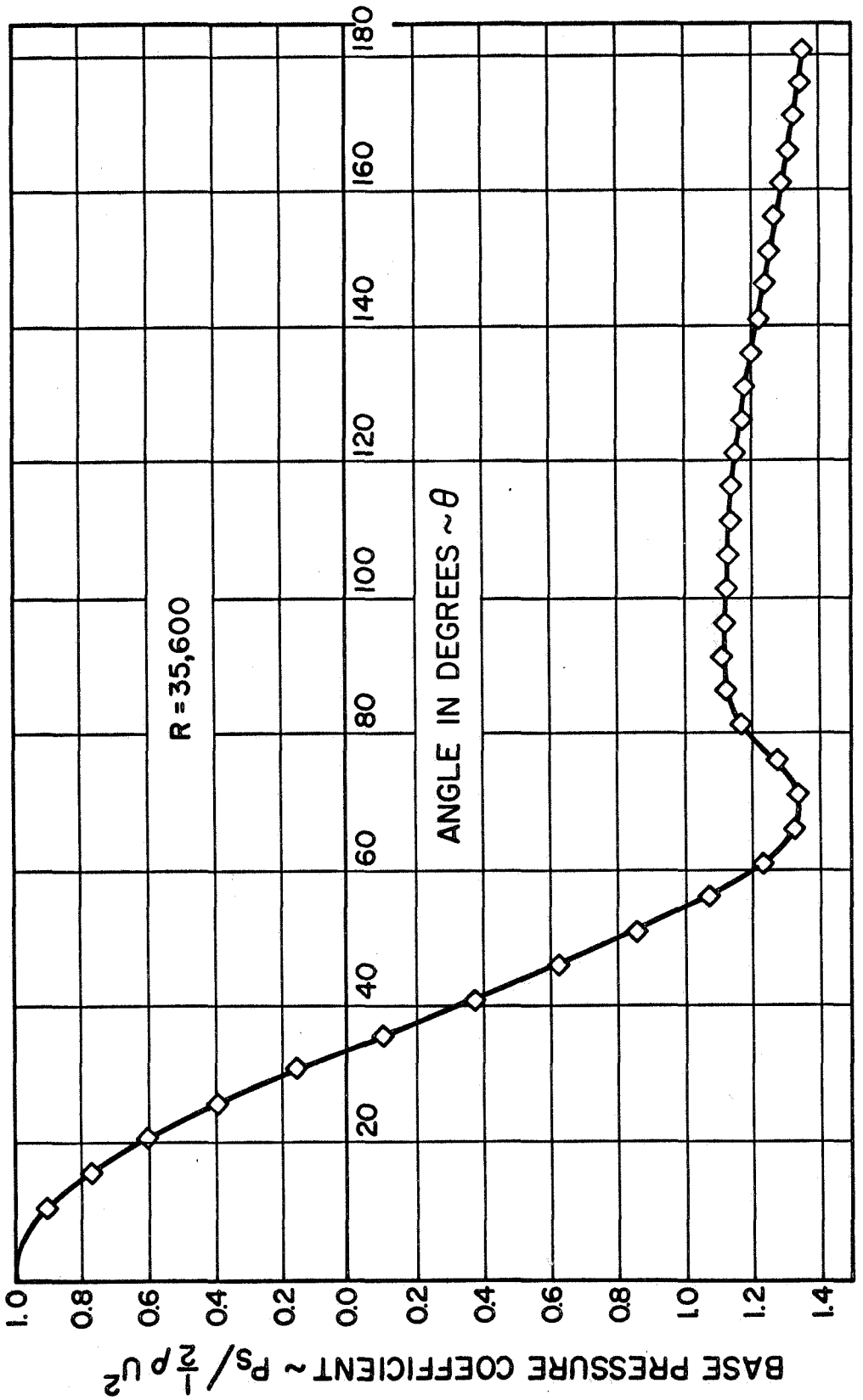

FIGURE 38 PRESSURE DISTRIBUTION OVER CIRCULAR CYLINDER, R = 35,600, D = 1.50 IN.

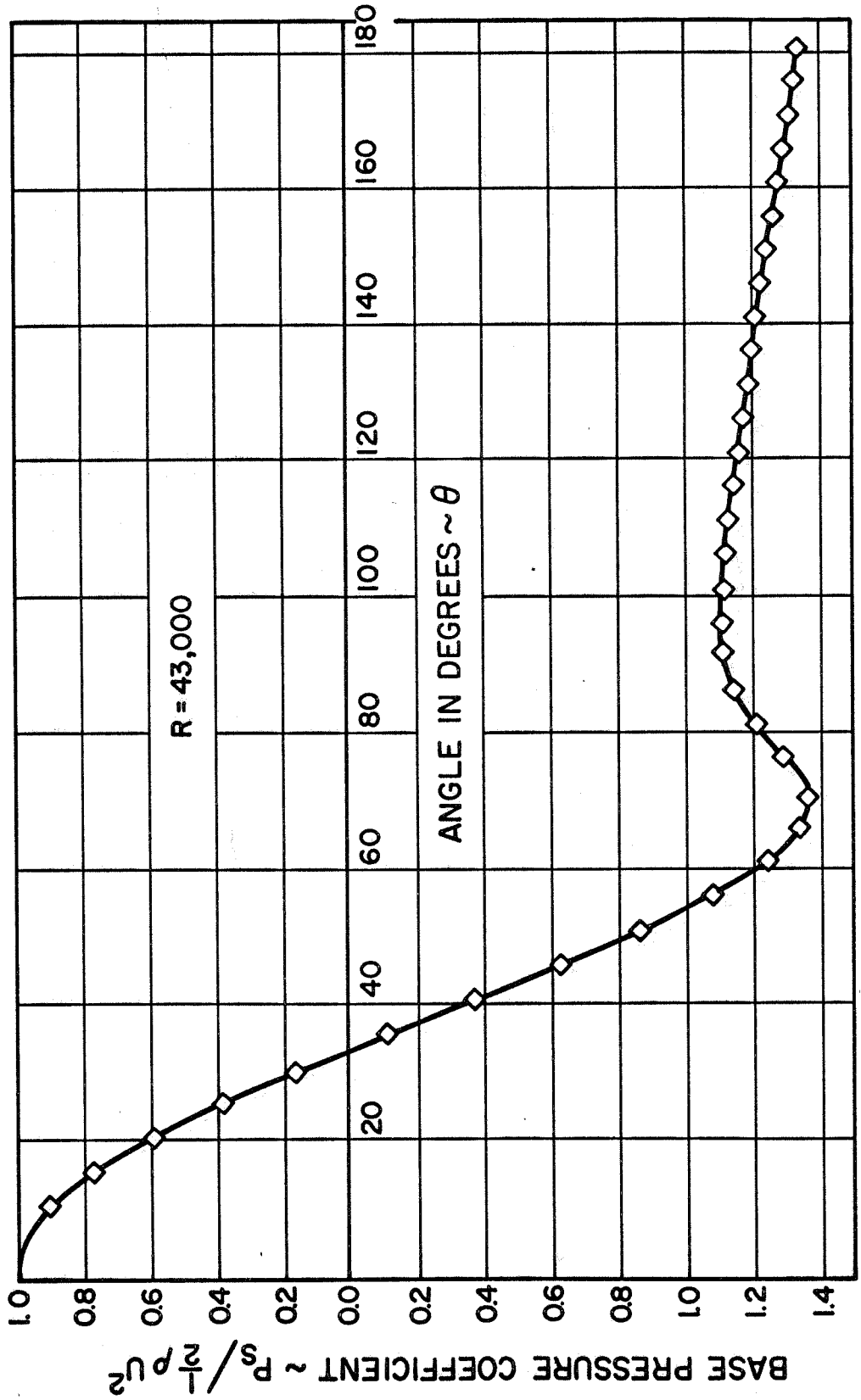

FIGURE 39 PRESSURE DISTRIBUTION OVER CIRCULAR CYLINDER, R = 43,000, D = 1.50 IN.

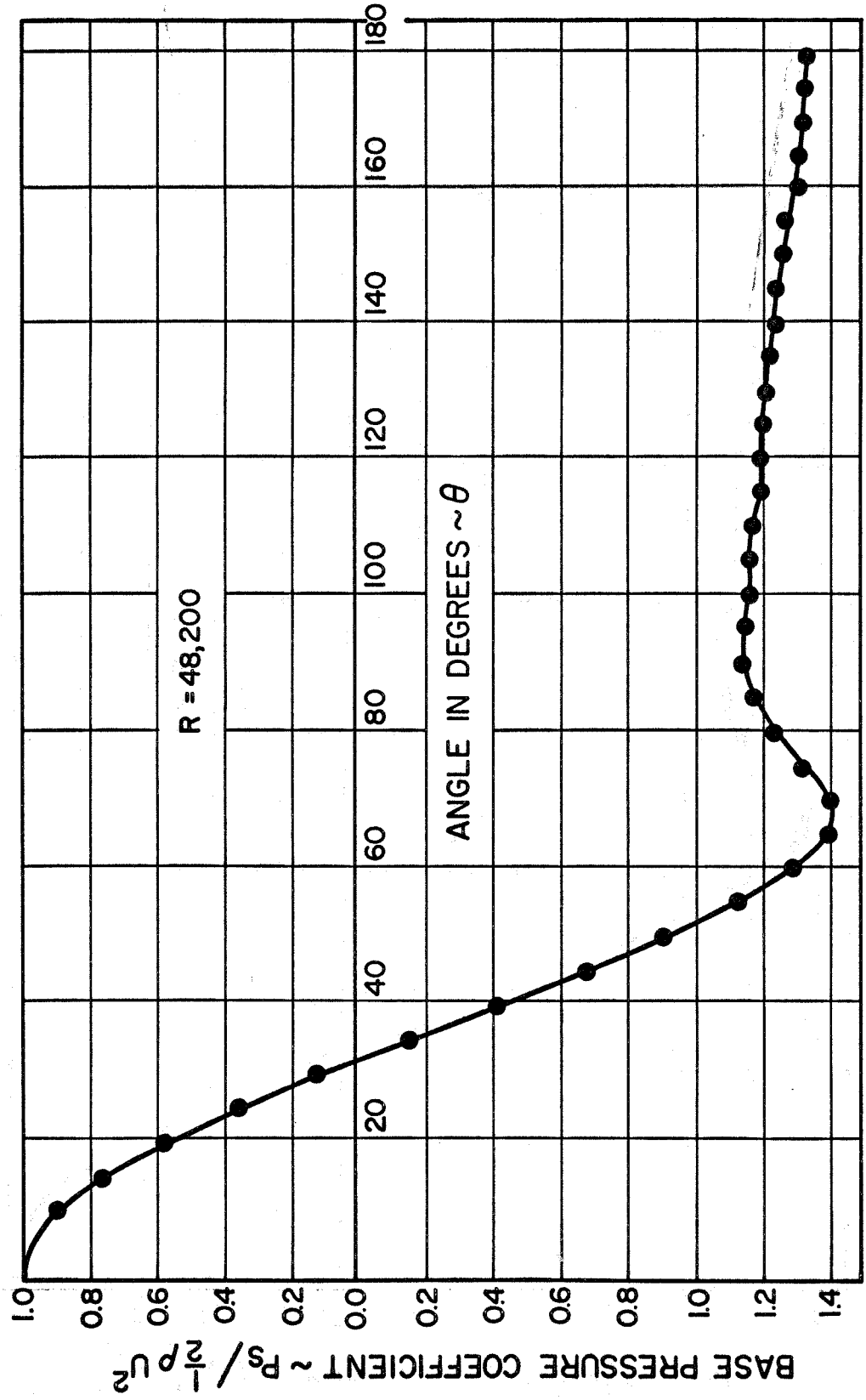

FIGURE 40 PRESSURE DISTRIBUTION OVER CIRCULAR CYLINDER, R = 48,200, D = 2.25 IN.

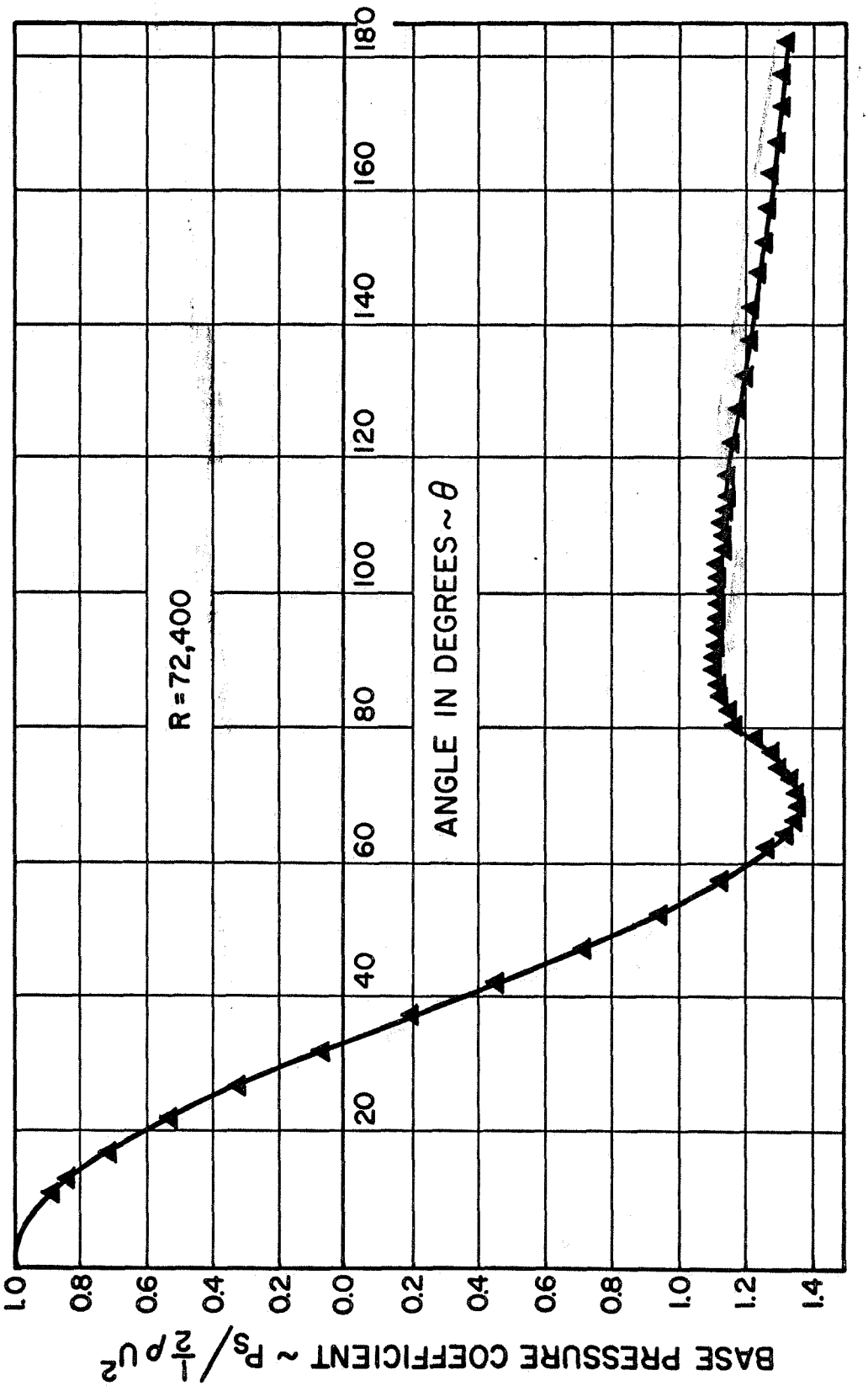

FIGURE 41 PRESSURE DISTRIBUTION OVER CIRCULAR CYLINDER, R = 72,400, D = 1.00 IN.

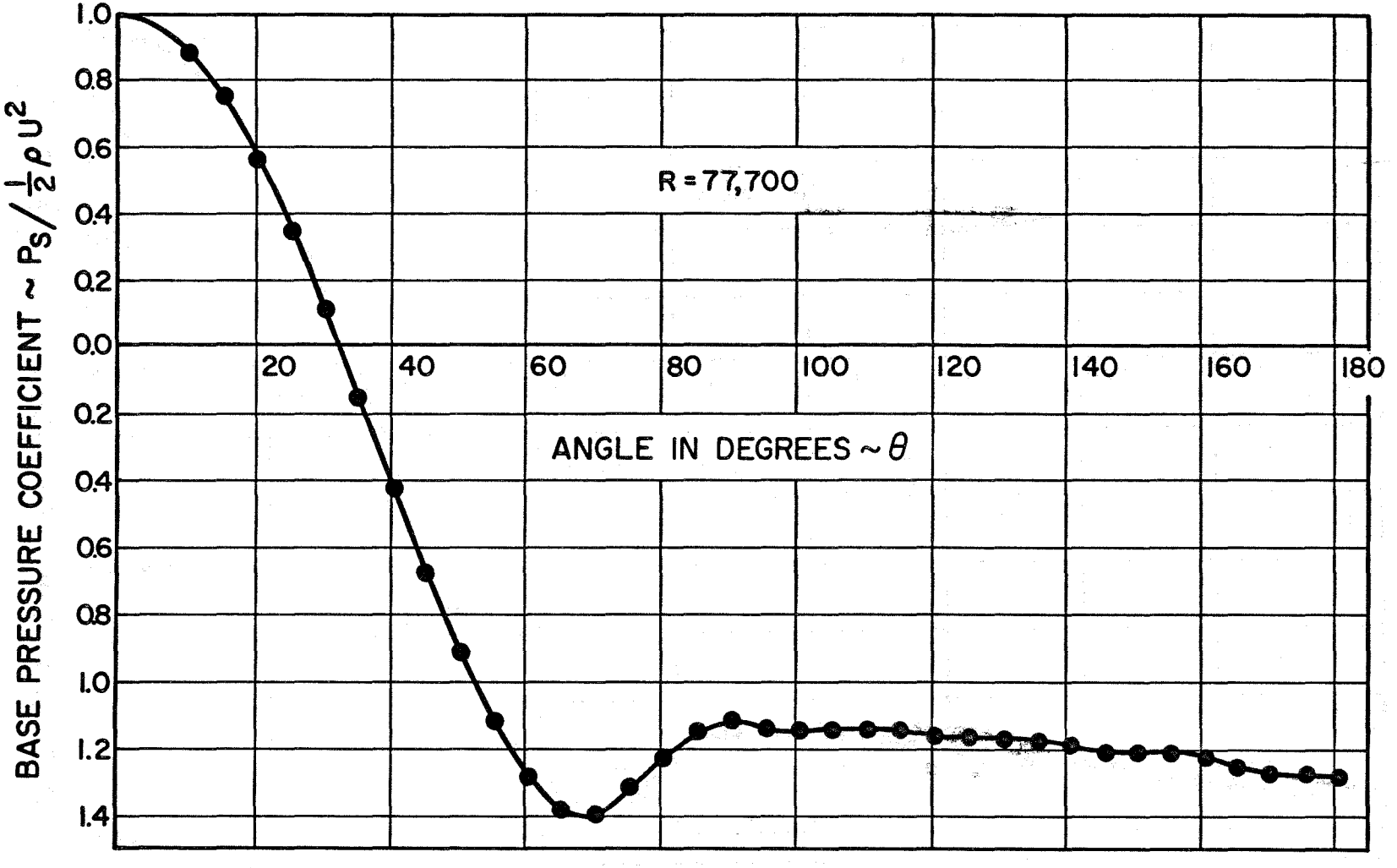

FIGURE 42 PRESSURE DISTRIBUTION OVER CIRCULAR CYLINDER, R = 77,700, D = 2.25

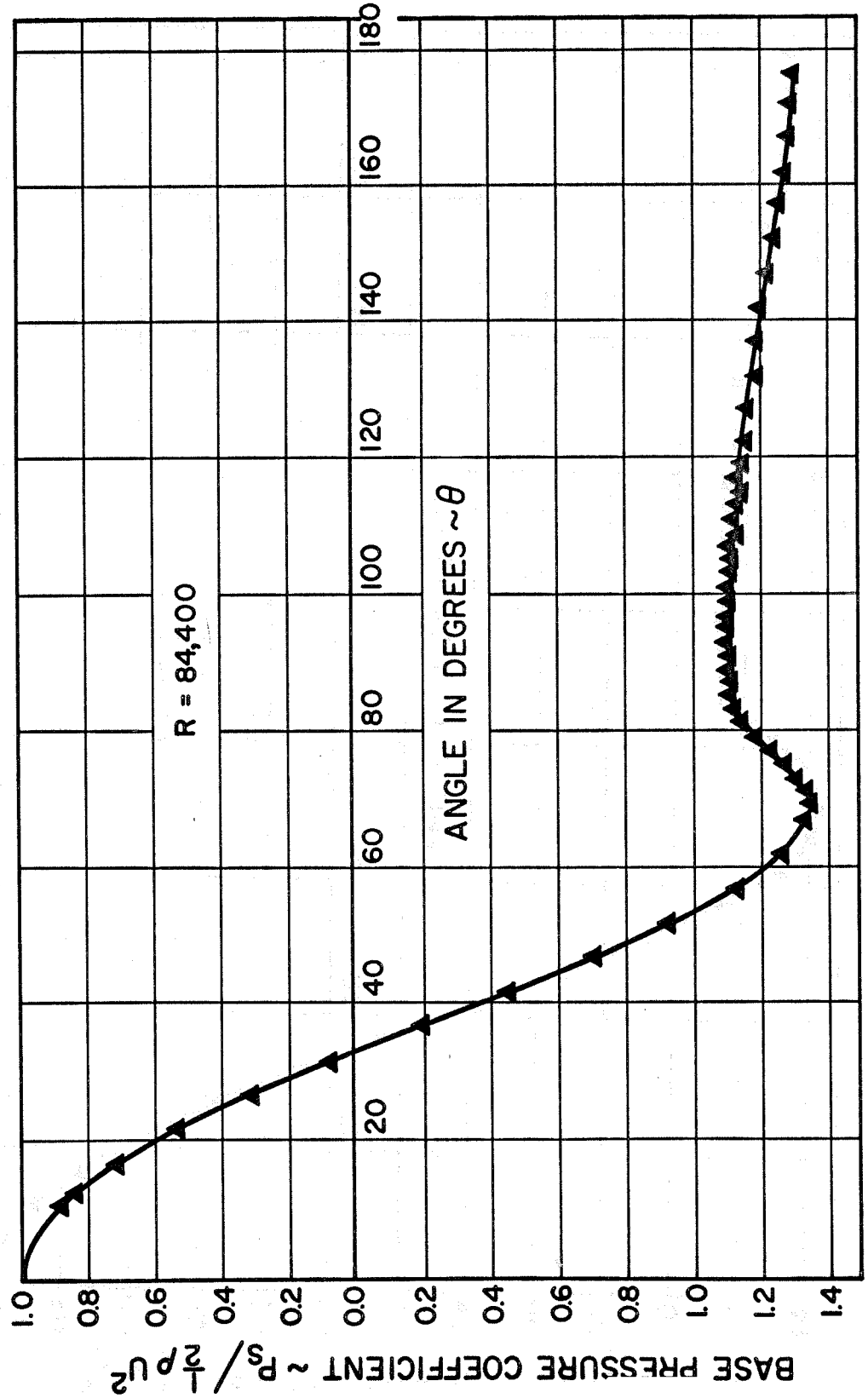

FIGURE 43 PRESSURE DISTRIBUTION OVER CIRCULAR CYLINDER, R = 84,400, D = 1.00 IN.

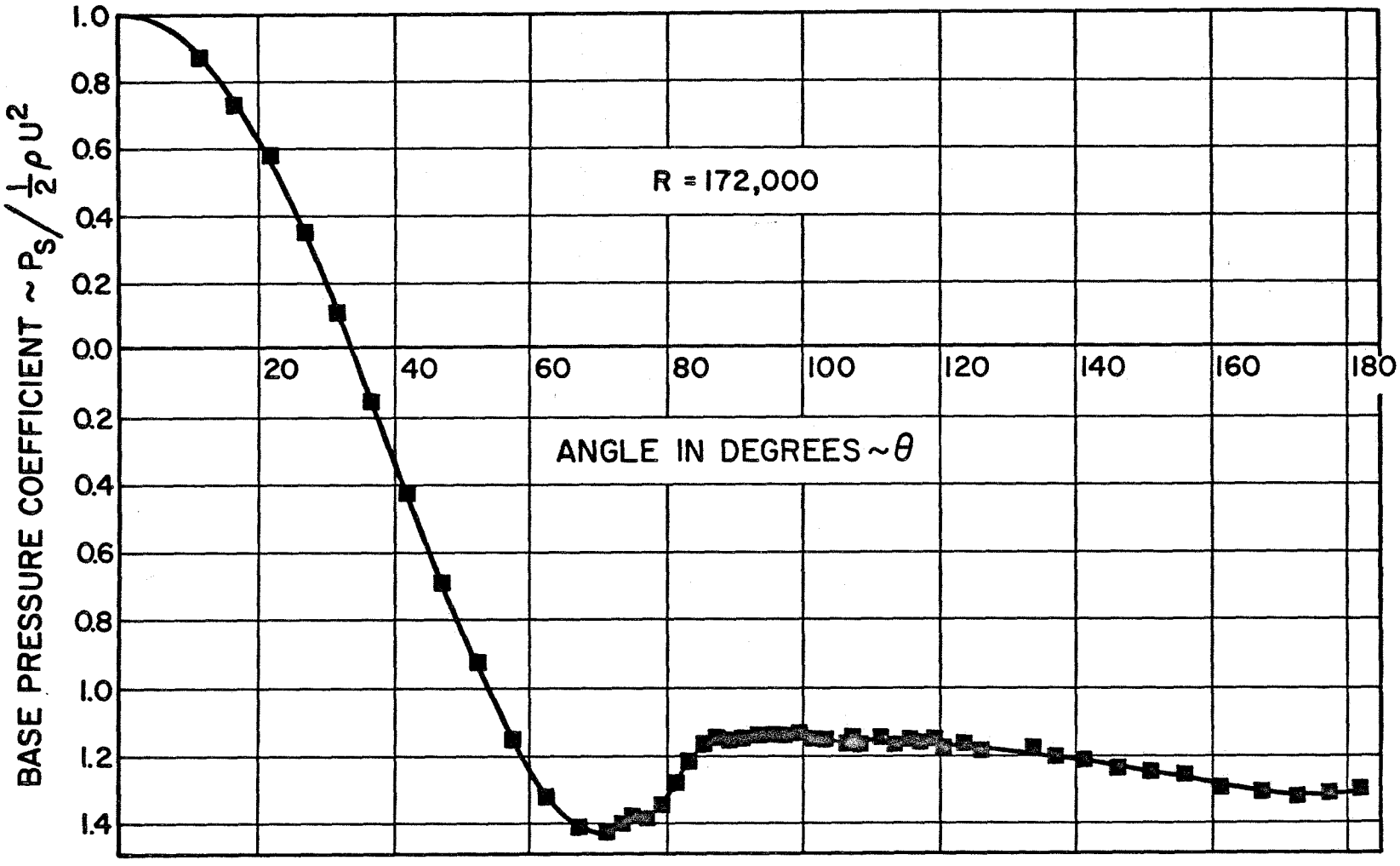

FIGURE44 PRESSURE DISTRIBUTION OVER CIRCULAR CYLINDER, R=172,000, D=3.50 IN.

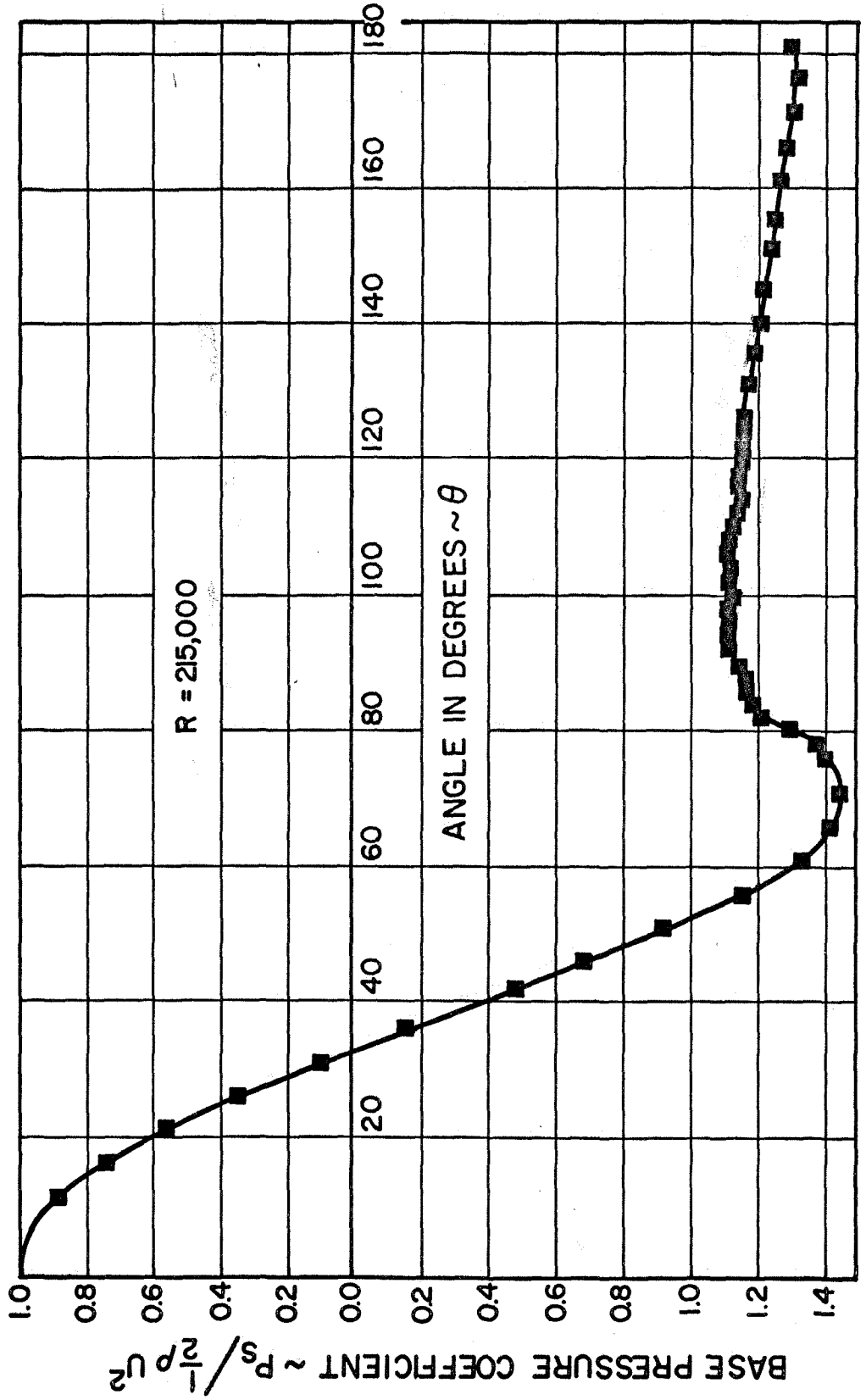

FIGURE 45 PRESSURE DISTRIBUTION OVER CIRCULAR CYLINDER, R = 215,000, D = 3.50 IN.

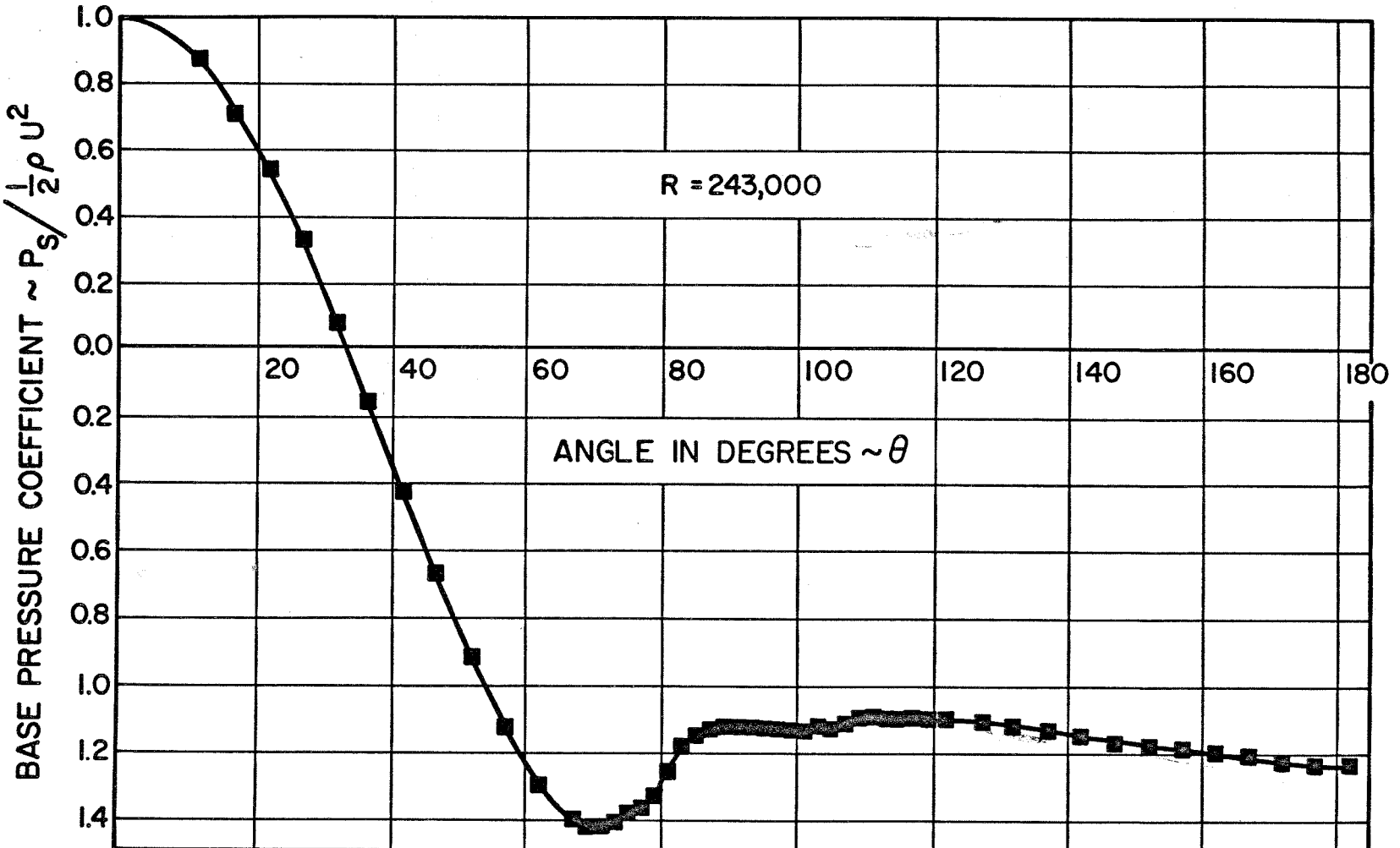

FIGURE 46 PRESSURE DISTRIBUTION OVER CIRCULAR CYLINDER, R = 243,000, D = 3.50 IN.